Defect Characterization in Heterogeneous Civil Materials Using Ultrasound

A Dissertation
Presented to
The Academic Faculty

By

Chi-Won In

In partial Fulfillment
of the Requirements for the Degree
Doctor of Philosophy in the
School of Civil and Environmental Engineering

Georgia Institute of Technology

May 2013

Defect Characterization in Heterogeneous Civil Materials Using Ultrasound

Approved by:

Dr. Laurence Jacobs, Co-Advisor
School of Civil & Environmental Engineering
Georgia Institute of Technology

Dr. Kimberly Kurtis, Co-Advisor
School of Civil & Environmental Engineering
Georgia Institute of Technology

Dr. Jin-Yeon Kim
School of Civil & Environmental Engineering
Georgia Institute of Technology

Dr. Reginald DesRoches
School of Civil & Environmental Engineering
Georgia Institute of Technology

Dr. Karim Sabra
The George W. Woodruff School of Mechanical Engineering
Georgia Institute of Technology

Date Approved: December 20, 2012

ACKNOWLEDGEMENTS

First of all, my deep gratitude goes to my two advisors, Dr. Laurence Jacobs and Dr. Kimberly Kurtis for providing me the opportunity, direction, encouragement and support to complete this research. I would also like to thank Dr. Reginald DesRoches and Dr. Karim Sabra for giving me valuable suggestions for my research.

I would like to express my gratitude to Dr. Jin-Yeon Kim, for his inspiring discussions throughout all phases of my work. His help on the ultrasonic experimental instrumentation is greatly appreciated.

I want to thank the fellow PhD and Master students in my group, Dr. Jun Chen, Dr. Holland R. Brett, Katie Matlack, Krzysztof Lesnicki, Matthias Seher, Kevin Arne, and Gun Kim for the technical assistances as well as good friendship. The nice atmosphere in our lab is always a good reason that I enjoy the life at Georgia Tech. Particularly I would like to thank Seher Matthias for his fruitful discussion on FE simulation of diffuse ultrasound used in Chapter 4 and Dr. Holland R. Brett for providing all self healing specimens and fruitful discussion on self healing process used in Chapter 5. I would like to thank Georgia Department of Transportation for the financial support.

Last but most importantly, I am deeply indebted to my parents. I thank my parents for their wholehearted support given for the every step I took in my life. Their unlimited encouragement is constantly the force which drives me to accomplish my goals.

TABLE OF CONTENTS

LIST OF TABLES

LIST OF FIGURES

LIST OF SYMBOLS

ρ	The mass density
E	The Young's modulus
G	The shear modulus
C_{LW}	The longitudinal wave speed in Teflon
C_R	The Rayleigh wave speed in asphaltic concrete
D_R	Rayleigh wave diffraction correction
E	Spectral ultrasonic energy
E^*	Ultrasonic spectral energy density without dissipation
f	Frequency
$H(f)$	Transfer function
$\alpha(f)$	Attenuation coefficient
Φ_0	Initial phase angle
$v(f)$	Phase velocity
P	Spectral energy density of the source
P_0	Amplitude of spectral energy source density
D	Diffusivity
D^e	Effective diffusivity
σ	Dissipation
$S_0(f)$	Source spectrum at z=0
$S_i(f)$	Spectra of each signal propagating the distance between two transducers
t	Time

SUMMARY

Asphalt and Portland cement concrete constitutes a significant portion of the total infrastructure all over the world. It has been reported that much of this concrete infrastructure is now approaching or has already passed its original design life. Thus it is critical to be able to quantitatively assess the condition of these concrete components. In order to rehabilitate or repair the civil infrastructure, nondestructive evaluation (NDE) techniques have been of great interest for infrastructure management agencies. However concrete components present several specific NDE challenges that must be addressed. . Concrete naturally exhibits large scale heterogeneous microstructure with a great deal of local material property variability,

For this reasons, many conventional NDE techniques that work well for steel and other homogeneous materials cannot be applied to concrete; concrete is unable to transmit high frequencies, as the heterogeneity of the concrete causes signals of smaller wavelengths or wavelengths equal to the nominal aggregate size to be scattered and severely attenuated. Nevertheless, progress has been made towards accurate and reliable in-place NDE of concrete structures and materials, for example impact echo, ultrasonic pulse velocity method, and the ultrasonic wave transmission method. However, the detection of smaller sized defects or remote defects that are located away from the testing location still pose problems. In addition, the large size and potential limited access conditions of civil structures raise additional challenges.

To overcome the limitations of current NDE techniques for concrete, this research considers two different types of ultrasonic waves (coherent and incoherent wave) to quantitatively characterize and monitor defects in heterogeneous concrete materials. The global objective of this research is to determine the feasibility and applicability of using these ultrasonic waves as a global, rapid, reliable, and non-biased technique for the routine screening of defects or monitoring of concrete structures and materials. Three different problems are considered: 1) characterization of segregation in asphaltic concrete, 2) crack depth determination in pier cap of concrete bridge structure, and 3) monitoring of self-healing process in cement-based concrete.

This research characterized fundamental ultrasonic properties of asphaltic concrete (wave speed, attenuation, dynamic stiffness) in the frequency range from 40 kHz

to 100 kHz. This property measurement method has been applied to evaluate segregation in asphaltic concrete. The diffuse ultrasonic technique has been successfully developed and applied to measure small crack depth and to predict self healing in concrete. This development opens up a wide range of application in concrete for high resolution, reliable, and rapid inspection of heterogeneous materials and structures

1. INTRODUCTION

1.1 Background

Asphalt and Portland cement concrete constitutes a significant portion of the total infrastructure all over the world. Much of this concrete infrastructure is approaching or has passed its original design life. Therefore, at present, it is in poor condition, as described by the report card of the American infrastructure (ASCE, 2009). In that report, it is estimated that a $2.2 trillion investment is needed to return the condition of the infrastructure to acceptable levels for 5 years. Before appropriate rehabilitation can be prescribed, however, the condition of the structures must be assessed. Nondestructive evaluation (NDE) techniques that can detect, localize and characterize damage, deterioration and discontinuities in concrete are of great interest to infrastructure management agencies, this is important for concrete structures since internal discontinuities may remain hidden from view, yet significantly compromise the overall integrity of the structure.

Early detection of discontinuities is the most effective way to reduce maintenance and rehabilitation costs, thereby improving public safety. The deterioration and damage of concrete structures can be described by a variety of physical and environmental damage modes. Common discontinuity modes include delamination/ spalling, cracks and segregation in concrete structure. In other cases, the geometry or size of a concrete element should be verified in a nondestructive fashion: for example, verifying the thickness of pavement slabs or the depth and shape of poured concrete shafts that act as the supporting foundations for tall buildings. Finally, the strength and stiffness development of early age concrete over time may be needed.

Concrete structures present several specific challenges that must be overcome before NDE can be applied effectively. The structures usually are large in size. As a result, much time is needed to adequately test the entire structure and deep material penetration is often difficult to achieve. In addition, concrete naturally exhibits large scale inhomogeneous material structure and a great deal of local material property variability. Structural concrete is composed of graded mineral aggregates, up to 30mm (1.2in) in size, bound by an inorganic cement matrix. In addition, most structural concrete contains a grid of reinforcing steel bars or cables. For these reasons, many conventional NDE techniques that work well for steel and other homogeneous materials cannot be applied to concrete. Concrete is unable to transmit high frequencies, as the inhomogeneity of the concrete causes signals of smaller wavelengths or wavelengths equal to the nominal aggregate size to be highly scattered and attenuated. For example, high frequency pulse/ echo A-scan or C-scan analysis cannot be applied directly to concrete because of the intensive backscatter caused by the aggregates. Nevertheless, some forms of ultrasonic tests have been developed and found application in concrete structures to determine the properties of concrete.

In the 1930s, Powers (Powers, 1938), Obert (Obert, 1939), Hornibrook (Hornibrook, 1939), and Thomson (Thomson, 1940) were the first to conduct extensive research using vibrational techniques such as the resonant frequency method for concrete. Concurrently, the development of through thickness ultrasonic wave velocity measurement, commonly referred to as the ultrasonic pulse velocity method, began in Canada called the soniscope (Leslie & Cheesman, 1949) and England called the ultrasonic tester (Jones, 1948) as late as the 1940s. Over the next several decades,

additional advancements in ultrasonic testing of concrete have been introduced, both for practical field application and for laboratory research purposes. (e.g., the echo methods (impact-echo and pulse-echo) for thickness measurements (Bradfield & Gatfield, 1964; Howkins, 1968; Mailer, 1972; Sansalone, Lin, & Streett, 1997), flaw detection (Posston & Sansalone, 1997; Sansalone & Carino, 1989), and integrity testing of piles (Brendenberg & Ed., 1980; L. D. Olson & Wright, 1990; Stain, 1982; Vankuten & Middendorp, 1982), the impulse-response method to test piles (Davis & Hertlein, 1991; L. Olson & Church, 1986), Drilled shafts (Finno & Gassman, 1998), and bridge deck (Davis & Hertlein, 1990) and the spectral analysis of surface waves (SASW) method to determine the thickness of pavements and elastic moduli of layered pavement systems.(Heisey, Stokoe II, & Meyer, 1982; Jones, 1962b; Nazarian & Stokoe II, 1986; Nazarian, Stokoe II, & Hudson, 1983).

Recently, Progress toward improved and innovative application of NDE for civil engineering materials and structures such as attenuation measurement (Suaris & Fernando, 1987), Laser generation and detection (Jacobs & Whitcomb, 1997), peak frequency of ultrasonic wave (Sellick, Landis, Peterson, Shah, & Achenbach, 1998), high frequency technique (S. Popovics, Bilgutay, Karaoguz, & Akgul, 2000), and noncontact ultrasonic technique (Purnell, Gan, Hutchins, & Berriman, 2004) has been reported. Nevertheless, through thickness wave velocity test has remained the most common ultrasonic tests and the only ones standardized for use in concrete in field investigation.

The most of common feature of the recently proposed methods is that inferences about internal conditions of concrete structures are made based on the effect that the structure has on the propagation of stress waves. In all cases, stress waves are introduced

into the test object and the surface response is monitored. Access to only one surface is mostly required in field application. Depending on the details of the testing configuration and the measured response, different information is obtained about the concrete structures.

1.2 Research Motivation

Progress towards accurate and reliable in-place nondestructive evaluation of concrete structures and materials has been achieved over the past several decades. A wide range of physical phenomena is incorporated into current ultrasonic inspection techniques in these concrete systems. And, some nondestructive evaluation (NDE) tasks have been successfully performed in heterogeneous material with current technology; for example near-surface, larger sized (> 10 cm) volumetric defects and cracks in concrete structures are possible. However the detection of smaller sized defects, defects located away from the testing location, and defects in inhomogeneous materials still pose problems. Moreover, the large size and potential limited access conditions of civil structures raise additional challenges.

For instance, in impact-echo method, when applied and interpreted properly, the presence and depth of internal air-filled flaws can be detected, especially those that are oriented parallel to the testing surface. However, it can be difficult to interpret especially for complicated test specimen geometries. Furthermore, impact-echo is not sensitive to small voids (smaller than half the pulse wavelength) and vertically-oriented cracks (McCann & Forde, 2001). Similarly, in ultrasonic phase velocity method, cracks, voids and other defects in a concrete member can be detected by variations in ultrasonic wave

velocity. However, only large cracks and voids, generally larger than the transducer contact face, will cause measurable reduction in velocity, so that the detection of small size of crack or void could be hard to achieve (Jones, 1962a). Also, in impulse response technique, the test has the benefit of being rapid and simple to carry out, and the resulting dynamic stiffness estimation is useful in characterizing the complete pile system (ACI, 1998). However, analysis of impulse response could be uncertain if the data are clouded by other effects. Also, complete data are often not obtained for long piles ($L/d > 30$) or piles embedded in stiff soil systems because of leakage of wave energy.

New research and developments in NDE technology for concrete structures have focused on solving the described issues. These limitations of existing test methods urge the development of an ultra-accelerated, but still simple and reproducible test method for the routine screening of defects or monitoring of concrete structures and materials. In accordance with these current problems and aspects and in order to overcome the limitations of current NDE techniques for concrete, this research considers two different types of ultrasonic waves (coherent and incoherent waves) to quantitatively characterize and monitor defects in heterogeneous concrete materials. The global objective of this research is to determine the feasibility and applicability of using these ultrasonic waves as a global, rapid, reliable, and non-biased technique for the routine screening of defects or monitoring of concrete structures and materials. Three different problems are considered: 1) characterization of segregation in asphaltic concrete, 2) crack depth determination in pier cap of concrete bridge structure, and 3) monitoring of self-healing process in cement-based concrete.

1.3. Research Objectives

The global objectives of this research are to understand physical based principles of coherent or incoherent ultrasonic waves in heterogeneous media, to determine the feasibility of using these ultrasonic waves as a global, rapid, reliable, and non-biased technique, and to develop in-field application technique in concrete materials.

Part Ⅰ: Segregation Detection by coherent waves

Five detailed main objectives are:

1) To understand existing NDE techniques to determine their effectiveness at distinguishing segregated asphaltic concrete samples from non-segregated ones which are comprised of the same mix design. This first step verifies the feasibility of ultrasonic surface wave techniques for segregation detection of asphaltic concrete.

2) To understand physical based principles of the Rayleigh surface wave and modeling concept in asphaltic concrete and to develop measurement concept of generation and detection method (using wedge) by ultrasound. Acoustic parameters such as attenuation and phase velocity are chosen to differentiate the level of segregation from sound asphalt.

3) To develop diffraction correction factor numerically to calculate exact attenuation values using the developed contact or non-contact methodology. In a time-parallel manner, to investigate attenuation parameters in top and bottom segregated samples with baseline values measured in sound one and to verify if the developed methodology in contact manner is feasible.

4) To develop theoretical model of the developed acoustic techniques. Then, simulation results from the model are correlated with the experimental measurements to verify how segregation does affect the waveform, especially for attenuation parameters, which are then compared to those conducted experimentally.

5) To apply the proposed techniques in a fully non-contact manner for both segregated and non-segregated samples. Verify a feasibility of the non-contact method and specify what are the existing hindrances to measure attenuation parameters by this technique. To recommend requirements for the corresponding limits to identify segregation level by fully non-contacted ultrasonic Rayleigh wave technique.

Part Ⅱ: Determination of Crack Depth by incoherent waves

Five detailed main objectives are:

1) To understand existing NDE techniques to determine their effectiveness at characterization of crack depth in laboratory scale to field study and also a literature review in diffuse wave theory and its application applied to fluid and optics is a preliminary step for its feasibility to characterize the material properties of heterogeneous materials.

2) To understand the physical based principles of the diffuse wave approximation in elastic solids and develop measurement concept by diffuse ultrasound and demonstrate the capability of diffuse ultrasonic methods to assess through cover cracks in reinforced concrete bridge pile caps.

3) To evaluate material parameters such as diffusivity and dissipation at the various degrees of defect (e.g. microcracks and surface cracks) compared to those from

sound concrete. This step serves as the foundation for the rest of work since it verifies the trend that material parameters are related to the degree of defect in materials.

4) To develop a theoretical model (using ANSYS) of the developed diffuse technique. Then, simulation results from the model are correlated with the experimental measurements to verify the trend that surface crack depth is linearly dependent on lag time (the arrival time of maximum diffuse energy)

5) To perform the proposed technique to characterize different crack geometries and size (e.g. inclined crack, two cracks spaced closely, and closed cracks), and more complex configurations (fluid filled crack or with reinforced bar) as well as real cracks in bridge pier caps (full scale concrete component) to examine capability of the developed technique and to get a sense of how it can be adapted and should be modified to different situations that could arise in the field application.

Part Ⅲ: Monitoring of Self-healing Process by incoherent waves

Five detailed main objectives are:

1) To understand existing NDE techniques to determine their effectiveness at monitoring the extent of self healing process in cement based materials. Emphasis will be placed on their limitation, current implementation status of the techniques, and how the phenomenon of autogeneous self healing in cement-based composite has been known to date.

2) To benchmark the performance of the proposed diffuse ultrasound method and evaluate material parameters such as diffusivity, dissipation, and the arrival time of maximum energy of the various degree of defects (e.g. tension or flexure crack)

compared to those from controlled uncracked concrete. After and during exposure to self healing environments, such material parameters will be monitoring over time.

3) To track the progress of self healing with varying mix design and crack configuration. In conjunction, the visual test method is carried on in a time parallel manner. The results by ultrasonic diffuse technique are compared with results from measurement on surface crack width over time.

4) To investigate how different supplementary materials such as fly ash, slag, and metacaolin would lead to self healing process which is the issues of being affected by the constituent entities and change of diffusion parameters (diffusivity, dissipation, and the ATME) over time according to five different mix designs.

5) With the existing limits specified in traditional methods, the corresponding limits of parameters defined in diffuse ultrasonic methods are recommended for the identification of autogeneous self healing in cement based materials.

1.4 Outline of the Document

The proposal document will be organized into six chapters. Chapter 2 provides a literature review of existing NDE technique for each research category. Chapter 3 presents the background of coherent surface wave propagation and characteristics and its applicability to detect segregation on asphaltic concrete in both contact and non contact manners. Chapter 4 introduces incoherent field approach which is well defined in concrete materials and its applicability to estimate simple surface vertical crack depth with ANSYS simulation. Chapter 5 explain autogenuous self healing process occurred in Portland cement concrete and continuously incoherent field is applied to monitor self

healing process over 120 days with crack crack width measurements. Chapter 6 presents the conclusion of the research and gives recommendations for future research.

2. LITERATURE REIVEW

In this section, a thorough overview of current existing methods for characterization of segregation in asphaltic concrete, crack depth determination, and monitoring of self healing process in cement based concrete with their limitations are presented first. In addition, a brief introduction is given to the recent work on the use of acoustic techniques to study each proposed problem.

2.1 Segregation characterization in asphaltic materials

2.1.1 Background of Segregation in asphaltic concrete

In asphaltic concrete pavements, segregation is said to occur in the finished mat when coarse aggregate materials are localized in some areas and fine aggregate materials in others. Higher air content and lower asphaltic content in coarse aggregate-rich regions can accelerate pavement distress, such as pothole formation and raveling, and these regions also tend to exhibit lower tensile strength and reduced fatigue life. In regions where the fines are concentrated, lower void and higher asphalt contents are typical. This can lead to a greater incidence of permanent deformation (i.e., “rutting”) and flushing. Thus, segregation is associated with reduced pavement performance. When segregation is identified in pavements, those sections may be replaced or reductions in contractor compensation may be made. Therefore, accurate and rapid assessment of pavement segregation is necessary for quality assurance.

2.1.2 Testing Methods for Defects in Asphaltic Concrete

In recent years, various destructive and nondestructive techniques have been applied to detect and evaluate defects in asphaltic concrete, such as ground penetrating radar (GPR) (Sebesta & Scullion, 2003; Stroup-Gardiner & Brown, 2000), infrared imaging (IR) (Sebesta & Scullion, 2003; Stroup-Gardiner, 2000; Stroup-Gardiner & Brown, 2000), nuclear density gages (NDG) (Stroup-Gardiner, 2000; Stroup-Gardiner & Brown, 2000), thermography (Stroup-Gardiner & Brown, 2000), and a lab-based technique, X-ray tomography (XRT) (Shashidhar, 1999). All these techniques have limitations and disadvantages in that they either require expensive equipment (all), have safety issues (NDG), or the results are not directly related to the mechanical properties of asphaltic concrete (GPR and X-rays). For example, X-rays and GPR provide optical images and dielectric constant maps, respectively, and not direct information concerning the material's mechanical properties; both require a large amount of data collection to construct an adequate image; and GPR requires knowledgeable personnel for data interpretation. Few ultrasonic/seismic methods have been used for detecting the defects in asphalt concrete (Kobori & Udagawa, 2001; J. Popovics et al., 2008; Ryden, Lowe, & Cawley, 2007; Tigdemir, Kalyoncuoglu, & Kalyoncuoglu, 2001) in spite of the advantages. The status of this research is still preliminary and it is primarily because of the lack of suitable sensors to implement the ultrasonic techniques to a real pavement system.

Traditionally, segregation has been identified visually by inspection of the pavement surface for non-uniformity. However, the subjectivity of this approach can lead to conflict between the inspector and the contractor. Alternatively, sand patch testing can

be performed by ASTM E 965. These measurements, while providing a quantifiable measure of surface texture not available by visual inspection alone, are restricted to the pavement surface, and, as a result, segregation that is not apparent at the surface will not be detected. Also, limits must be defined for pavements with varying surface texture. Recently, attempts have been made to use rolling density gauges (or "Nuclear Density Gages") to identify segregation from longitudinal profiles to measure the variation in pavement mat density. The technique, even with its associated health issues, has been used with mixed success, with Michigan DOT and Missouri Transportation and Highway Department researchers noting that gage measurements did not always detect segregation which was visually apparent. Kansas DOT has found that segregation can be reduced when using these gages on the job site, but noted that the test procedure can be time consuming. The Kansas DOT also noted that the accuracy of the gages seemed to depend on the mineralogy and gradation of the aggregate present. Most recently, thermography, infrared imaging (IR) and ground penetrating radar (GPR) have been used to assess segregation, but thermography cannot distinguish between gradation and temperature types of segregation, while the analysis of IR and GPR data requires a high degree of operator skill and interpretation.

2.1.3 Ultrasonic Rayleigh Surface Wave Techniques for Asphaltic Concrete

A large amount of research has already been performed on the generation of Rayleigh surface waves in metallic alloy and cement-based materials. Rayleigh surface waves have been used to characterize acoustic properties (attenuation and phase velocity) of Portland cement-based materials (Aggelis & Shiotania, 2007; Goueygou, Abrakam, & Lataste,

2008; Jacobs & Owino, 2000; Neuenschwander, Schmidt, Luthi, & Romer, 2006; Zhu & Popovics, 2005; Zhu & Popovics, 2007). It has been shown that, in general, the attenuation criteria are more sensitive and reliable than the velocity criteria to the existence of structural defects such as cracks.(Zhu & Popovics, 2005; Zhu & Popovics, 2007) Piwakowski et al. (Piwakowski, Fnine, Goueygou, & Buyle-Bodin, 2004) investigated techniques to launch Rayleigh surface waves in mortar and concrete. They examined the relative efficiencies between using different wedge materials and coupling materials and concluded that Teflon and a gel type agent are relatively better as wedge and coupling materials. Aggelis and Shiotani (Aggelis & Shiotania, 2007) experimentally studied the effect of simulated cracks in mortar samples on the wave speed and attenuation of longitudinal and surface waves, while Goueygou et al. (Goueygou et al., 2008) conducted a comparative study between two NDE techniques to assess damage (surface breaking cracks) in concrete structures and reported that the technique based on the ultrasonic surface waves is more sensitive than the electric resistivity measurement.

A fundamental understanding of the frequency dependent attenuation in these materials is, therefore, critical to enhance the application of this technology. However, there are few studies that are concerned with the *quantitative* determination of the absolute attenuation in a heterogeneous and viscoelastic material such as asphaltic concrete. Neuenschwander et al. (Neuenschwander et al., 2006) investigated the effects of sulfate interaction in mortar samples using leaky Rayleigh waves. Popovics et al. (J. S. Popovics, W.-J. Song, M. Ghandehari, et al., 2000) used Rayleigh surface waves to measure the depth of the surface crack in concrete. Dunning et al. (Dunning, Karakouzian, & Dunning, 2007) used the air-couple ultrasonic transducers to evaluate

air-void contents in hot-mix asphalt concrete blocks. Their measurements were done in a transmission mode in which two air-coupled transducers are sending and receiving longitudinal ultrasonic wave signals transmitted through an asphalt block.

References (J. Popovics et al., 2008; Ryden et al., 2007; Zhu & Popovics, 2005; Zhu & Popovics, 2007) use the air-coupled sensors for receiving the leaky Rayleigh waves while they use ultrasonic contact transducers or impact hammers for generating the Rayleigh waves. There is no reported research on the fully noncontact ultrasonic detection and characterization in an asphalt concrete pavement that was found in the literature review.

2.2 Crack depth determination in concrete

2.2.1 Background of Diffuse ultrasound in elastic solids

In the heterogeneous elastic body, random and multiphase media, acoustic wave cannot propagate in directions which do coincide with the incident wave after numerous scattering event caused by multiphase characteristics, especially in the case that scatterers are comparable to the wavelength of incident wave, which is usually the so-called diffuse or incoherent field. Also, there are two bulk wave mode conversions happened, different from fluid medium, thereby, complicating to extract reliable information without assumption.

Because of this complex physical phenomenon, especially in heterogeneous material, recently, diffusion approximation has been paid attention and utilized in elastic solids by adding additional dissipation term, which is negligible in fluid acoustics application, first by Weaver (Weaver, 1998) to characterize aluminum foam microstructure with varying pore size and distribution and polycrystal like heat treated

still at high frequencies(5-15Mhz) (Weaver, 1990a), after his basic theoretical background of diffusion theory for anisotropic and inhomogeneous bodies (Weaver, 1982).

In early 2000's, Anugonda et al.(Anugonda, Wiehn, & Turner, 2001) first extended the diffusion wave approach to real concrete materials and suggested theoretical predictions using ultrasound frequencies from 100 kHz to 900kHz with the diffusion parameters by a 1-D diffusion equation (Anugonda et al., 2001), In (Becker, Jacobs, & Qu, 2003), the diffuse method has successfully been applied to characterize the microstructure of cement-based materials by a 2-D diffusion theory(0.3-2Mhz), Punurai et al. (Punurai, Jarzynski, Qu, Kurtis, & Jacobs, 2007) employed the method to characterize dissipation in cement paste, while Ramamoorthy (Ramamoorthy, Kane, & Turner, 2004) used the diffuse method to detect large surface cracks and to quantify their depth. Additional theoretical studies were conducted through the use of the elastodynamic finite integration technique (EFIT) (Schubert & Koehler, 2004). The 2-D concrete beam was modeled by using aggregates and air-filled voids embedded in a homogeneous cement paste matrix. Deroo (Deroo, Kim, Qu, Sabra, & Jacobs, 2010) also extended this technique to application of monitoring ASR damage level by 2D and 3D cuboid model.

A systematic approach for modeling diffuse wave field caused by the multiple scattering process is to use the principle of conservation of energy in the form of the equation of radiative(energy) transfer and exploit statistical signal analysis methods to examine the scattered energy. In other word, The diffusion process is probabilistic, which treats only the statistical aspects of the flow of energy, the total energy is

conserved, and the equation that governs the energy flow is the diffusion equation with an additional term representing linear dissipation. In the diffusive field, it takes much longer that the time in which the stress wave propagating onto a solid body containing many scatterers goes into the diffusive field compared to the typical time between the randomizing scattering events of an ultrasonic wave. For example, the diffuse fields evolve on time scales on the order of hundreds of micro seconds. This time scale may be contrasted with the direct travel time across the specimens that may take only a few microseconds. The longer the energy remains in the specimens, the more information about the microstructure the propagating wave can gather.

2.2.2 Previous Testing methods for Determination of Crack Depth in Cement Concrete

Well-designed and constructed concrete bridge structures are inherently durable and are expected to be relatively maintenance free during many years of service. In contrast to the common perception that concrete is relatively inert, it is in fact a very complex material whose properties can change significantly with time. Some of these changes can be positive, such as long-term strength gain obtained through continued cement hydration. Other changes can be detrimental to the concrete, resulting in the development of premature surface breaking crack or material deterioration resulting from freeze and thaw cycle, alkali-aggregate reactivity (ASR), etc. Also it naturally influences the bridge's capability to carry traffic load and their failure over time, currently the monitoring of these defects is primarily conducted by visual inspection, with the disadvantage that no judgment can be made of how severe (deep) the cracks (defects)

into the materials. Hence it is inevitable to evaluate the depth, quality, strength and penetration of the surface breaking crack of existing concrete bridge over time, which will result in the need for testing equipment and cost effective techniques that can nondestructively collect data on existing bridges to determine their present condition, to predict the remaining life, and to establish effective maintenance and rehabilitation programs.

Recent research has focused on using nondestructive evaluation (NDE) methods to estimate the depth of a surface breaking crack using ultrasonic methods. However, established quantitative NDE methods that use ultrasound are difficult to apply to cement-based materials. The main issues are the scattering due to the presence of water and randomly distributed, multi-scale solid inclusions (e.g., hydration products, unhydrated cement, fine and coarse aggregate) and the very high attenuation due to their intrinsic viscosity, porosity (spanning 10-9 to 10-1m) and pre-existing microcracks (i.e., present prior to loading or environmental exposure). Clearly, using traditional ultrasound to detect damage such as cracks in concrete is exceedingly complex. Complicating these issues is the fact that traditional low frequency ultrasonic techniques have difficulty in differentiating between microstructural features (e.g., porosity and solid phases) and damage, because they all scatter the ultrasonic waves in somewhat similar ways. One manifestation of this material complexity is that ultrasonic signals in concrete can be severely distorted due to the multiple-scattering effect and the shape of an ultrasonic wave will change as it propagates through a concrete specimen. This introduces difficulties in accurately interpreting the signals and drawing parameters for a quantitative analysis on the damage status. Thus, to characterize surface breaking cracks

in concrete components, a variety of advanced ultrasonic NDE techniques are necessary. In this section, several NDE techniques used for crack damage assessment of concrete are discussed.

Impact echo

This method utilized transient stress waves (Carino, Sansalone, & Hsu, 1986) for nondestructive testing of concrete. A short duration mechanical impact (an impulse hammer) generates low frequency stress waves which are detected by the receivers at a distance. This method is applied for flaw detection in concrete structures such as circular columns (J. S. Popovics, Achenbach, & Song, 1999). The frequency range for these experiments varied from 0 to 100 kHz. A frequency of 100 kHz corresponds to a wavelength on the order of few centimeters in concrete. Though widely used, the method requires a highly skilled and experienced technician to interpret the recorded echo signals in the waveform, in both amplitude and frequency domains. The method was subsequently studied by researchers (J. S. Popovics, Song, Chandehari, Subramaniam, & Achenbach, 2000; Sansalone, Lin, & Streett, 1998) to study concrete cracks.

The pulse echo method

The pulse-echo method used to characterize flaws or inclusions in materials by detecting the echo of pulsed stress waves. The pulse-echo method carried through the impact echo developments with minor changes in technique. The method utilized ultrasonic transducers to generate the stress waves as compared with an impact by a metal ball in the impact echo method. The method tests concrete structures using low frequency waves

generated by the transducer. The frequency used in this process of testing varies between $0 - 200$ kHz (Carino et al., 1986). However, there exists a limit for the detectable size of flaws in this technique. (Mix, 2005). It may be a solution to increase the frequency of signal to get a smaller size resolution. But the production of high amplitude waves is difficult. Thus, the effectiveness of the pulse-echo method is reduced in comparison with time-of-flight and later evolved techniques.

Pulse-velocity Method (Time of flight method)

The pulse-velocity method refers to the measurement and comparison of phase velocity of a pulsed stress wave propagating a certain distance along defined samples (ASTM, 2009; Hevin, Abraham, Pedersen, & Campillo, 1998; Y. Lin & Su, 1996; Liu, Lee, Wu, & Kuo, 2001; Sansalone et al., 1998). The travel time is obtained by observation of the phase difference of incident signal and received signal, and thus the phase velocity can be calculated by the division of path length over the travel time. If there is a flaw or crack inside the material, the wave may be delayed and cause a decrease in the phase velocity. Several recent research papers purport to determine non-destructively the depth of surface breaking cracks in concrete using elastic stress wave time of flight (wave velocity) techniques (Bazant & Planas, 1998; Hevin et al., 1998; Sansalone et al., 1998). Time of flight techniques were also used to predict the influence of fluid filling in the crack volume (Sansalone et al., 1998). In these studies, the crack depth is determined if the velocity of wave propagation in the intact concrete is known and a particular wave path and wave pulse-crack interaction are assumed. The frequency range for these experiments varied from 0 to 100 kHz.

Surface wave method

Surface cracks in concrete have been characterized by surface wave method have been utilized to characterize and investigate surface cracks (J. S. Popovics, W.-J. Song, M. Chandehari, et al., 2000; Song, Popovics, Aldrin, & Shah, 2003) in the range of 0 to 70 kHz. The work on curved cracks commonly found in concrete structures was investigated using surface wave techniques (Sansalone et al., 1998). Surface wave methods have also been used to characterize the micro structural properties of concrete such as grain size, porosity of micro crack distribution (Owino & Jacobs, 1999). However, the penetration depth of surface waves is on the order of a wavelength. Hence methods that utilize surface waves are in general, insensitive to deeper cracks. To detect these surface breaking deeper cracks, low frequencies must be used. These can be difficult to generate with sufficient energy without damaging the surface.

Wave-energy transmission (WET) technique.

Wave energy transmission (WET) method has been developed by (J. S. Popovics, W.-J. Song, M. Ghandehari, et al., 2000; Shin, Zhu, Min, & Popovics, 2008; Song et al., 2003) and has been found to be sensitive to the existence of surface breaking cracks. The WET is a technique that is modified from the traditional TOF measurement setup, measures the energy of transmitted surface waves and relates the energy to the crack depth. This technique has been shown to be more robust than the traditional TOF technique. Since this technique uses relatively low frequency ultrasound (<70kHz), the best resolution of this technique is depth measurements up to plus/minus 5 cm. This indicates that the

ultrasonic measurement requires highly accurate devices, experience in data processing and/or an accumulated data base.

Limitation of previous NDE techniques in concrete

It has been shown that most of all NDE techniques used in characterization of defect or crack in concrete structure have their own limitation such as their sensitivity and repeatability, commonly resorting to the highly experienced technician or needing particular inference or information to correlate damage level existed in concrete; the measurable changes as a function of increasing damage are often too small to be considered reliable in many cases. Especially in attenuation measurement, the researchers (Suaris & Fernando, 1987) have reported that measurable changes were not achieved until after 50% of the fatigue limit and repeated accuracy in these types of measurement is difficult to achieve. Especially for the TOF method to measure surface breaking crack depth presented in (Hevin et al., 1998; Y. Lin & Su, 1996; Y. C. Lin, Liou, & Tsai, 1999; Sansalone et al., 1998), it does not always provide reasonable crack depth estimation in the case that crack tips are ill-shaped and crack is filled with dust and or water, also wave speed in intact concrete structure should be known previously. In addition, in the surface wave energy transmission (WET) method, it can be significantly malfunctioned by near field scattering effects (signal enhancement and oscillation in transmission coefficients) unless there is enough distance between sensor and crack; it is necessary to have at least larger than h/λ (ratio of crack depth to wavelength) >1.5 to minimize the near field effects (Kee & Zhu, 2011).

2.2.3 Ultrasonic Diffuse Wave Techniques for Concrete

It has been reported by previous researchers that diffuse ultrasound techniques have many advantages compared to the previous NDE methods. Most importantly, the diffuse fields can be examined at higher frequencies at which the previous NDE methods are impossible and wave fronts are destroyed, thus offering higher sensitivity to small scale damages or cracks as well as to deep scale cracks, which takes place in concrete such as ASR, freeze-thaw damage or interlocking cracks of shrinking or creep process. Also it is not necessary to determine the wave velocity and other wave propagation parameters (wave path, interaction with geometry of the slab). Especially compared to WET technique, the resolution (minimum distinguishable crack depth) can be much better than in the WET technique (theoretically 5-10 times better).

As compared to the traditional ultrasonic NDE techniques, the diffuse ultrasonic technique exploits a fundamentally different physical phenomenon of ultrasonic propagation in strongly inhomogeneous materials such as concrete, i.e. diffusion of ultrasonic energy (analogous to the thermal conduction in solids) (Page, Schriemer, Bailey, & Weitz, 1995; Sheng, 2006; Weaver, 1998; Zhang et al., 1999). These early discoveries in physics first proved theoretically and experimentally that diffuse approximation is reasonable in high frequencies in inhomogeneous media and these form the foundation of the present research project. Hereby, the goal is to achieve more reliable measurements of crack depth in concrete. However, as this method is model-based, it requires an analytical or numerical model in order to investigate the interaction of the diffuse ultrasonic field with a surface breaking crack and to characterize the depth

of the crack. The finite element method is an established method for this purpose and yields a simple and cost-effective approach to this problem.

The diffuse ultrasonic technique has proven to be applicable to concrete structures (Anugonda et al., 2001; Becker et al., 2003; Deroo et al., 2010; Punurai, Jarzynski, Qu, Kurtis, et al., 2007), where the changes in the microstructure of cement-based materials were investigated. Further, Deroo et al (Deroo et al., 2010) related the scattering parameters (diffusivity and dissipation) of the diffuse field to microstructural damage in cement-based materials which occurred due to alkali-silica reaction and thermal loading. It has been shown that with increasing microstructural damage, the diffusivity also decreased. The finite element method has been first introduced for the analysis of the interaction of a diffuse field with a surface breaking crack by Ramamoorthy et al. (Ramamoorthy et al., 2004). In their research, the influence of a vertical crack on the ultrasound diffusion was investigated using an own finite element implementation, in order to simulate crack depth measurements. Seher recently investigated the finite element simulation of the diffuse ultrasonic measurement (M. Seher, C.-W. In, J.-Y. Kim, K.E. Kurtis, & L.J. Jacobs, 2012) using a commercial FEA simulation package (ANSYS). In this investigation, variously different geometrical configurations of surface breaking cracks are numerically simulated to see how the diffuse ultrasound interacts with cracks in different geometries and the factors that limit the applicability of the diffuse ultrasonic technique. Simulated geometries include partially closed crack, non-vertical crack, two parallel cracks, and a crack with a rebar underneath. More recently, Quiviger et al. (Quiviger, Payan, Chaix, Garnier, & Salin, 2012) studied effect of the

presence and size of a macro-crack on ultrasonic diffusivity in concrete. Their results show that the overall diffusivity can be changed by the presence of a macro-crack.

Diffuse methods also allow an additional parameter to be accessed directly-ultrasonic dissipation. Attenuation of ultrasound is due to both scattering and dissipation. Typically the scattering process conserves energy, but dissipation results in actual energy loss from the propagating wave. Traditional ultrasonic attenuation measurements cannot distinguish between these two very different mechanisms. The attenuation measured by traditional measurements is really the combined effect of the scattering and dissipation. However, diffuse ultrasound methods are possible to measure this parameter directly.

Overall, the current trend in this research indicates that researchers started looking at the diffuse ultrasonic technique as a technique alternative to the traditional NDE technique for the crack depth measurement.

2.3 Monitoring Crack Condition under Self-healing process in concrete

2.3.1 Background of self healing in concrete

The phenomenon of autogeneous self healing in cement-based composite such as concrete has been known and paid attention for many years, first reported by Abrams (Abrams, 1925), and self sealing of uncracked material (Hearn, 1992; Hearn & Morley, 1997). It has been reported that some cracks in old concrete structures are sealed with white needlelike structure, suggesting that cement based materials could have the ability to self-seal its own cracks with chemical products by itself. Many researchers have put a lot of efforts to understand this self sealing phenomenon in concrete. It has been postulated that rainwater and carbon dioxide in air could aid cracks to be self sealed in

crack of concrete. Later, a number of researchers (Edvardsen, 1999; Reinhardt & Joos, 2003) have noted that water flow through cracked concrete have been gradually reduced with time and the most likely reasons of the decrease in flow with time is attributed to autogenous healing of cracks.

According to the reported literature, even while the individual finding may differ, trends within these studies are very clear. Firstly, self healing can occur in a variety of environmental conditions ranging from underwater to cyclic wet dry exposures. Secondly, adequate concentrations of certain critical chemical species are essential to exhibit self healing mechanisms; the formation of calcium carbonate, which is resulted from the reaction between unhydrated cement and carbon dioxide (CO_2) dissolved in water, also by chemical formation of precipitation of calcium hydroxide (Ter Heide, 2005).

- Formation of calcium carbonate or calcium hydroxide

  1) Calcium hydroxide is a reaction product of the hydration of concrete. Calcium hydroxide in the area of the crack can dissolve in the water inside the crack and precipitate at the crack surface:

$$Ca(OH)_2 \leftrightarrow Ca^{2+} + 2OH^-$$

  2) CO_3^{2-} comes from the CO_2containing water:

$$CO_2 + H_2O \leftrightarrow CO_3^{2-} + 2H^+$$

  3) Ca^{2+} is liberated from calcium hydroxide, dissolved from the cement paste:

$$Ca(OH)_2 \leftrightarrow Ca^{2+} + 2\ OH^-$$

4) To form calcium carbonate, the water in the crack has to contain dissolved carbon dioxide. The chemical reaction of the formation of calcium carbonate is as follows:

$$Ca^{2+} + CO_3^{2-} \leftrightarrow CaCO_3$$

Thirdly and potentially most importantly, the width of the concrete cracks has been found to be play a role and very critical for self healing to take place and the rate of healing depends on the initial effective crack widths because self healing is associated with the chemical formation within the cracks. For example, cracks with an initial effective width less than 50 microns reduce to 20 microns within 24 hours, and cracks with an initial effective width between 50 and 100 microns reduce to an effective width of 20 microns within seven days (Clear, 1985). Other studies show that cracks with initial effective widths of 200 microns after sufficiently long water exposure can completely seal after five to seven weeks (Edvardsen, 1996). In addition, mechanical blocking, obstruction of narrow crack areas with ultrafine materials, and swelling and rehydration of the hardened cement paste on the crack walls are shown to be main possible causes to self healing in concrete.

2.3.2 Self healing examination methods

In the published literature, a number of techniques have been used to detect self healing or quantify the extent of self healing in cement based materials. In this section, to develop a more comprehensive understanding of self healing in cement based material, the testing methods used in diagnosis of self healing process are overviewed and discussed. Usually,

transport and mechanical properties are examined to quantify degree of self healing in concrete.

Dynamic modulus measurement (resonant frequency measurement)

It provides a quick means to assess the presence of self healing. The material dynamic modulus measurement appears to be a particularly promising technique to monitor the extent and rate of autogeneous healing. It has been adapted to measure the extent and rate of self healing in cracked concrete (Yang, Lepech, & Li, 2005), when healing is seen as reduction in material damage. Jacobsen(Jacobsen & Sellevold, 1996) have recorded resonant frequency of concrete samples deteriorated to various degree and examine self healing could be the important factor that concrete have better frost durability in field than when submitting samples to freeze/thaw cycles in water. Also it is shown that Freeze/thaw led to substantial loss in resonance frequency and subsequent self healing gave a substantial recovery of the frequency. (Jacobsen, Marchand, & Homain, 1995; Jacobsen & Sellevold, 1996)

Uniaxial tension text

It is used to determine self healing of mechanical properties. To assess the quality of self healing in concrete, the magnitude of recovered mechanical properties were measured under uniaxial tensile loading. First, deliberate damage was introduced by tensioning a coupon specimen to predetermined strain levels followed by unloading. After exposure to a healing environment, the specimen is then reloaded in direct tension to analyze the recovery magnitude of tensile strength, stiffness and strain capacity in concrete. These

properties were then compared with those measured before damage (in the case of elastic stiffness) and with those after damage but before self healing.

Water permeability test

Water permeability test(Edvardsen, 1999; Jacobsen, Marchand, & Boisvert, 1996; Lepech & Li, 2005; Ramm & Biscoping, 1998; Reinhardt & Joos, 2003; Wang, Jansen, Shah, & Karr, 1997) is used to measure the transport property, permeability coefficient, of material either uncracked, cracked/damaged, or rehealed by examining the recovery of transport property through permeation. The extent of self healing is examined by monitoring the flow rate or quantity of water passing through the cracked specimens. The change in the coefficient of permeability of concrete with respect to time is used to measure the amount of self healing which has occurred. Typically, a gradual reduction in this coefficient is used to infer self healing taking place in the specimen. There are two type of experimental setup for water permeability test (a falling head test and a constant head test), which are both adapted by Wang et al. (Wang et al., 1997) A falling head test was used for specimens with a low permeability, while a constant head test was used for specimens (such as those with large crack width) with permeability too high to practically use the falling head test. The permeability test is typically used to examine self healing of a single crack although it can be applied to water permeability through multiple cracks.

Microscopic observation and analysis

The quality of healing is likely influenced by the type of self healing products formed inside the crack. Surface chemical analysis (XEDS) and environmental scanning electron

microscopy (ESEM) are used to analyze these chemical composition and morphology of the self healing product. These techniques are particularly useful in verifying the chemical makeup of self healing compounds, essential in identifying the chemical precursors to self healing and ensuring their presence within the composite. (Jacobsen et al., 1995)

Ultrasonic phase velocity (UPV) method

Ultrasonic pulse velocity (UPV) measurements have been used to assess the healing capacity of damaged specimens with crack. (Abded-Jawad & Haddad, 1992) it is reported that although UPV measurement can detect the occurrence of crack healing, this method cannot accurately determine the extent of crack healing. (Aldea, Song, Popovics, & Shah, 2000). Jacobsen et al.(Jacobsen & Sellevold, 1996)have reported that subsequent self healing after various freeze/thaw cycling can be monitored by Ultrasonic Pulse Velocity (UPV). It has been shown that UPV has been changed moderately in accordance with the stage of deterioration and also depends on how much the specimens were deteriorated (Jacobsen & Sellevold, 1996) mechanical properties. (M. Sahmaran, Keskin, Ozerkan, & Yaman, 2008) have researched using UPV method to investigate influence of fly ash on self healing process by measuring the rate of loss or increase UPV in concrete.

Stress Wave Energy Transmission Technique (WET)

Stress wave energy transmission technique(Aldea et al., 2000) was used to characterize the process of self healing and quantify the extent of healing in concrete. Based on the experimental observation, the signal transmission decreased with increasing initial crack

width and the signal transmission of cracked specimens increased with time after exposure to a healing environment. It has been demonstrated that ultrasonic signal transmission measurement, performed under laboratory conditions, is a very sensitive indicator of the presence of cracking damage in concrete (Sellick et al., 1998). Also, it is noted that signal transmission measurement is more sensitive to the extent of cracking in concrete than UPV measurement (Song, Popovics, & Achenbach, 1999). However, the practical application of signal transmission measurements in concrete has been restricted because of the disrupting effects of source, receiver, and coupling variability. In addition, this transmission measurement is unable to clearly distinguish among crack widths above 100um. (Aldea et al., 2000)

2.3.3 Ultrasonic Diffuse Wave Technique for Monitoring Self-Healing Process

As mentioned in previous chapter, diffuse ultrasonic techniques have demonstrated their capability to characterize microcracking and to measure the depth of large cracks in cement based materials. Deroo et al. (Deroo et al., 2010) quantified microcracking damage in concrete due to alkali silicate reaction (ASR) and thermal shock and by measuring ultrasonic diffusivity and dissipation. It has also been confirmed that diffusivity is sensitive to microcracking and microstructural behavior as also indicated in (Becker et al., 2003; Punurai, Jarzynski, Qu, Kurtis, et al., 2007; Schurr, Kim, Sabra, & Jacobs, 2011). Ramamoorthy et al. (Ramamoorthy et al., 2004), In et al. (In, Kim , Jacobs, & Kurtis, 2012), and Seher et al. (M. Seher et al., 2012) have numerically and experimentally shown that the diffuse ultrasonic technique can measure the depth of surface opening cracks using the arrival time of maximum energy (ATME).

In this research, assessment of the capabilities of the diffuse ultrasonic technique for quantifying the degree of self-healing of cracks in concrete will be conducted. The theory of ultrasonic diffusion in concrete and the diffuse ultrasonic measurements carried out on five different mix designs with two types of cracks will be described later. Then, The diffuse ultrasonic parameters from a two-dimensional (2-D) diffusion model are evaluated to characterize the self-healing process and microscopic measurements of crack width over a 120 day exposure period is compared to verify the sensitivity of the technique to crack healing.

CHAPTER 3

CHARACTERIZATION OF SEGREGATION IN ASPHALT CONCRETE

3.1 Technical Approach

This section briefly describes characteristics and composition of asphaltic concrete, physical principle of the Rayleigh wave, methodology to generate and detect the Rayleigh wave and ultrasonic measurement procedure and modeling of attenuation and scattering of the Rayleigh wave to characterize segregation in asphalt concrete.

3.1.1 Fundamental Physical Principle and Measurement Concept

In asphaltic concrete, which is commonly used for the construction of highway and airport pavements and is limited only to one side access in construction area or in service, the ultrasonic Rayleigh surface wave is regarded as possible solution to assess the pavement quality or characterize defects such as segregation or rutting in one side access limitation. It provides one good feature that a major portion of wave energy is confined in the surface area i.e. in the depth of one wavelength, and thus is highly sensitive to the material property changes and defect near the surface. For example, the Rayleigh wave in frequency range of 10 to 100 kHz can be used to investigate segregation both on the top and bottom of the asphalt pavement mat with penetration depth of 1.8 to 18cm. Physically, the Rayleigh surface wave amplitude gradually decays due to both dissipation effect by viscoelasiticity in the constituent materials (the asphalt binder and aggregate) and the scattering by aggregate in asphaltic concrete. Especially in

such a material, the scattering effect is more dominant than in Portland cement concrete because of the high aggregate volume fraction (80-85%). In addition, the Rayleigh wave can further attenuate if a volume of segregation exists in its wave path. This is because the segregation contains higher amount of air voids which will act as an additional source of scattering, and thus the scattering portion in the attenuation will increase; this increase is expected to be considerable in view of the typical amount of air voids in segregation (up to 15%).

This concept is schematically shown in Figure 3.1 Here, the attenuation of the Rayleigh wave amplitude in a non-segregated asphalt pavement is taken as a base-line reference and the attenuation in a suspected area is compared to this base-line attenuation to make a judgment regarding the existence of the segregation in that area. Note that due to the additional scattering effect of the segregation, the amplitude of the waves transmitted through the volume with segregation will be lower than the base-line reference and therefore, the attenuation coefficient of the segregation is higher than that of the non-segregated reference asphalt, as shown in Figure 3.2. A comparison between these two, that is, the increase in the attenuation, can also provide additional information about the overall size of the segregation in the area through which the Rayleigh surface waves are transmitted. While the detailed geometrical shape of segregation might be difficult to determine, the existence, location and size may be determined, provided that the measured Rayleigh wave signals are of high quality.

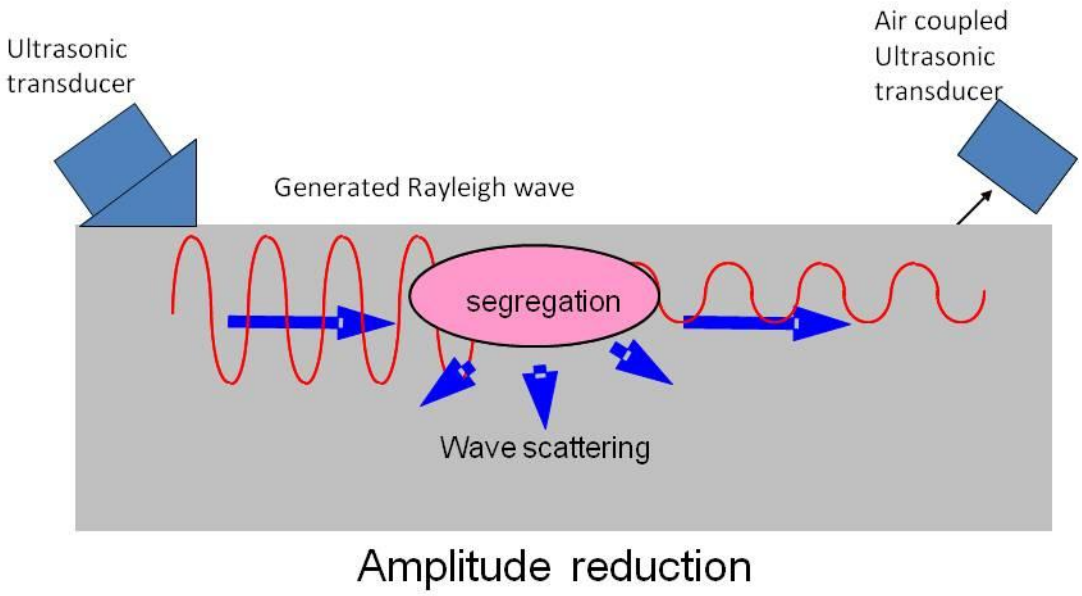

Figure 3.1 A schematic showing the measurement concept: Rayleigh surface waves generated by an ultrasonic wedge transducer are scattered by the segregation and their amplitude is reduced during this course. Rayleigh waves with reduced amplitude are detected by a non-contact ultrasonic transducer and received signals are analyzed to calculate the location and size of the segregation.

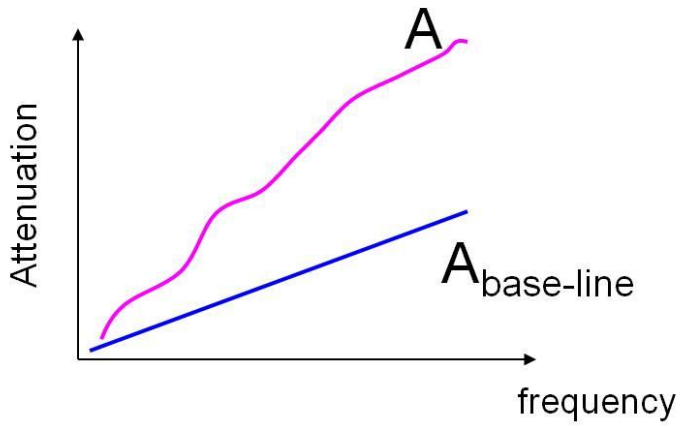

Figure 3.2 Attenuation coefficients from non-segregated asphalt (base-line) and segregated asphalt are shown. This difference is to be measured and will provide

information about the existence and size of the segregation in the area where the measurement are performed.

In general, the wave attenuation is frequency-dependent and is higher at higher frequencies. This attenuation is produced by the mismatch in material properties between the surrounding medium and the scattering object (segregation): $\Delta\rho = \rho_s - \rho_a$, $\Delta E = E_s - E_a$, $\Delta G = G_s - G_a$, where the subscripts *s* and *a* denote the segregation and the good asphalt, respectively, and ρ is the mass density, E the Young's modulus, and G the shear modulus. Therefore, given that the frequency-dependent attenuation coefficient, $\alpha(f)$, is accurately obtained, mechanical properties of the segregation can be established using a scattering model analysis and an inversion procedure. In order to quantitative measure of the severity of given segregation, the non-uniformity index (NUI) is defined as the sum of absolute normalized values of the differences in the mechanical properties:

$$NUI = \frac{1}{3}\left[\left|\frac{\Delta\rho}{\rho_a}\right| + \left|\frac{\Delta}{E_a}\right| + \left|\frac{\Delta}{G_a}\right|\right]. \tag{3.1}$$

so that the NUI of a non-segregated asphalt material is zero and that of a severely segregated material approaches. The entire procedure to determine segregation properties and location in asphaltic concrete is summarized in Figure 3.3

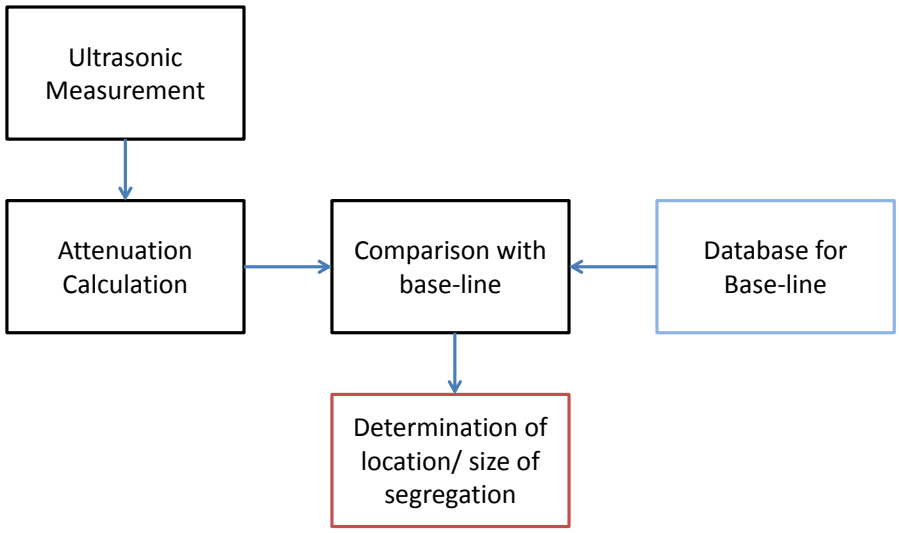

Figure 3.3 Procedure for the determination of segregation properties and location

3.1.2 Generation and Detection of Rayleigh Surface Waves

In this research, contact and noncontact method are considered to generate and detect the Rayleigh surface waves in an asphaltic concrete. The contact method has been widely used and shown to be most efficient to generate and detect the Rayleigh wave [Rose 1999]. In contact method, a wedge-shaped shoe is used to launch the Rayleigh wave into the material from a longitudinal wave generated by an ultrasonic transducer that is mounted on the inclined side of the wedge at Rayleigh critical angle and detect the Rayleigh wave from receiving. Recently, the noncontact ultrasonic method using transducer or microphone has given rise to an attention as a newly emerging NDE technique. In the noncontact method, technically, a very strong sound wave in the ultrasonic frequency range is generated in the air and directed toward the solid material, and the acoustic (sound) wave transmitted into the solid material propagates as a Rayleigh surface wave or other type of elastic wave, then leaky Rayleigh wave is detected from other receiving transducer or microphone.

The transducers used in this research are shown in Figure 3.4. Those in Figure 3.4(a) are the contact transducers (Ultran 100 kHz with a 50 mm diameter) and wedges (Teflon) and those in Figure 3.4(b) are the noncontact transducers (Ultran 100 kHz with a 50 mm diameter).

(a)

(b)

Figure 3.4 (a) contact transducers and wedge (b) air coupled ultrasonic transducers

3.1.3 Modeling Concept

Since the asphalt concrete is an inhomogeneous material consisting of various size of aggregate and asphalt binder, the modeling of attenuation and scattering of Rayleigh waves is not straightforward. In order to simplify this random variation in geometry and mechanical properties (inhomogeneities) of the microstructure in asphaltic concrete, effective medium is considered to obtain the gross or overall or average properties of the inhomogeneous material so that the average response of the materials can be predicted. Please refer to (Christensen, 1979) for this micromechanical approaches in detail.

Briefly speaking, it is assumed that inhomogeneous volume (the segregated asphalt concrete) is embedded in another inhomogeneous medium (the normal asphalt concrete). The mechanical properties of the original, non-segregated asphalt concrete may be written as $\rho(r)$, $E(r)$ and, $G(r)$ which are taken to be randomly varying as a function of space. Then it is treated as an effective medium whose properties (ρ_a, E_a, G_a) are homogeneous and constant in space. These imaginary effective properties are determined such that they contain all characteristics of the material that come from microstructural features. In the same way, the inhomogeneous properties of the segregation are replaced with homogeneous effective properties (ρ_s, E_s, G_s).

Figure 3.5(a) shows schematically the homogenization concept and Figure 3.5(b) shows how the complex original problem is simplified through this homogenization procedure. Finally, the simplified problem poses itself as a wave scattering by a localized inhomogeneity in a homogeneous uniform medium. In the model work in the following sections, this homogenized asphalt pavement model is used.

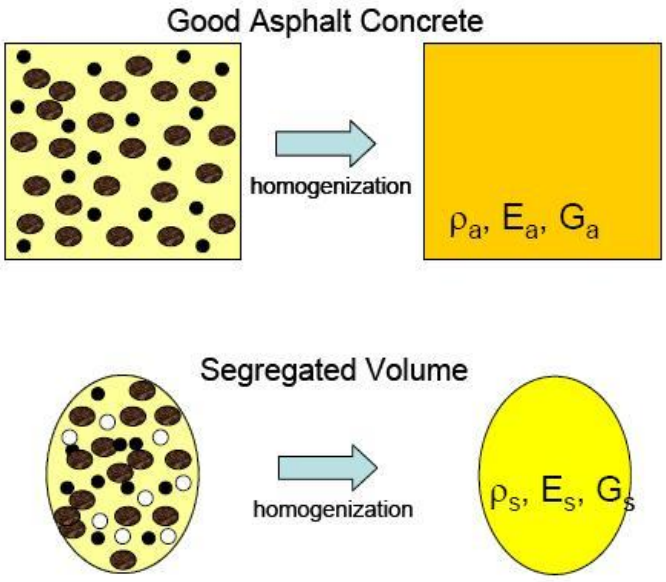

(a)

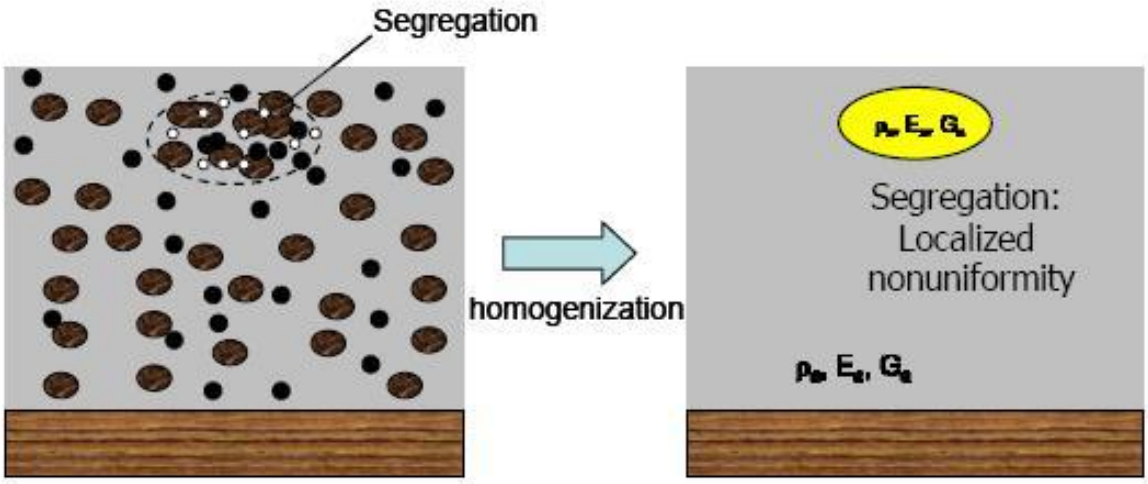

(b)

Figure 3.5 Homogenization of (a) surrounding medium and segregation and (b) the whole asphalt pavement layer.

3.2 Development of ultrasonic measurement setups and procedures

This section provides preliminary measurement for the material properties of asphaltic concrete measured at an ultrasonic frequency and wedge design to generate and detect ultrasonic Rayleigh surface wave for an ultrasonic measurement system and diffraction correction required to calculate absolute attenuation at frequency range from 10 to 150 kHz for three different configuration setups. Based on experiment setups, preliminary results are discussed.

3.2.1 Preliminary Measurements

Asphaltic concrete is heterogeneous material consisting of an asphalt cement matrix as a binder and mineral aggregate (the mineral filler, fine and coarse aggregate) that are mixed together, heated, placed, and compacted. The typical composition of asphaltic concrete by mass is approximately 95% aggregates and 5% asphalt binder. By volume, the composition is approximately 80-85% aggregates, 9-17% asphalt binder, and 3-6% air. Note that the asphalt cement matrix is a highly viscoelastic material, and is much more viscoelastic than the cement matrix used in Portland cement concrete. Also, note that the viscoelastic behavior of the asphalt is also variable with temperature, aging and load duration; Asphalt tends to behave in an elastic fashion at lower temperatures, under rapid loading, or when the material has aged, while viscous behavior dominates at higher temperatures, under long-term loading, and in unaged asphalt.

A set of preliminary measurements is performed on a typical asphaltic concrete specimen to obtain a set of ultrasonic characteristics of asphaltic concrete with no segregation at ambient temperature. First, the longitudinal and Rayleigh wave speeds are

measured on a typical asphaltic concrete specimen, and those are used to determine the overall materials properties of asphaltic concrete (all at 100 kHz). Table 3.1 shows the mechanical properties and the shear wave speed of this typical asphaltic concrete specimen determined from the measured wave speeds. The through transmission method combined with spectral analysis (Sachse & pao, 1978) is used to measure the longitudinal wave attenuation in a frequency range from 50-600 kHz (punurai, Jarzynski, Qu, Kim, et al., 2007; Punurai, Jarzynski, Qu, Kurtis, & Jacobs, 2006). The measured attenuation coefficients are presented in Figure 3.6 along with a comparison to Portland cement paste (punurai, Jarzynski, Qu, Kim, et al., 2007; Punurai et al., 2006). Note that the Portland cement paste results are only included for comparison purposes. Figure 3.6 shows the high attenuation in asphaltic concrete, approximately two times higher than the Portland cement paste, which illustrates its highly heterogeneous and viscolelastic nature of asphaltic concrete. The results in Figure 4.6 are used to determine an operational frequency range of 40-100 kHz, and also for the wedge design discussed in the next section. The predicted Poisson's ratio, 0.32, is in the range of typical asphalt concrete, 0.3-0.35 (Huang, 1993).

Longitudinal wave speed	**3750m/s**
Rayleigh wave speed	**1800m/s**
Shear wave speed	**1890m/s***
Density	**2414kg/m^3**
Elastic Modulus	**22.7GPa***
Shear Modulus	**8.6GPa***
Poisson ratio	**0.32***

* Calculated values from measured wave speed and density

Table 3.1 Material properties of asphalt concrete puck measured at 100 kHz

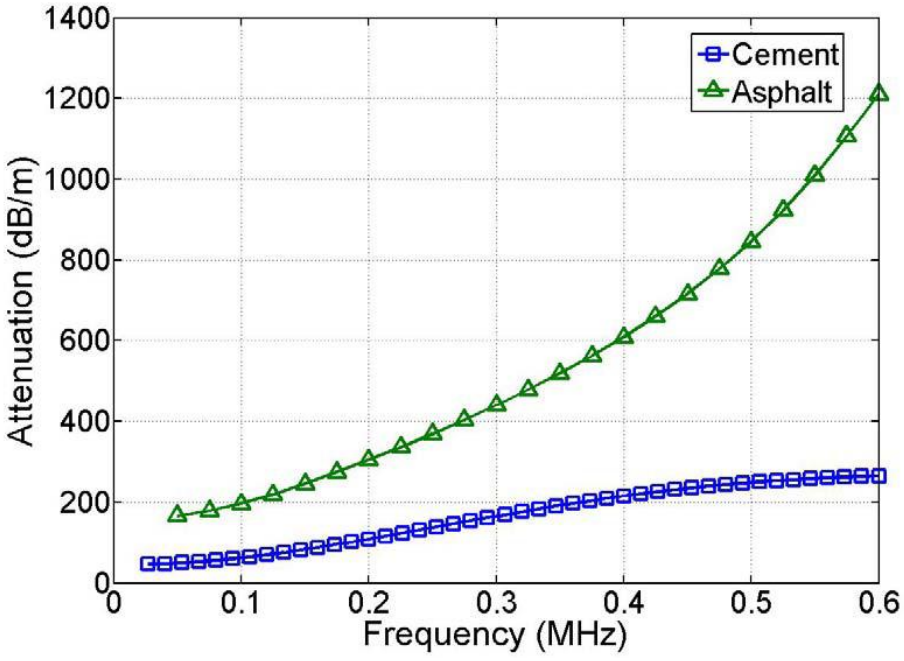

Figure 3.6 Longitudinal wave attenuation in Portland cement paste and asphalt concrete

3.2.2 Wedge Design

This section describes precisely how the wedge is designed and manufactured. Extensive research has been done on the efficient generation of Rayleigh surface waves in metals, composites and cement-based materials. Rose (Rose, 1999) provides a brief summary of techniques including an angle beam transducer (wedge), a periodic array or comb transducer, a laser source and a mechanical hammer. The frequency bandwidth from a laser source is too high for a heterogeneous and viscoelastic medium such as asphaltic concrete, and a mechanical hammer (or steel ball) can be inconsistent and unreliable for quantitative NDE. As a result, this research will employ the wedge technique to generate Rayleigh surface waves in asphaltic concrete.

A wedge is used to create longitudinal waves that are incident to the lower half space (the asphaltic concrete in this case) at the Rayleigh critical angle such that the incident longitudinal waves are mode-converted to Rayleigh surface waves. Based on the asphaltic concrete's material properties, Teflon is selected for the wedge material as in (Ryden et al., 2007); the longitudinal wave speed in Teflon is very low (1350m/s) which is sufficiently slower than the Rayleigh surface wave speed (1800m/s) in asphaltic concrete, so that the wave path in the wedge is minimized. From Snell's law (Viktorov, 1967), the critical angle of the wedge is given by

$$\theta = \sin^{-1}\left(\frac{C_{LW}}{C_R}\right) \tag{3.2}$$

where C_{LW} is the longitudinal wave speed in Teflon and C_R is the Rayleigh wave speed in asphaltic concrete as shown in Figure 3.7.

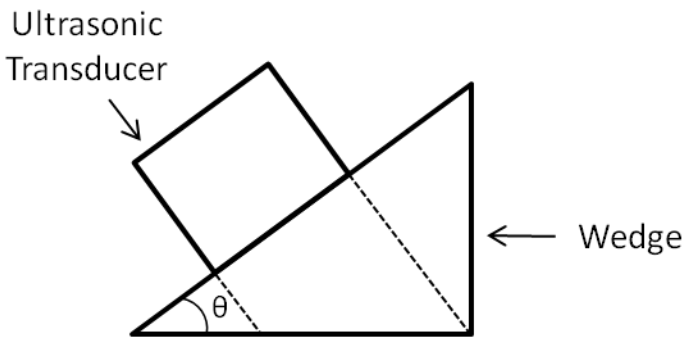

Figure 3.7 Wedge and the ultrasonic transducer mounted on the wedge.

In general, it is extremely difficult to exclusively generate only Rayleigh surface waves because the generating transducer has a finite-size aperture and does not produce a perfect plane wave; the incident beam spreads some as it propagates in the wedge so that the entire incident longitudinal wave front does not hit the specimen surface exactly at the Rayleigh critical angle. Although the Rayleigh surface wave will carry most of the incident wave energy, this spreading effect will cause bulk waves to be generated in the specimen. To decrease this effect, the propagation distance in the wedge material should be as short as possible, so the wedge shape is designed such that a ray from the transducer's upper edge will hit the leading edge of the wedge (Viktorov, 1967)**.**

3.2.3 Diffraction Correction for Rayleigh Surface Waves

These beam spreading (diffraction) effects can cause large errors in attenuation measurements, unless they are accounted for. Therefore, it is necessary to separate the diffraction effects from the measured attenuation and to isolate only the material attenuation contribution. Correction for (or removal of) the diffraction effects can be

done numerically by calculating the output of a simple transducer shape (Rogers & Van Buren, 1974).

As described in the next section, this research considers three different transducer arrangements – wedge transducers for both generation and detection, a wedge transducer to generate (transmitter) and a point microphone receiver, and wedge transducer generation and an air-coupled ultrasonic receiver. Following (Alberto Ruiz & Nagy, 2002), an apodized surface wave displacement distribution is generated by the elliptical footprint of the circular piston on the surface. By modifying the model in (Alberto Ruiz & Nagy, 2002), an approximate diffraction model for the wedge transmitter and wedge and air-coupled receivers is proposed in the following form, using a cosine displacement distribution as an apodization function for both the transmitting and receiving wedge transducers.

$$D_R(\varsigma) = \sqrt{\frac{s}{2\pi i}}\,\frac{1}{2}\int_{-1}^{1}\cos\left(\xi\frac{\pi}{2}\right)d\xi\int_{-1}^{1}\cos\left(\xi'\frac{\pi}{2}\right)\times\frac{e^{is\left(\sqrt{(\xi-\xi')^2+\varsigma^2}-\varsigma\right)}}{\sqrt[4]{(\xi-\xi')^2+\varsigma^2}}\,d\xi' \tag{3.3}$$

where $\varsigma = z/a$, $\xi = x/a$, $\xi' = x'/a$, $s = ak$ is the normalized frequency, a is approximately the radius of the transducer. Here, z is the axis of wave propagation and x is the axis perpendicular to the z-axis, referring to Figure 3.8. Note that Equation (3.3) is easily obtained by including a cosine distribution function in the receiver integral of Eq. (14) in [Alberto and Nagy 2002].

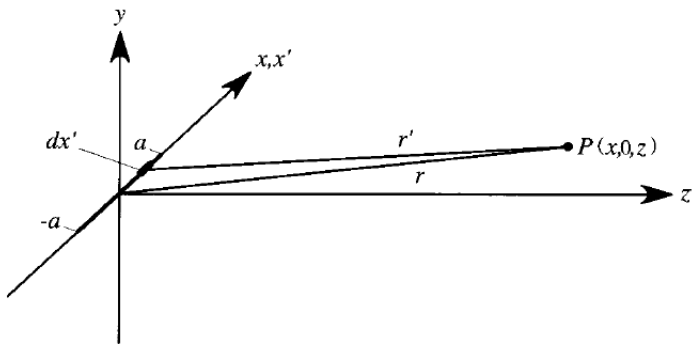

Figure 3.8 Coordinate system used to calculate the ultrasonic field of a line source on the free surface of an elastic half-surface.

In a similar fashion, an apodized model for the wedge transmitter and a point receiver is proposed as

$$D_R(\varsigma) = \sqrt{\frac{s}{2\pi i}} \int_{-1}^{1} \cos\left(\xi' \frac{\pi}{2}\right) \times \frac{e^{\left(\sqrt{(\xi')^2+\varsigma^2}-\varsigma\right)}}{\sqrt[4]{(\xi')^2+\varsigma^2}} d\xi' \tag{3.4}$$

Note that the microphone is assumed to be a point receiver so the apodization function in the first integral in Eq. (3.3) becomes a delta function, $\delta(\xi)$. Figures 3.9 (a) and (b) show the calculated normalized diffraction corrections versus frequency for a Rayleigh surface wave generated and detected by both a pair of wedge transducers (50 mm diameter), and for wedge generation (50 mm diameter) and microphone detection (point), with separation distances of 60 and 80 mm, respectively. The distance from the center of the elliptic footprint to the leading edge of the wedge is 30 mm. This distance is considered to be part of the Rayleigh wave propagation distance, and must be accounted for in the propagation distance calculations. Therefore, separation distances of 60 and 80 mm

correspond to propagation distances of 120 and 140 mm when both the transmitter and receiver are wedge transducers.

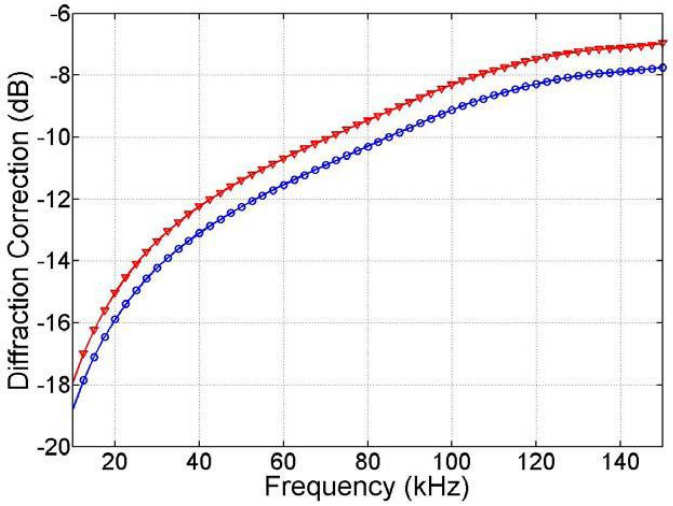

(a)

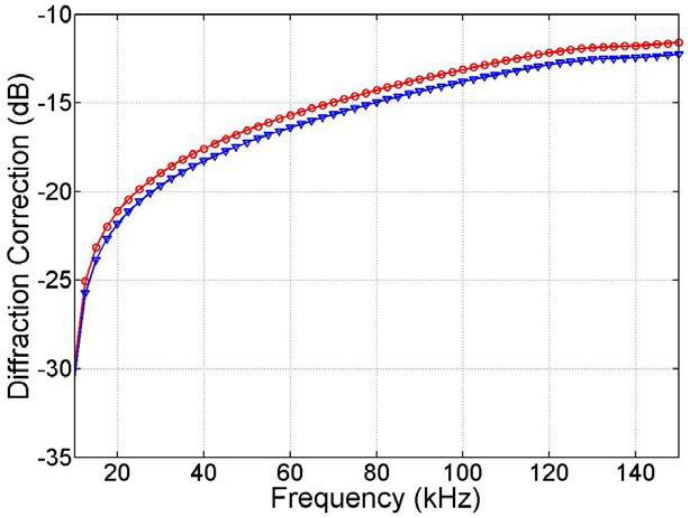

(b)

Figure 3.9 The calculated normalized diffraction corrections versus frequency for surface wave by a pair of wedge transducers (a) in 120 mm and 140 mm propagation distance in asphalt concrete and by wedge and microphone (b) with 50 mm diameter in 90 mm and 110 mm propagation distance.

3.2.4 Experimental Setups

Figure 3.10 shows the experimental setup that consists of a pulser/receiver (Panametrics 5072PR) for generating an electrical pulse signal, a transmitting transducer , a receiving transducer, an oscilloscope, and a computer for post signal processing and data analyses. In this research, four different measurement setups have been developed and evaluated. The first setup uses the contact transducer for both generation and detection, the second and third ones use the contact transducer for generation and the noncontact transducer (air-couple transducer and microphone) for detection, and the fourth one uses the air-coupled transducer for both generation and detection of the Rayleigh wave in the asphalt concrete samples.

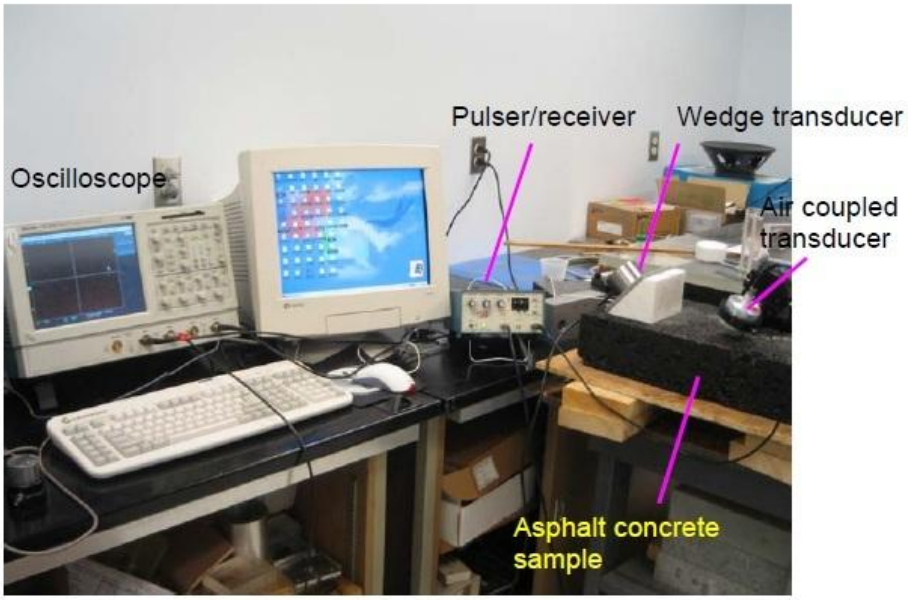

Figure 3.10 the experimental setup.

3.2.4.1 Setup #1: Wedge transmitter and wedge receiver

In the setup #1, both the transmitting and receiving sensors are wedge transducers as shown in Figure 3.11.this setup includes a pulser-receiver (Panametric 5072PR), a pair of contact transducers (Ultran-GRD100-D50, 100kHz) on wedges, a digital oscilloscope and a personal computer. The temperature of the specimen in all measurements is stabilized at 22ºC within ±1ºC in order to assure the accuracy of the attenuation measurements. Note that the absorption rate in the asphalt matrix is sensitive to changes in temperature. The critical angle to generate Rayleigh surface waves in asphaltic concrete is found to be around 49º with a Teflon wedge from Snell's law. Vacuum grease is used as the couplant, and Rayleigh surface waves are detected with a second wedge receiver at different propagation distances of $z_1, z_2, ..., z_n$. Signal averaging (over 1000 signals) is used to improve the signal-to-noise ratio (SNR), the sampling rate is 125 Mega-samples/second, and a Hann (Hanning) window with a low pass filter (500 kHz) is used.

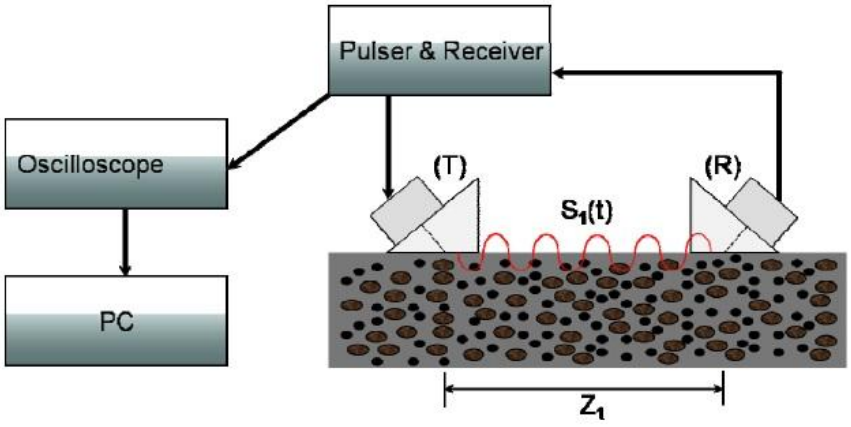

*Propagation distance (z_1) is the distance between the centers of elliptic footprints

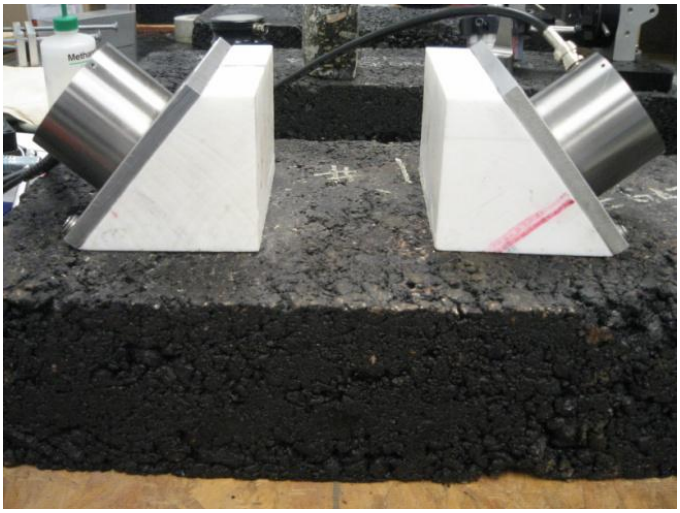

Figure 3.11 Setup # 1: Wedge to Wedge measurement

Two typical measured time-domain Rayleigh surface signals with propagation distances of 120 and 140 mm, their Hanning-windowed segments, and their frequency spectra are shown in Figure 3.12. While there are some longitudinal wave contributions with small amplitudes running in front of the Rayleigh surface wave, it is clear that most of the energy is carried in the Rayleigh surface wave. It is noted that there is also some signal reflected from the back of the transducer (a characteristic of a narrow band ultrasonic transducer at low frequencies) following the major signal portion, which also makes it difficult to isolate a single wave packet of Rayleigh surface waves.

The spectral ratio analysis (Sachse & pao, 1978) is used to determine the attenuation and phase velocity from the measured time-domain Rayleigh surface wave signals; spectral analysis compares the amplitude and phase spectra of two time-domain signals which have traveled along two different propagation paths in the same specimen. In brief, denote the input and output signals as $S_0(f)$ (source spectrum at z=0) and

$S_i(f)$ (spectra of each signal propagating the distance between the two transducers) and a transfer function as $H(f)$. The transfer function $H(f)$ can be presented as

$$S_i(f) = S_0(f)H(f) \tag{3.5}$$

$$H(f) = D_R(z)e^{-\alpha(f)z}e^{i(\omega t - \kappa(f)z + \phi_0)} \tag{3.6}$$

where *z* is the total distance traveled by the signal and $\alpha(f)$ is the attenuation coefficient, Φ_0 is the initial phase angle and $D_R(z)$ is the Rayleigh wave diffraction correction term in Equation (4.3). The distance traveled by the wave from the transmitter to the receiver can be presented as

$$z = 2z_{wedge} + 2\left(z_{couplingmaterial}\right) + z_{Rayleighwavepropagation} \tag{3.7}$$

Thus, the corresponding expressions for the attenuation and the phase velocity can be expressed as

$$\alpha(f) = \frac{\ln\left(\frac{S(z_1)}{S(z_2)}\right) - \ln\left(\frac{D_R(z_1)}{D_R(z_2)}\right)}{z_2 - z_1} \tag{3.8}$$

$$v(f) = \frac{2\pi f\left(z_2 - z_1\right)}{\arg\left(\frac{S_1}{S_2}\right)} \tag{3.9}$$

where "arg" designates the argument of the complex number. In this signal processing, the same time frame (*t=0*) is used for the first and second signals; there is no other source of phase shift in addition to that due to the propagation, that is, $\arg\left(\frac{S_1}{S_2}\right)$.

The diffraction correction is made only for the Rayleigh wave propagation and thus for the distance between the center of the elliptic projection areas under the wedges. It should be noted that this is not exact, and the diffraction effects in the wedges should also be taken into account. For example, for a distance z_1 the total diffraction correction would be $D(z_1) = D_L^{TW}(z_w) D_R(z_w; z_1) D_L^{RW}(z_w; z_1; z_w)$, where the superscripts TW and RW denote the transmitting and receiving wedges, z_w is the propagation distance in the wedge, the subscripts L and R denotes longitudinal and Rayleigh waves. In a similar way, the total diffraction correction for another distance z_2 will be $D(z_2) = D_L^{TW}(z_w) D_R(z_w; z_2) D_L^{RW}(z_w; z_2; z_w)$. First, the diffraction correction for the longitudinal wave in the transmitting wedge (the first term) remain equal regardless of the Rayleigh wave propagation distance, and thus does not need to be considered. The diffraction corrections for the receiving wedge will be different because the apertures of the incoming waves at the two different locations are different, so they should be taken into account. However, in the experiment that is presented in the next section, the Rayleigh wave propagation distances z_1 and z_2 (120 mm and 140 mm) are large enough so that the wave-front will be quite flat. Moreover, the difference between the two propagation distances is only 20 mm, which introduces a small change in the diffraction effect. Therefore, it is assumed that $D_L^{RW}(z_w; z_1; z_w) / D_L^{RW}(z_w; z_2; z_w) \approx 1.$, that is, the diffraction effects in the wedge at two different propagation distances in the far-field will be approximately the same.

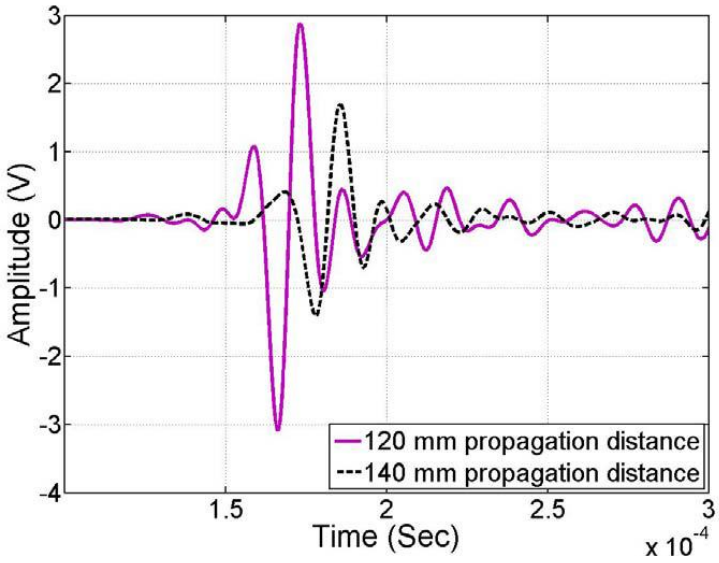
Amplitude (V)
Time (Sec)
x 10^-4
120 mm propagation distance
140 mm propagation distance

(a)

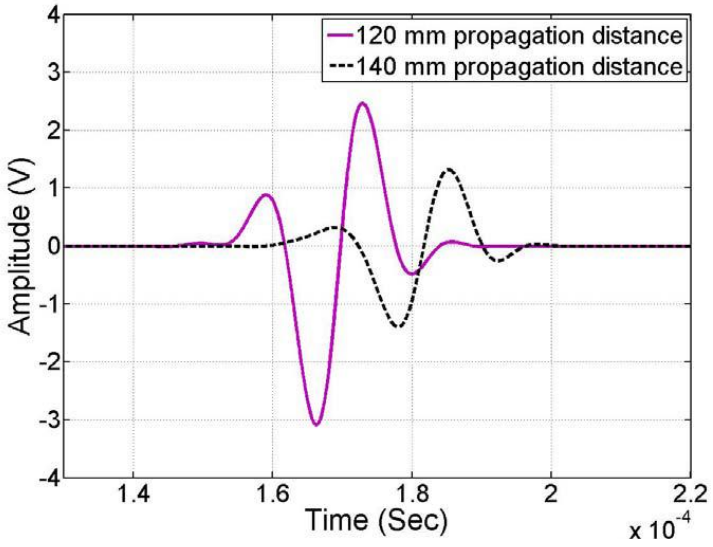
Amplitude (V)
Time (Sec)
x 10^-4
120 mm propagation distance
140 mm propagation distance

(b)

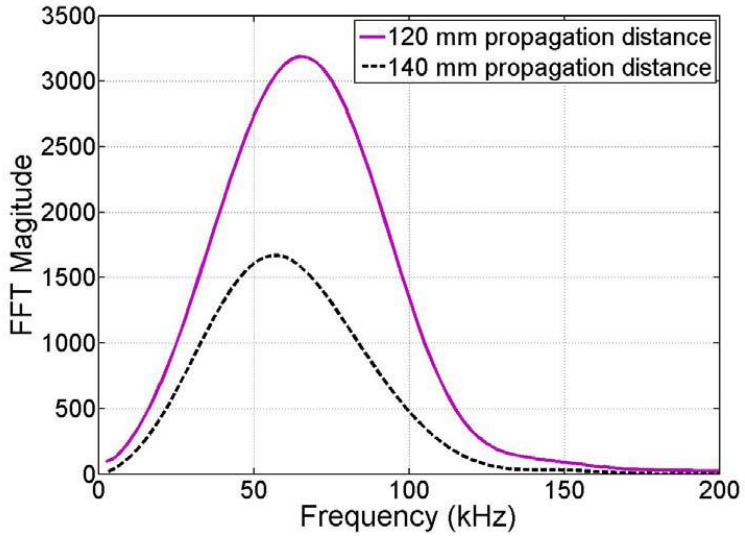

(c)

Figure 3.12 (a) Received original signal with wedge receiver obtained at two propagation distances (120 mm and 140 mm) (b) example of received, Hann windowed signals shown in (a) and (c) spectra of signals shown in (b).

3.2.4.2 Setup #2: wedge transmitter and microphone receiver

Setup #2 is similar to setup #1 except that the receiver is now a point, non-contact microphone (G.R.A.S. 40BE prepolarized free-field condenser microphone) that has a frequency range from 10-100 kHz. This setup measures the leaky Rayleigh surface waves instead of the pure Rayleigh surface waves. The critical angle for the microphone to detect these leaky Rayleigh waves determined from the Snell's law is 11º as shown in Figure 3.13. The lift-off distance (from the specimen) is 1 mm. Figure 3.14 shows two typical measured time-domain Rayleigh surface wave signals with propagation distances of 90 and 110 mm, their Hanning-windowed segments, and their frequency spectra. The spectral analysis technique is again used to determine the attenuation coefficient and

phase velocity and the diffraction correction Equation (3.4) is now used in Equations (3.6) and (3.8). Since the propagation distance from the specimen to the microphone is small and the wave speed in the air is much lower, the diffraction effect for this air path is neglected.

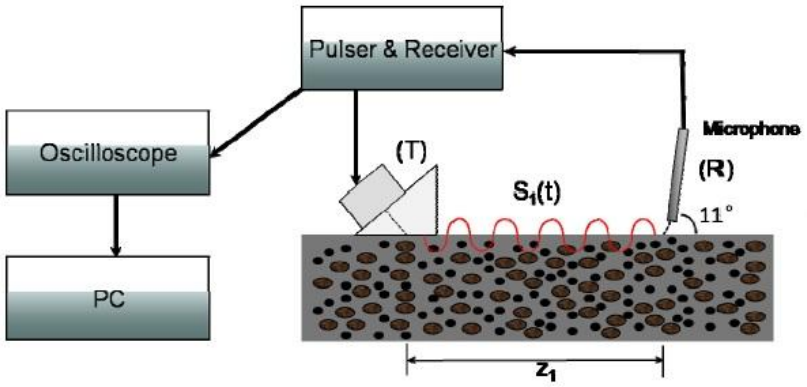

*Propagation distance is the distance between the center of the elliptic footprint and the tip of the microphone

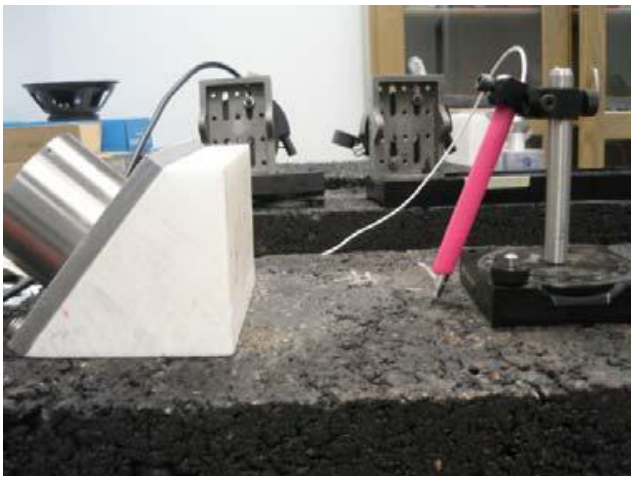

Figure 3.13. Setup #2: Wedge to microphone measurement.

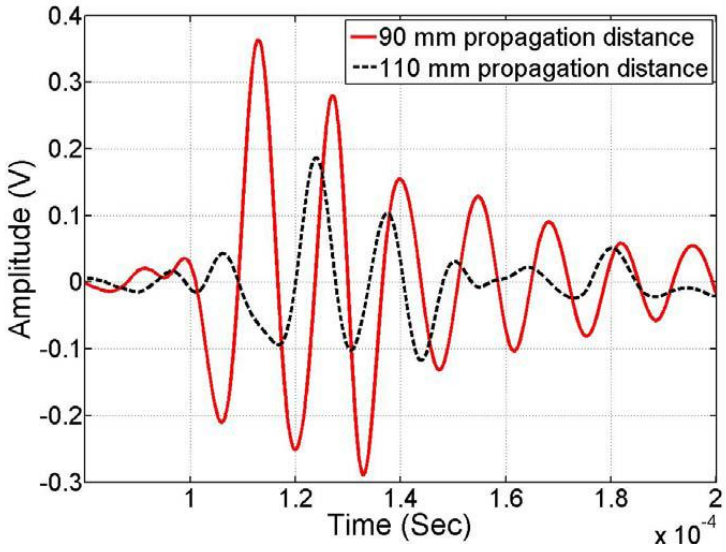
90 mm propagation distance
110 mm propagation distance
Amplitude (V)
Time (Sec)
x 10^-4

(a)

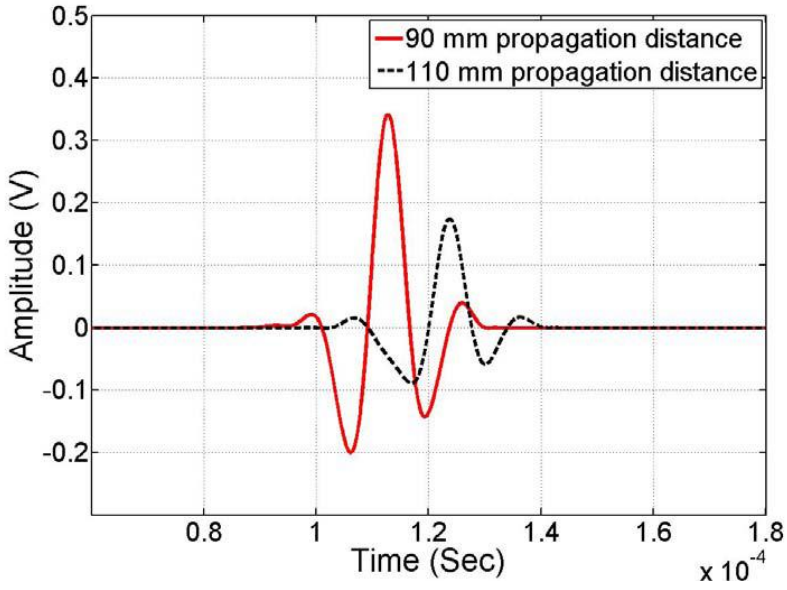
90 mm propagation distance
110 mm propagation distance
Amplitude (V)
Time (Sec)
x 10^-4

(b)

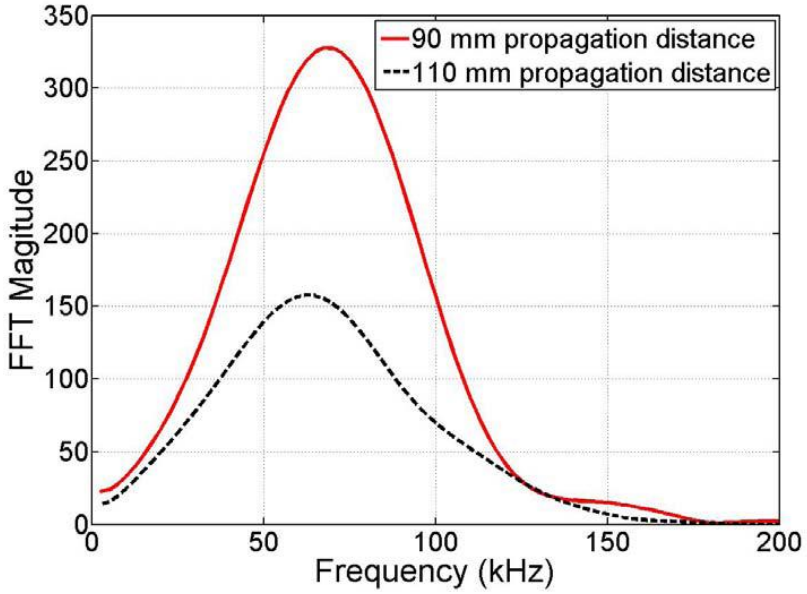

(c)

Figure 3.14 (a) received original signal with microphone obtained at two propagation distances (90 mm and 110 mm) (b) example of received, Hann windowed signals shown in (a) and (c) spectra of signals shown in (b).

3.2.4.3 Setup #3: wedge transmitter and air-coupled ultrasonic receiver

Setup #3 is identical to the setup #2 except the receiver is now a non-contact, air-coupled ultrasonic transducer (Ultran 100 kHz with a 50 mm diameter). This setup also measures the leaky Rayleigh surface waves at a critical angle of 11º as with the microphone. Figure 3.15 shows two typical measured time-domain Rayleigh surface wave signals with propagation distances of 90 and 110 mm, their Hanning-windowed segments, and their frequency spectra. The diffraction correction Equation (3.3) is now used in Equations (3.6) and (3.8). As in the setup #2, the diffraction effect in the air path is neglected. The time-domain signals shown in Figures 3.12, 3.14, and 3.15 look quite different. This is because the frequency spectrum of the received signal is modified by

the frequency characteristics (magnitude and phase) of the receiving transducer. Note that the three receiving transducers used in this research have different transduction principles and materials, which is the reason for the different transducer time and frequency characteristics.

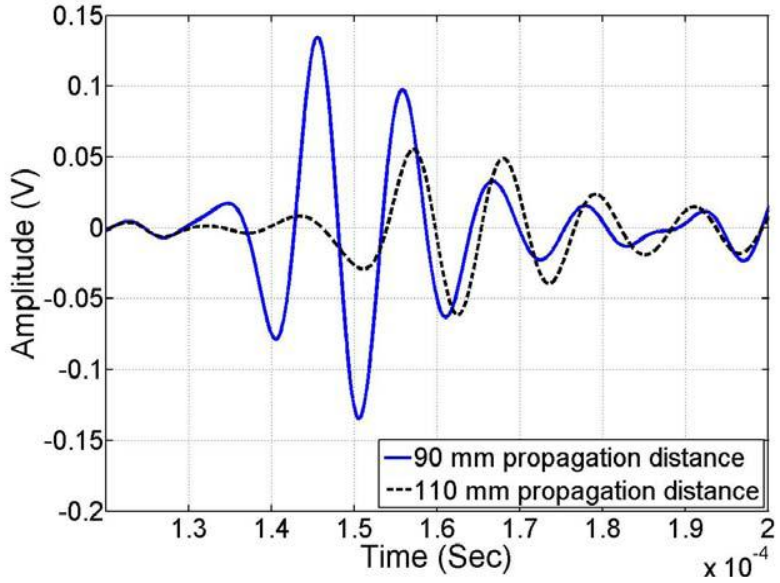

(a)

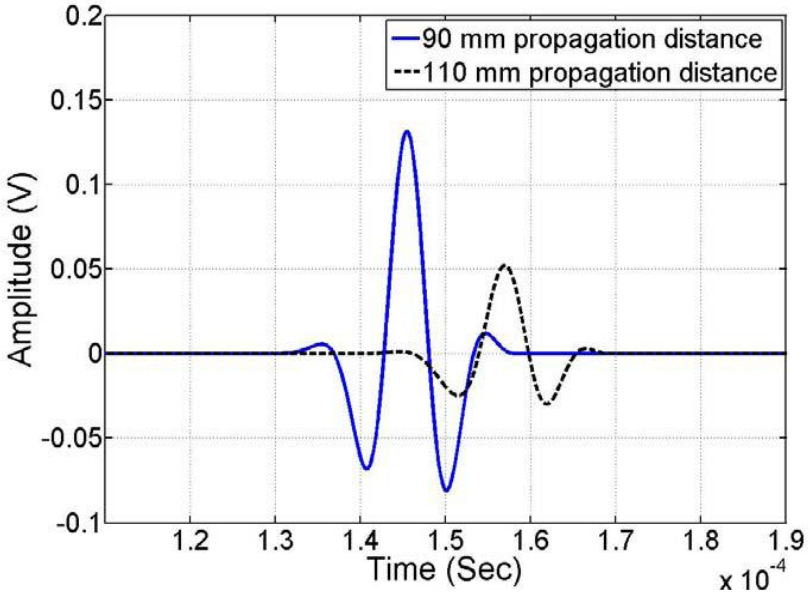

(b)

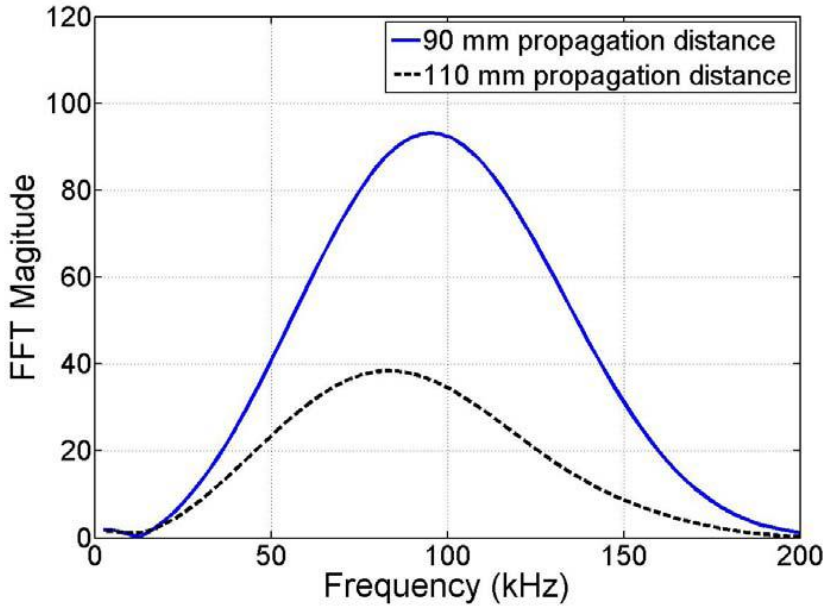

(c)

Figure 3.15 (a) received original signal with air coupled sensor obtained at two propagation distances (90 mm and 110 mm) (b) example of received, Hann windowed signals shown in (a) and (c) spectra of signals shown in (b).

3.2.4.4 Setup #4: fully noncontact (air-coupled) ultrasonic method

Setup #4 is identical to setup #3 except the transmitter is now an air-coupled ultrasonic transducer (100 kHz nominal center frequency with a 50 mm diameter) so that this setup excites and detects the Rayleigh surface waves in a fully noncontact manner. The excitation and reception angle is 11º as explained in Section 3.2.4.3.

Unlike setups #1-#3, this setup has an issue of relatively weak excitation (large impedance mismatch between air and asphaltic concrete) and accordingly difficult detection of ultrasonic signals (high attenuation due to viscoelastic characteristics of asphaltic concrete). To ensure Rayleigh waves are generated and detected in a fully non-

contact fashion. First, the setup is applied to a 1.5” thick Plexiglas plate as shown in Figure 3.16. Figure 3.17 shows the ultrasonic signal. As expected, most of Rayleigh wave energy is reflected at the boundary between air and asphaltic concrete. Note that energy reflection ratio at these material interfaces is 0.9996 so that less than one percent of longitudinal wave is mode converted into Plexiglas. A wave packet is observed exactly at the expected arrival time of the Rayleigh wave in the obtained ultrasonic signal as shown in Figure 3.17.

Figure 3.16 noncontact experimental setup in a 1.5” thick Plexiglas plate.

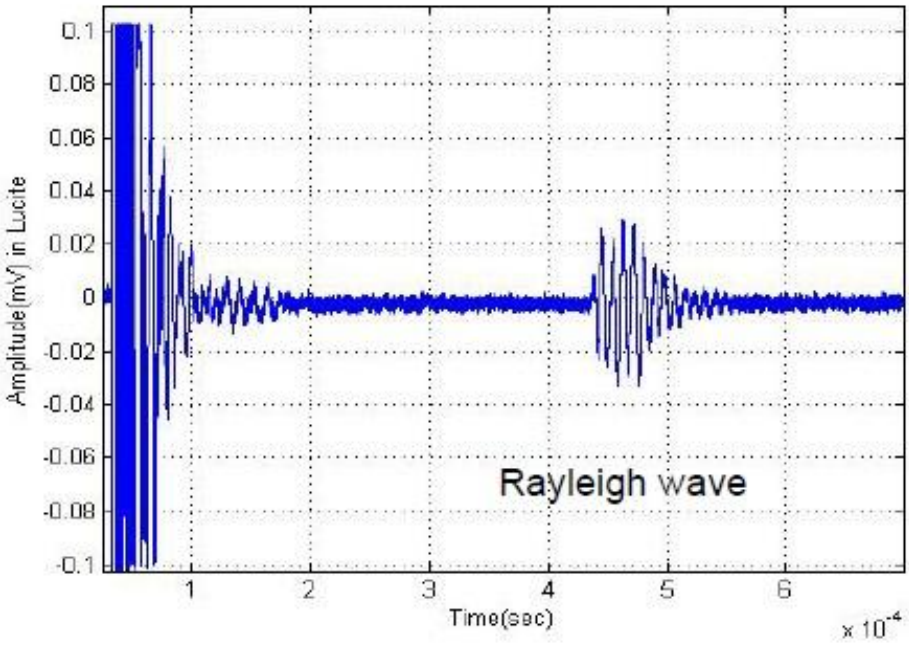

Figure 3.17 Detected ultrasonic signal from the Plexiglas.

Next, the setup #4 is applied to an asphalt concrete specimen without segregation as shown in Figure 3.18. Both the input power level and the pre-amplification level in the pulser/receiver are set to 360 Volts and 60dB, respectively. Note that energy reflection ratio at these material interfaces is 0.9998 so that only half the Rayleigh wave energy transmitted into Plexiglas can be propagating into asphaltic concrete. Figure 3.19 shows the ultrasonic signal transmitted through asphaltic concrete. The expected arrival time of Rayleigh waves is marked by a circle, where an ultrasonic signal with very small amplitude appears. As expected, due to the large acoustic impedance mismatch between the surrounding medium (air) and the material (asphaltic concrete) as well as the higher surface roughness, most of energy is reflected into air. Moreover, the transmitted acoustic energy dies out quickly within a small distance of propagation due to the high attenuation

at the frequencies considered in this study (50-100 kHz), such that they cannot be used for any further reliable analysis for attenuation.

In conclusion, in order to generate stronger ultrasonic Rayleigh wave signals in this material, an ultrasonic generator which can supply higher voltage input to the ultrasonic transducer and a transducer that can handle such high voltage input and has a higher electrical-mechanical transduction coefficient are needed.

Figure 3.18 setup #4: the noncontact generation and detection setup with separation distance, 10 cm.

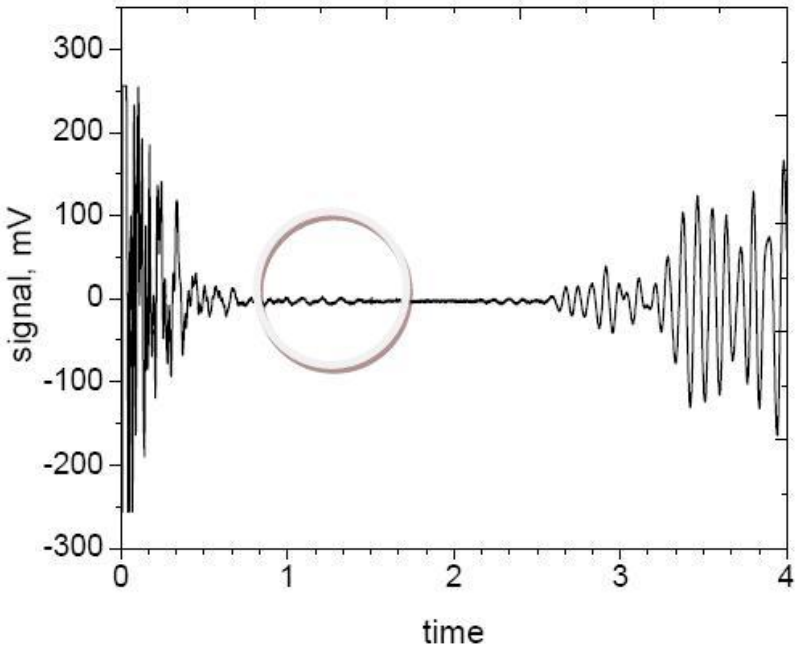

Figure 3.19 transmitted ultrasonic Rayleigh wave at separation distance 10 cm

3.3 Sample preparation

Asphaltic concrete samples were prepared in accordance with the requirements of the Georgia Department of Transportation (Section 828—Hot Mix Asphaltic Concrete Mixtures) (GDOT, 2011) with a size of 120×250×610 mm (depth × width × length). Table 3.2 gives the material type for the baseline design and the design gradation is presented in Table 3.3 Compaction was performed with a vibratory plate tamper and the samples were manufactured with a uniform distribution of aggregate. Two samples, one with no segregation, the second with a top segregation were produced by the Construction Materials Services, Inc., Locust Grove, GA. All two have the same dimensions and vary only with the segregation. Figure 3.20 shows pictures of the two actual samples.

Source Type	Location	Material Type
Aggregate	Valcan-Barin, Georgia Blakely, Georgia	Limestone
Asphalt Cement	Ergon-Bainbridge, Georgia	PG 67-22

Table 3.2 Aggregate and asphalt cement source

Sieve Opening Size (mm)	% Passing
37.5	.
25	100
19	99
12.5	78
9.5	60
4.75	--
2.36	33
0.3	12
0.075	5
Percent AC	4.2

Table 3.3 Aggregate gradation

(a)

(b)

Figure 3.20 (a) Non-segregated; (b) Segregation on top

3.4. Attenuation Measurements in Non-segregated and Segregated Samples

Figure 3.21 shows the phase velocity (v) and attenuation (α in dB/m) for Rayleigh surface waves measured with the three different setups as a function of frequency. It is observed that there is weak dispersion in the frequency range of interest, 40-100 kHz. Thus, it can be said that the phase velocity can be approximated as a frequency independent constant in this frequency range; the average phase speed of a Rayleigh wave in asphaltic concrete is approximately 1800 m/sec. Similar weak dispersion has been observed in Portland cement concrete specimens (Jacobs & Owino, 2000; punurai, Jarzynski, Qu, Kim, et al., 2007; Punurai et al., 2006). The frequency dependent attenuation plot in Figure 3.20 shows an increase in attenuation with increasing frequency, so the term $e^{-\alpha(f)z}$ commonly acts as a low pass filter causing a narrowing of the signal bandwidth.

A comparison of the phase velocity measured with the three setups (the wedge, microphone, air-coupled sensor) shows good agreement with a 5% error between them. However, attenuation values in each of the three cases show a greater variation; in the case of the microphone detection, the attenuation curve becomes flat and starts to decrease at around 90 kHz. This behavior is due to the fact that the operational frequency response range of the microphone is only up to 90 kHz. The wedge receiver results may also be biased because it is difficult to make consistent surface contact at each propagation distance. The point receiver microphone is sensitive to spatially incoherent structural noise that occurs due to local material variations in this heterogeneous medium (the multiple wave scattering effect). On the other hand, the air-coupled transducer has a finite-size aperture that averages the measured wave over this transducer area, thus reducing the effect of spatially incoherent noise. It is clear from Figure 3.21 that the wedge generation along with air-coupled detection (with a finite-size transducer) can be most effectively used to characterize Rayleigh waves in asphaltic concrete; the non-contact air-coupled ultrasonic receiver is the most repeatable, robust, and fastest (for scanning) receiver for the ultrasonic characterization of asphaltic concrete.

Figure 3.22 shows error bars for the attenuation results measured with the three different setups. Twenty-five measurements performed at different locations in the specimen are averaged, with the error bars giving the range of distributions. In each measurement, the wedge transducers are completely removed and then reattached. The maximum error ranges are 75 dB/m, 42dB/m, and 36 dB/m for the wedge-wedge transducer setup, the wedge-microphone setup and the wedge-air-coupled transducer setup, respectively. The average error ranges are 69dB/m, 30dB/m and 34dB/m for these

three setups. Overall, the air-coupled receiver produces the smallest error range. Even though both are non-contact receivers, the air-coupled receiver performs better than the microphone because of the averaging effect in its relatively larger surface area. When the wedge-wedge transducer setup is used, a large number of measurements are required to obtain a representative attenuation measurement of the material. However, when one specific spot is measured, the error bars are observed to be much lower than the above value. In addition, it appears that the attenuation values have some degree of location dependence. There are a number of potential sources for the relatively large error range and the location dependence. First, the sample surface is relatively flat but still has a slight local curvature; this can lead to an incomplete and inconsistent contact between the surfaces of the wedge and specimen. Second, even though the contact pressure on the wedge transducer is maintained as constant as possible, the contact condition varies in each measurement due to the inherently porous nature of the asphalt surface. Third, the specimen has localized surface cracks that are possibly due to the hardening of asphalt binder with time. Finally, the variation of the signal shape due to the above-mentioned error sources causes some difficulty in consistent windowing of the signals.

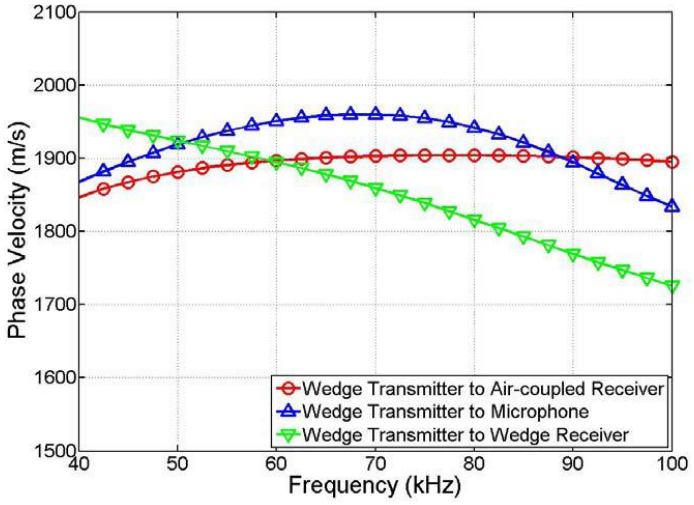

(a)

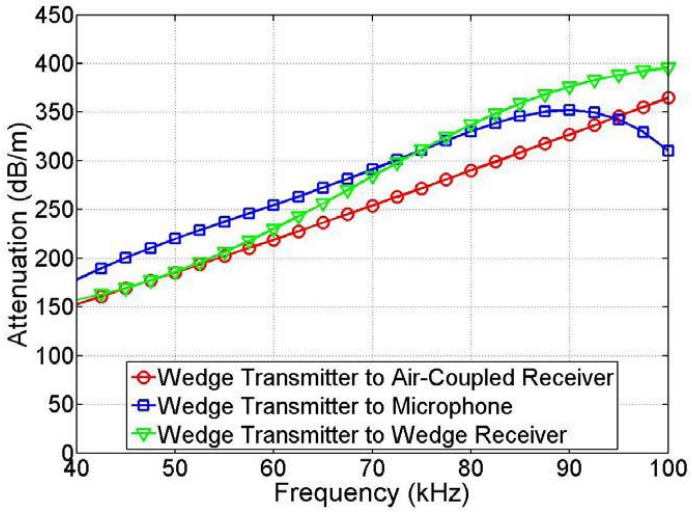

(b)

Figure 3.21 (a) Comparison of Phase velocity of Rayleigh wave with three techniques (b) Comparison of Attenuation of Rayleigh wave with three techniques

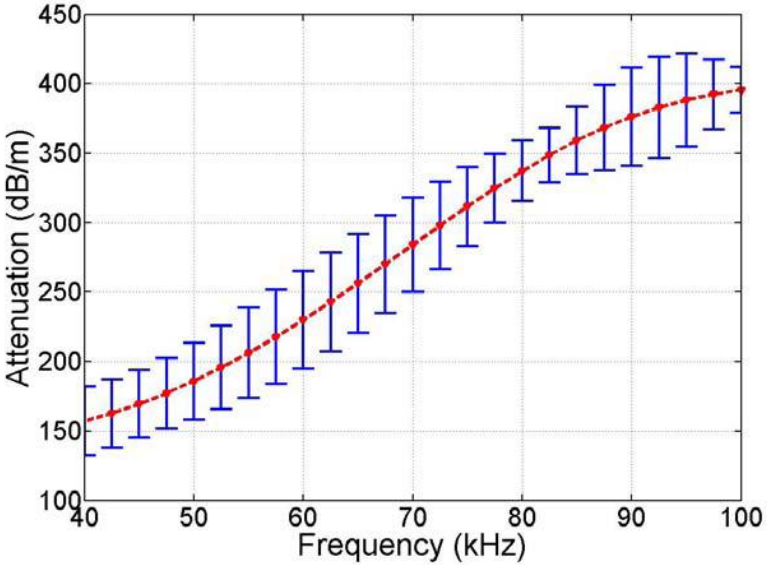

(a)

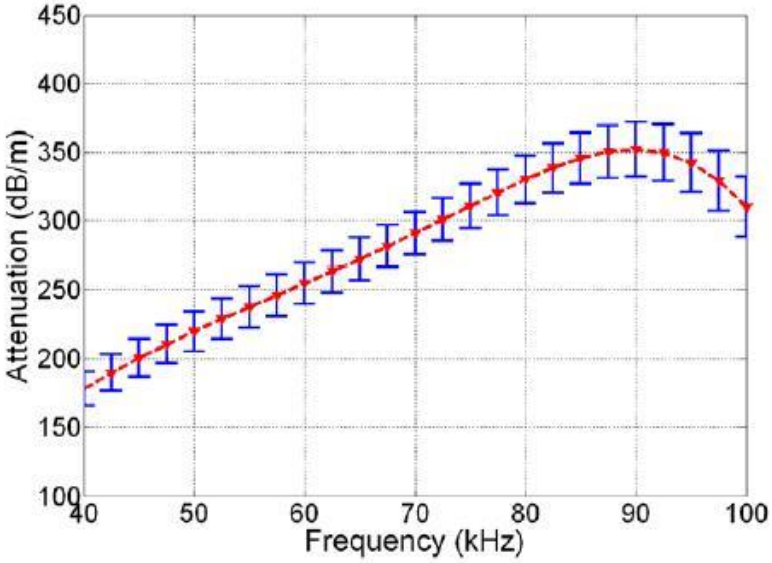

(b)

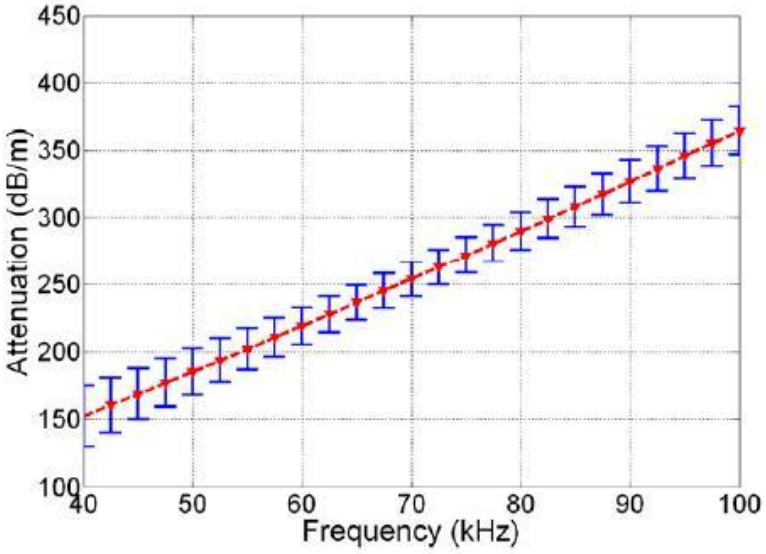

(c)

Figure 3.22 Error bars of the attenuation measured with the wedge transmitter and different receivers: (a) Wedge transducer; (b) Microphone; (c) Air-coupled transducer.

Figure 3.23 compares the time-domain signals measured using the contact transmitter and noncontact receiver for the sample with the top segregation and the sample with no segregation. It is clearly seen that the signal amplitude reduces significantly and this can be used to detect and size the segregation on top of the asphalt pavement. Figure 3.24 shows the results of a preliminary measurement of the attenuation in the asphaltic concrete specimen with top segregation, compared with the attenuation of an asphaltic concrete specimen with no segregation.

More details about the segregated sample and measurement will be reported elsewhere and note that experimental setup #3 is used to make these measurements and the segregation sample has a segregation volume of extent 300mm and a depth of 50 mm. Figure 3.24 shows that there is a considerable difference between the attenuations for these two materials in the frequency range of 20-40 kHz while the error ranges increase with frequency and do get a bit overlapped at the frequencies in 30-35 kHz. This qualitatively demonstrates that the proposed technique may be used to detect segregation in asphaltic concrete specimens.

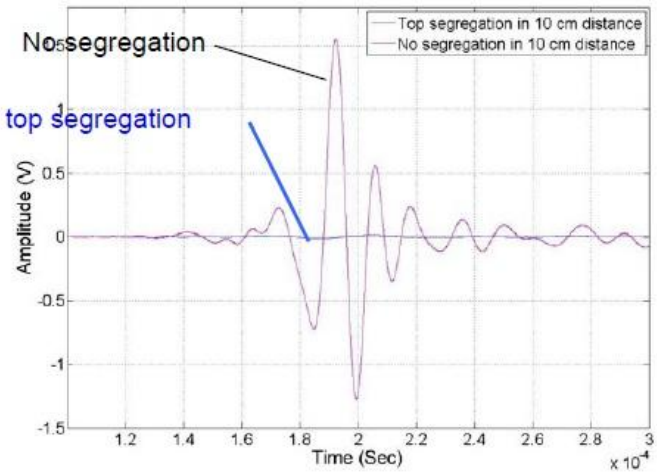

Figure 3.23 Time-domain signals from the samples with a top segregation and no segregation

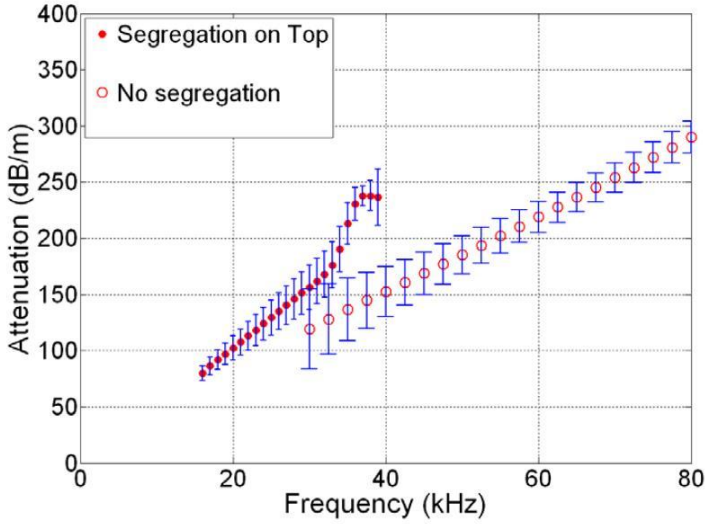

Figure 3.24 Comparison of attenuation spectra measured from asphalt concrete samples with no segregation and with segregation on top.

3.5 Conclusions and recommendations

This research examines the effectiveness of using wedge, microphone, and air-coupled sensor techniques to characterize the material properties of asphaltic concrete. The dispersion and attenuation characteristics of asphaltic concrete have been quantitatively measured in the frequency range from 40 to 100 kHz. It is observed that the wedge to the air-coupled sensor (with a finite-size aperture) technique of Experimental setup #3 appears to be the most reliable in characterizing Rayleigh waves in the present viscoelastic and heterogeneous medium. A preliminary measurement qualitatively demonstrates that the proposed measurement procedure can be used to detect segregation in asphaltic concrete specimens. Future research will employ this method to quantitatively characterize the amount of aggregate segregation in asphaltic concrete.

Due to its different aggregate content, a segregated area will have a local attenuation coefficient either considerably higher or lower than the non- segregated area. Therefore, a judgment regarding the existence of segregation can be made by comparing the local attenuation coefficients. Results obtained in the current research can serve as reference data for the attenuation coefficient of the non- segregated area. It is proposed that a high-frequency Rayleigh wave scattering and propagation model can provide quantitative information about the aggregate content in the segregated area. However, the fully noncontact measurements (experimental setup #4) show that the ultrasonic signal strength from an air coupled ultrasonic source is not sufficient enough to generate a reasonable Rayleigh wave signal that can detect segregation in asphaltic concrete. Thus it is recommended that in order to generate stronger ultrasonic Rayleigh wave signals in this material, an ultrasonic generator which can supply higher voltage input to the ultrasonic transducer and a transducer that can handle such high voltage input and has a higher electrical-mechanical transduction coefficient are needed.

CHAPTER 4

CRACK DEPTH DETERMINATION IN CEMENT BASED CONCRETE

4.1 Theoretical Approach

This chapter deals with the theoretical background of diffuse waves. First, elastic wave propagation in heterogeneous media will be presented, followed by the diffuse wave approximation in concrete and the governing equation with modified diffusion equation to treat it as heat transfer problem.

4.1.1 Elastic wave propagation in heterogeneous medium and diffuse field

In heterogeneous medium, an ultrasound wave field is scattered multiple times by scatterers therefore, consists of a coherent ballistic field and an incoherent diffuse field. Here the diffuse field is strongly scattered wave field by the scatterers; it is spatially incoherent and incoherent with the source signal in time and its phase is (approximately) randomized. If the phase information of the diffuse ultrasound field is neglected (this is a reasonable assumption when the scattered wave has lost its temporal and spatial coherence after many scattering events), the diffusion approximation can be used to describe the propagation of strongly scattered waves over a long distance; according to (Zhang et al., 1999), a minimum of 4 to 10 scattering mean free paths is needed for transition from ballistic to diffuse field, but it should also be pointed out that this is not universal and is dependent on the physical quantity under study, as well as the source-

detector geometry. After this transition, it is known that it is possible to treat the wave field on an energy basis rather than based on the displacement field. The evolution of the energy is then governed by the diffusion equation.

According to recent literature, The ultrasound diffusion approximation can be derived with either an incoherent random walk model (an approach similar to the derivation of heat transfer (Carslaw & Jaeger, 1990; Hill & Dewynne, 1987)) or by perturbative multiple scattering formalism (Weaver, 1990a). A formal derivation is given in (Sheng, 2006), less formal explanations are given in(Weaver, 1990b, 1998). In order to establish the ultrasound diffusion equation, several assumptions are made in the derivation. It is assumed that the scatterers are randomly distributed in the elastic solid and no resonance effects (as a result of high coherence of scattered waves) occur due to periodic distributions. Moreover, the scattering process is linear elastic, which means that no energy is lost during the interaction of the wave field with the scatterer. Furthermore, no change in frequency is assumed during the scattering process (linearity).

4.1.1.1 Diffuse wave approximation and its governing equation in concrete

Concrete is a strongly heterogeneous and multiphase medium in which scatterers (aggregates or voids) of various sizes are randomly distributed in a viscoelastic matrix (cement paste). Ultrasonic waves propagating in such a medium undergo repeated scattering; this effect is described as a function of a/λ, where a is the characteristic length of the scatterer and λ is the wavelength. The scattering effect is dominant in the intermediate frequency regime where $a/\lambda \sim 1$, or when the volume fraction of scatterers is fairly high. The initially coherent incident waves are quickly randomized and propagate

as an incoherent noise. The ballistic field decays in a distance of only a few times the wavelength from the source and the incoherent field that is superimposed on a ballistic field in the short distance becomes dominant (Cowan, Beath, Page, Liu, & Sheng, 1998). The macroscopic transport of ultrasonic energy in this process is similar to the well-known diffusion process while every single microscopic event is the wave propagation/scattering process. It has been shown that the average of the ultrasonic energy can be well approximated by the following dissipative diffusion equation (Page et al., 1995; Ramamoorthy et al., 2004),

$$D(f)\nabla^2\langle E(x,t,f)\rangle - \frac{\partial}{\partial t}\langle E(x,t,f)\rangle - \sigma(f)\langle E(x,t,f)\rangle = P(x,t,f), \forall x \in \mathrm{B}. \quad (4.1)$$

where $E(x,t,f)$ denotes the spectral ultrasonic energy per unit volume; the coefficients D and σ correspond to the frequency dependent diffusivity [m^2s^{-1}] and dissipation coefficient [s^{-1}] in domain B; $P(x,t,f)$ is the spectral energy density of the source; the symbol $\langle\cdot\rangle$ is the expectation operator as the distribution of the scatterers is random and thus $\langle E(x,t,f)\rangle$ denotes the average spectral ultrasonic energy per unit volume.

The solution to Eq. (4.1) requires a set of initial and boundary conditions. The initial condition is such that the initial spectral energy density in the domain B is zero:

$$\langle E(x,0,f)\rangle = 0, \forall x \in \mathrm{B}. \quad (4.2)$$

The boundary conditions are that the energy flux across the boundary surface $\partial\mathrm{B}$ of the domain B is zero (the Neumann's boundary conditions):

$$\nabla\langle E(x,t,f)\rangle = 0, \forall x \in \partial\mathrm{B}. \quad (4.3)$$

This condition can be understood as no transmission of ultrasonic energy from the solid to the surrounding air. In the following, Equation (4.1) is solved analytically for two-dimensional cases.

4.1.1.2 Analytical Solutions in a bounded 2-D domain

When the geometry of the domain B is simple, it is possible to obtain an analytic solution for Eq. (4.1), given the initial (Eq. (4.2)) and boundary (Eq. (4.3)) conditions and the forcing condition $P^*(x,y,t,f) = P_0\delta(t)\delta(x-x_0)\delta(y-y_0)$, which represents a spatial-temporal impulse at the location (x_0, y_0) and at time equal to zero with an amplitude of P_0. For the retrieval of the diffuse ultrasonic parameters, an analytical solution for a two-dimensional rectangular domain is employed (Ramamoorthy et al., 2004):

$$\langle E(x,t,f)\rangle = P_0\left\{1+2\sum_{n=1}^{\infty}\left(\cos(L_n x_0)\cos(L_n x)e^{-DL_n{}^2 t}+\cos(P_n y_0)\cos(P_n y)e^{-DP_n{}^2 t}\right)+4\sum_{n=1}^{\infty}\sum_{m=1}^{\infty}\cos(L_n x_0)\cos(L_n x)\cos(P_m y_0)\cos(P_m y)e^{-D(L_n{}^2+P_m{}^2)t}\right\}e^{-\sigma t} \quad (4.4)$$

where $L_n = n\pi/l$ and $P_n = n\pi/p$ with *l* and *p* being the dimensions of the rectangular domain. The variables x_0 and y_0 represent the location of impulse excitation and x and y depict the location of the receiver.

Diffusivity Coefficient

The diffusion coefficient *D(f)* is a frequency dependent material parameter. It has the unit [m^2/s] and determines the diffusion rate of the ultrasonic field. Higher values correspond to faster diffusion.

Dissipation Coefficient

The dissipation coefficient $\sigma(f)$ is a material parameter that represents the rate of loss of energy due to internal friction. It can be found that the loss due to dissipation are of a temporal nature and do not depend on the location *x* and *y* in the medium. The unit of dissipation is [*1/s*]. The frequency dependent dissipation is not to be mistaken with the acoustic attenuation which also accounts for the reduction of the wave amplitude due to the geometric attenuation.

Modification of diffusion equation

Another way to perceive the ultrasonic diffusion equation (4.7.1) is to view it as a modified heat conduction PDE as the dissipation term $\sigma\langle E(x,t,f)\rangle$ does not complicate the solution. With this modification,

$$\langle E(x,t,f)\rangle = \langle E^*(x,t,f)\rangle e^{-\sigma t}. \tag{4.5}$$

Substituting Eq. (2) into Eq. (1) yields the standard heat equation with no dissipation term:

$$D(f)\nabla^2\langle E^*(x,t,f)\rangle - \frac{\partial}{\partial t}\langle E^*(x,t,f)\rangle = P^*(x,t,f), \forall x \in \mathrm{B}. \tag{4.6}$$

Note that the elimination of the dissipation term makes it possible to directly adopt the modeling approach for heat transfer problems. The effects of the dissipation can be accounted for later by multiplying $e^{-\sigma t}$ to $\langle E^*(x,t,f)\rangle$ according to Eq. (2).

4.2 Development of Ultrasonic Measurement Setups and Procedures

This section describes methodology to generate and detect the diffuse wave and ultrasonic measurement procedure to determine the arrival time of maximum energy (ATME) from energy density curve to estimate the crack depth in concrete.

4.2.1 Generation of diffuse field in concrete

The transmitter and receiver in this research are Ultran WC 50 and GC500-D13 500kHz broadband transducers with a diameter of 12.5 mm. It should be noted that the diffuse field will converge to zero if it is averaged over random configurations or averaged in a finite volume, which is called phase cancellation (Page et al., 1995), because of the fact that diffuse wave is spatially and temporarily incoherent with the incident signal and its rapid spatial fluctuation in phase and amplitude, Hence it is inevitable to design transducers with a small surface area to avoid phase cancellation in measurement of the diffuse field.

For this purpose, a small cone is designed and manufactured. The bottom diameter of the cone is 5 mm, the top diameter is 2 mm, its thickness 2.2 mm. The cone is manufactured out of aluminum. The cone is attached with glue (LOCTITE Super Glue) to the center of the receiving transducer. Figure 4.1 shows a picture of a pair of transducers where the attached cone is clearly seen. Unfortunately, the added cone makes the transducer difficult to perfectly perpendicular to the surface, also to improve the consistent coupling conditions, a small clamp is accommodated to its fixture as shown in Figure. 4.2. In all measurements, the separation distance is 60 mm and the transducers are also placed far away from the specimen edges in order to avoid any possible edge effects.

Figure 4.1 Receiver and Transmitter

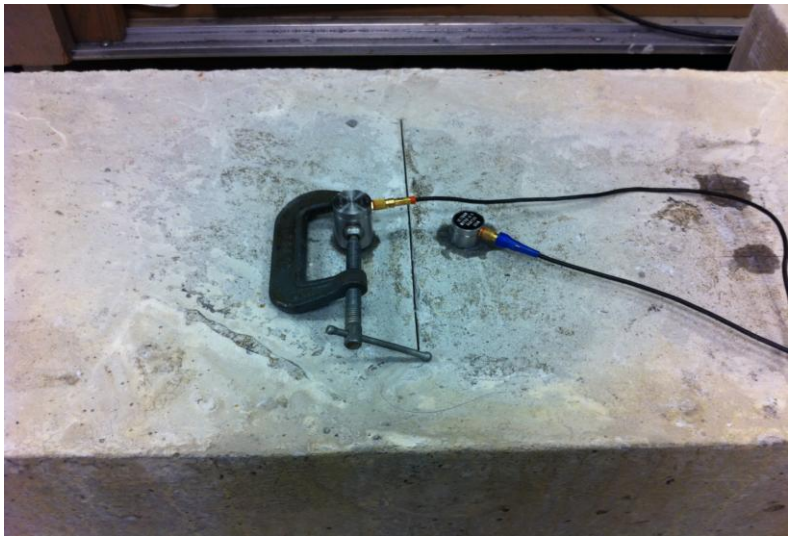

Figure 4.2 Accommodated clamp with transducers

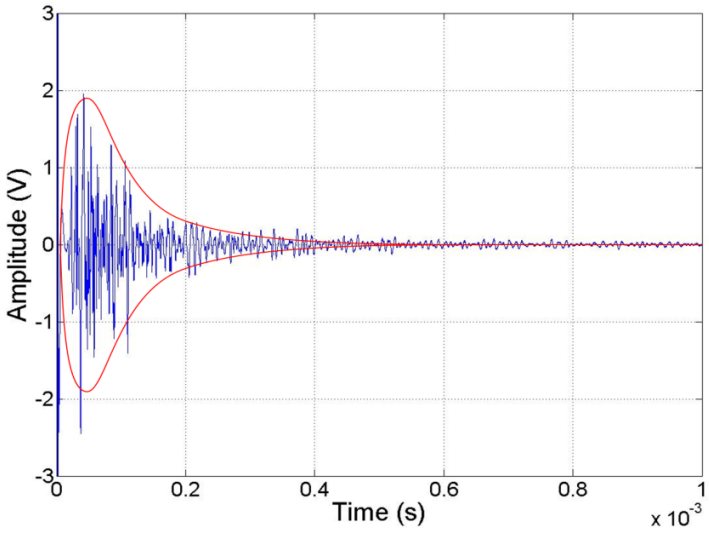

Figure 4.3: Typical diffuse ultrasound signal

4.2.2 Experimental Setups and procedures

4.2.2.1 Measurement setups

A high voltage pulse generator (Panametrics 5058 PR) is used to provide the source signal of 400 V which is sufficient for energy transmission into the concrete samples. In order to get a high signal-to-noise ratio (SNR) from the concrete samples, a pre-amplifier (DigitalWave DW2040G/A) – which amplifies the received signal by 40 dB – is used in series with a signal conditioning amplifier DigitalWave DW FTM4000, which allows an additional amplification of 20 dB. The amplifier also allows the setting of a lowpass and highpass filter. They are set to their respective minimum (20 KHz) and maximum (4 MHz) values. The transmitter and receiver in this research are Ultran WC 50 and GC500-D13 500kHz broadband transducers with a diameter of 12.5 mm. A schematic layout of the ultrasonic diffusion experimental setup is shown in Figure 4.4. A four channel digital Tektronix TDS 5034 B oscilloscope is used for this research. All

measurements are sampled with a sampling frequency *fs* of 50 MHz, recorded with 200000 record points, and then averaged 1000 times to obtain the signal to be processed. The impedance is always set to 1 M. The oscilloscope runs Windows 2000 as an operating system and allows saving the acquired waveforms in the *.dat format which is readable by Matlab. The files can be easily transferred to a PC using a flash drive for further signal processing. A viscous couplant is used to couple both of the transducers to the specimen. During the measurements, the transmitting transducer setup is fixed, while the receiving transducer is completely removed and reapplied three times to get a reliable data set and to give an error analysis

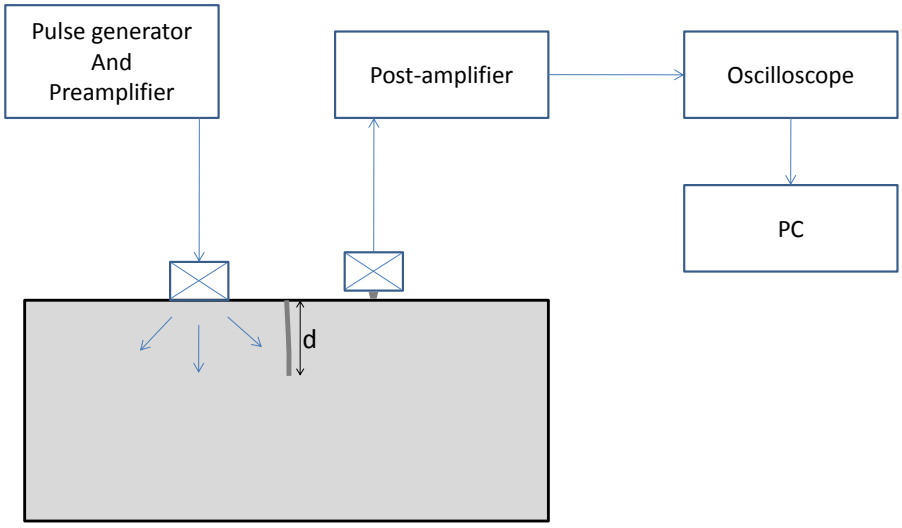

Figure 4.4 A schematic layout of the ultrasonic diffusion experimental setup

4.2.2.2 Calculation of the energy density evolution $\langle E(x,t,f)\rangle$ from measurement data

A time-frequency analysis with the following main steps is performed to calculate the measured spectral energy density $\langle E(x,t,f)\rangle$ at a certain frequency f (and at the

measurement point *x*). A typical time signal is shown in Figure 4.5 that is used as an example in the following sections.

1. Divide the time signal into overlapping time windows of length Δt . The window length is set to $\Delta t = 15\,\mu s$ and window overlap of 90 % between consecutive windows is applied. Multiply the signal of each time window with the Hanning window to smooth the signal edges. The Hanning window gives signal outside of the window center less weight, so the overlap makes sure that the whole time-domain signal is taken into account for the further calculations. More time points are available if the windows overlap more.

2. Calculate the discrete-time Fourier transform (DTFT) of each individual time window and square it. All the steps until here are done automatically by the Matlab function **spectrogram** which gives the resulting quantity from these three steps – the power spectral density – as one of its outputs. The power spectral density is basically a table of Fourier transforms for every time window centered at the center time of each time window.

3. Determine the spectral energy density of each time window in a certain frequency band by integrating the power spectral density in that bandwidth with width Δf centered around frequency f_c . The value used for this research is $\Delta f = 100 kHz$.

4. Construct a table of spectral energy density values that are assigned to discrete time points. The time points are centered in their respective time windows (centering assumes that the statistical signal properties like power spectrum are stationary over the length of the time window).

The resulting quantity is denoted with $\langle E(x,t,f)\rangle$. $\langle E(x,t,f)\rangle$ is not the ultrasonic spectral energy density itself, but differs from that by a factor related to transducer sensitivity and a factor relating the measured local mean-square motions detected by the transducer to the local strain and kinetic energy densities. That factor is unknown, but presumed constant (Weaver, 1998).

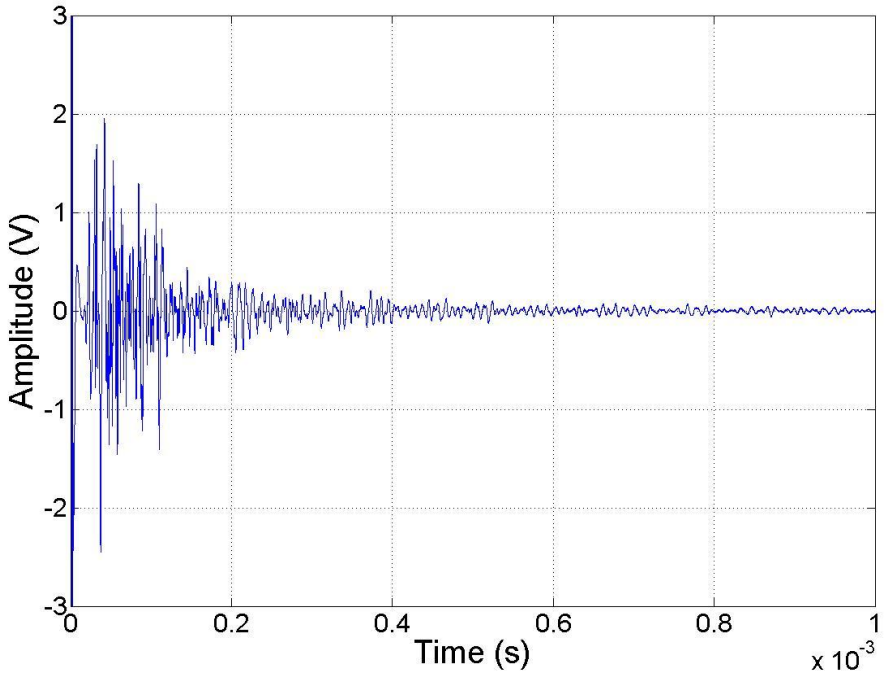

Figure 4.5 Typical diffuse ultrasound signal

4.2.2.3 Fit of an approximate solution in 2 D rectangular block

To recover the model parameters (P_0, D and σ) from the experimentally determined spectral energy density $\langle E(x,t,f_c)\rangle$ (calculated for a frequency band with center frequency f_c), the energy density curve is fit to the approximate two-dimensional model from Eq. (4.4). Only data on a limited time range in which the energy density is clearly above noise level can be considered for the curve fit. The coordinates of source and receiver are (x_0, y_0) = (0.14 m, 0.254 m,) and (x, y) = (0.20 m, 0.254 m,). The specimen dimensions are 0.615 m × 0.254 m × 0.325 m. The Matlab function **lsqnonlin** is used for the curve fitting procedure. It must be noted that the indices of the infinite series in Eq. (4.4) are selected to n = m = 250, which is determined by convergence test for Sufficient accuracy of the analytical solution. (Seher, 2011)

4.3. Sample Preparation

Three unreinforced concrete specimens are prepared for the diffuse ultrasonic measurements. All the specimens have the equivalent geometry shape with nominal dimensions (25.4 × 33 × 60.96 cm^3). All specimens are cast produced from ASTM C 150 Type I portland cement, natural sand, and coarse, crushed granitic gneiss aggregate as shown in table 4.1-4.3. The water-to-cement ratio is 0.45 by mass. After the components are mixed, fresh concrete are placed into wooden molds (30.48 × 40.64 × 68.58 cm^3). The artificial cracks (or notches) are created by inserting a lubricated steel plate of 1 mm thickness in the mold with a predetermined depth between 2.54 and 10.16cm. After the initial setting time, the steel plates are removed from the mold and the concrete is covered with plastic sheeting and left to cure for 24 h at ambient conditions. The molds are then stripped and the specimens were placed in a controlled environment nominally of 23^oC

and 95% relative humidity for a period of 28 days. After this curing period, the concrete specimens are stored in a laboratory environment until tested. The top surfaces of the samples are polished with an electric grinder to get a better contact condition for the ultrasonic transducers.

Table 4.1: Gradation of fine aggregate

Sieve size	Amount retained/ total weight (%)
# 4	6.2
# 8	7.1
# 16	14.8
# 30	18.7
# 50	33.0
# 100	15.8
Pan	4.4
Total	100

Table 4.2: Gradation of coarse aggregate

Sieve size	Amount retained/ total weight (%)
1/2"	33.3
3/8"	33.3
# 4	33.3

Table 4.3: Mix design for concrete sample

Coarse aggregate	1890 (lb/yd^3)
Fine aggregate	1130 (lb/yd^3)
Cement	720 (lb/yd^3)
Water	324 (lb/yd^3)

4.4 Measurements on Arrival Time of Maximum Energy Density

Experiments are first conducted on the uncracked concrete sample to recover the diffusivity and dissipation coefficients of the hardened concrete. A typical time-frequency analysis and curve fitting following the procedure described above are performed on the measured ultrasonic signals to retrieve diffusion parameter. Figure 4.6 shows the experimental spectral energy density corresponding to the time signal shown in Figure 4.5, together with its fitted model on the logarithmic scale. The recovered diffusion parameters at 500 kHz are 10 m^2/s and 21000 /s which agree well with those in a previously published paper (Anugonda et al., 2001). These parameters will be used in the numerical simulations to determine the predicted peak arrival time for different crack depths.

The experiments on the cracked specimens are essentially identical to those on the uncracked one. Transducers are placed 30 mm off on both sides of the crack. Figure 4.7 shows the measured ultrasonic waveform for the specimen with a 10.16 cm crack depth. In comparison with the result from uncracked sample (Figure 2), the delay of the pick arrival time is clearly seen (in this case $\Delta t=30\mu s$). This delay is due to the fact that the crack causes the energy propagation path to be longer, and hence will take more time to

reach the receiver; this also makes the effective diffusivity D lower. The delay in diffuse energy (the peak) is affected by the absence of diffuse energy transfer across the crack. The lag time, defined as the difference between the peak arrival times in the cracked and uncracked regions, is used to estimate the crack depth.

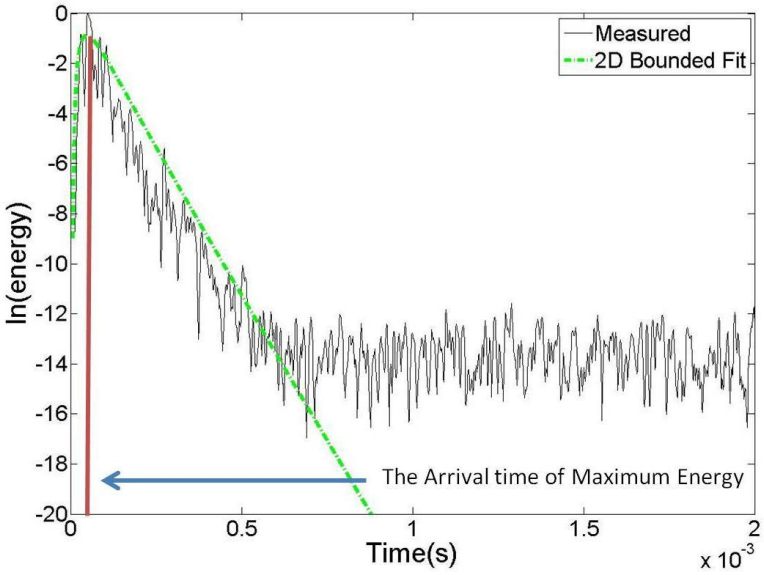

Figure. 4.6. Energy density curve and curve fitting in uncracked sample

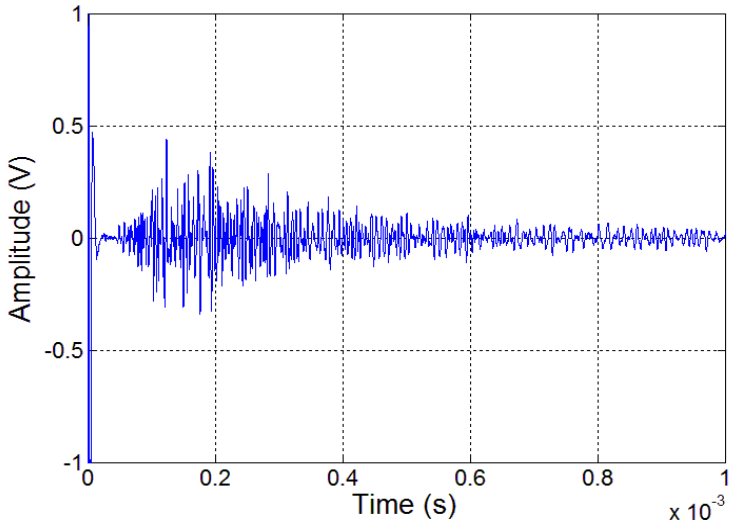

Figure 4.7 Diffuse ultrasound signal in 10.16cm cracked specimen

4.5 Model Analysis

Figure 4.8 show a flow chart of modeling procedure to determine crack depth in concrete. First, diffusion parameters (diffusivity and dissipation values) are retrieved from experimental measurements in uncracked regions of concrete. Then those diffusion parameters are used as an FE model input parameter using ANSYS (Seher, 2011) to simulate various crack configurations and depths. From these simulations, the peak arrival time of the energy is then determined from the numerical energy evolution curves and is compared with experimental measurements. The lag time as the difference between the peak arrival time in the cracked and uncracked regions is the measure used here to infer the crack depth. Lastly, the crack depths can be then estimated from the comparison of experimental results and numerical analysis.

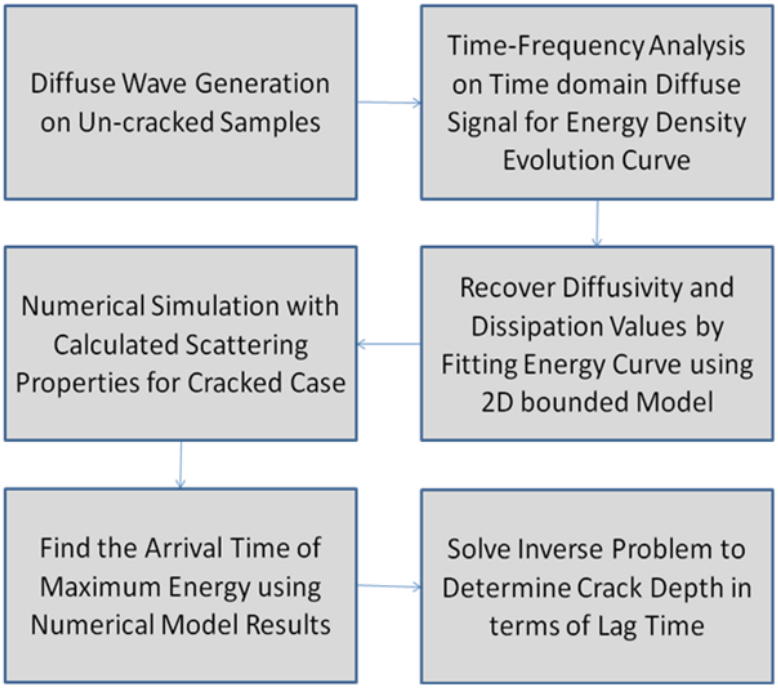

Figure 4.8: Flow chart of modeling procedure

4.5.1 Numerical modeling of Diffuse Wave Propagation

This research uses the commercial finite element software tool ANSYS in order to conduct the numerical simulations finite element code was developed (Seher, 2011) for solution of the diffusion equation given by equation 4.4 with forcing condition. The cross sectional details of the experimental specimens given in table 4.4 were used for creating a rectangular domain for this model. This approach has also been taken by Turner in (Ramamoorthy et al., 2004).

As discussed in theoretical approach section, the modified ultrasonic diffusion equation, which is treated as transient thermal problems in ANSYS, is used in this simulation. The rectangular domain was discretized and meshed with bilinear quadrilateral elements of the type “plane55” in ANSYS. The backwards Euler method is

used to approximate the time derivative of the ultrasonic spectral energy density for every integration step with Δt being the time step size: The typical time step used in this numerical integration is ranged from 10ns to 1us. Further information on this element type can be found in the ANSYS documentation (Ansys, 2010). To check for convergence of the numerical model, the analysis was carried out by varying the number of elements in the rectangular domain. It was found that the numerical solution compared well with the analytical solution for 6000 elements.

The boundary of the domain was modeled with Neumann boundary conditions (zero flux across the boundary) and the initial condition is assumed to be zero, as there is no ultrasonic energy in the domain at time zero. The ultrasonic material parameters in this research obtained from the experimental measurements on the specimen using the analytical solution for a bounded two-dimensional domain given in Equation (4.4) are given in Table 4.5.

Parameter	Height	Width	Depth
Dimension	600mm	250mm	325mm

Table 4.4 Dimensions of concrete block

Parameter	Diffusivity D	Dissipation σ
Value	10 m^2/s	21000 1/s

Table 4.5 Diffusivity and dissipation parameters at 500 kHz for the simulations.

Figure 4.9 shows a comparison of the experimentally measured diffuse energy with the numerical prediction for 10.16 cm crack depth with a separation distance of 60 mm. The results are scaled such that the initial rise of the experimental and numerical data matched. As a conclusion from the comparison between the experimental measurements and the FE simulations it can be said that the there is a good agreement yielding the applicability of the ultrasound diffusion approximation.

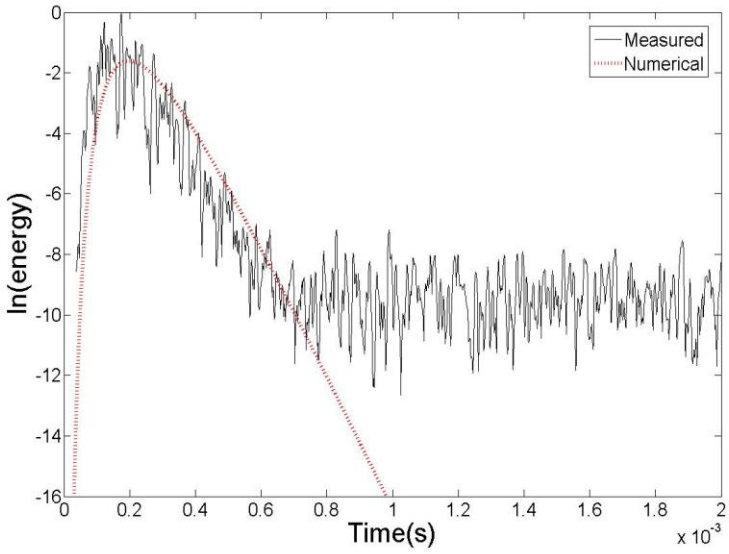

Figure 4.9 Comparison of the experimental diffuse energy curve with numerical energy curve in 10.16 cm crack sample

4.5.2. Crack Depth Determination via Lag Time

The lag time, defined as the difference between the peak arrival time of the diffuse energy in the cracked and uncracked regions, is the measure used here to infer the crack depth. By comparing the peak arrival time of the energy density curve across the crack (2.54 cm to 10.54 cm) with the peak arrival time of the data obtained at the uncracked region, the lag time for different crack depths was determined. Figure 4.10

shows the lag time obtained by numerical analysis for different crack depths. It is shown that the lag time increases with increases in crack depth, as expected.

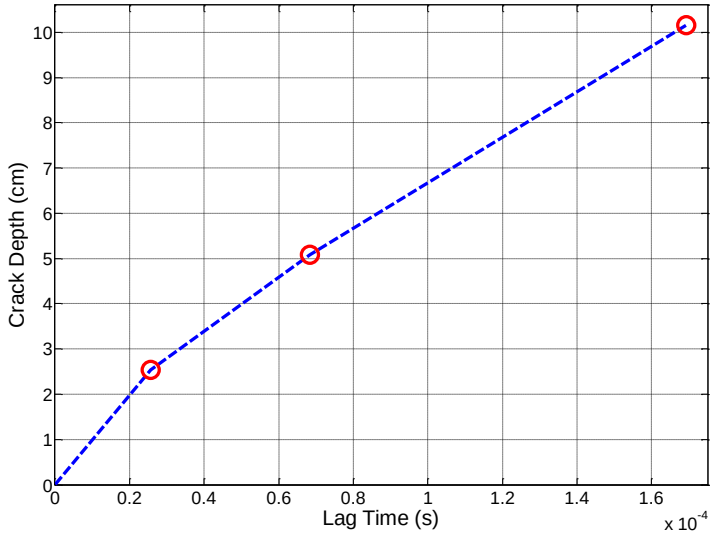

Figure 4.10 Lag time vs crack depth by numerical analysis

4.6 Application of diffuse technique to real vertical cracks in a concrete beam

This research continues the effort to generate cracks with appropriate depths and take measurements at different stages of crack growth, both opened and closed in a concrete beam. Figure 4.11 shows the measurement setup of the concrete beam (4.5 × 0.41 × 0.3m) undergoing four point bending to produce real cracks. As in the previous section, the same procedure is employed to estimate the depth of cracks in this concrete beam.

Figure 4.11: Concrete beam undergoing four point bending to obtain real cracks

4.6.1 Experimental procedure and results

The same transmitter and receiver used for the measurements in concrete block samples with various vertical crack depths are used in the experiment (Ultran WC 50 and GC500-D13 500kHz broadband transducers with a diameter of 12.5 mm). Also, the same small clamp is accommodated to the receiving transducer to improve the consistent coupling condition as shown in figure 4.12. In all measurements, the separation distance is fixed to be 60 mm and the transducers are also placed in the middle of the specimen far away from the specimen edges. A typical diffuse signal before cracking is shown in figure 4.13.

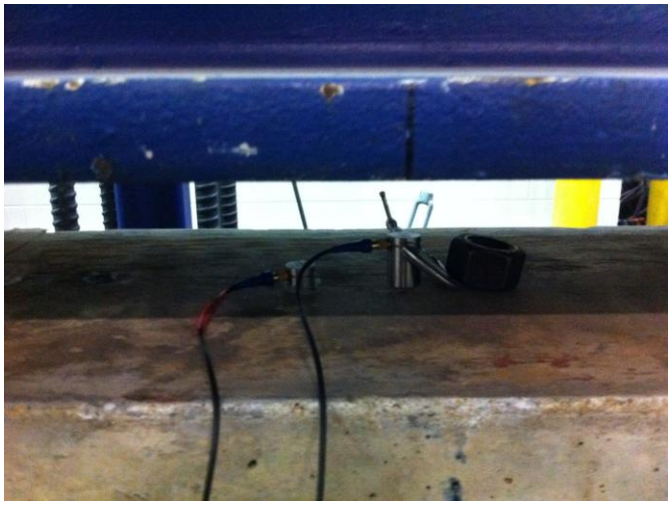

Figure 4.12 Transmitter and receiver on the surface of the concrete beam

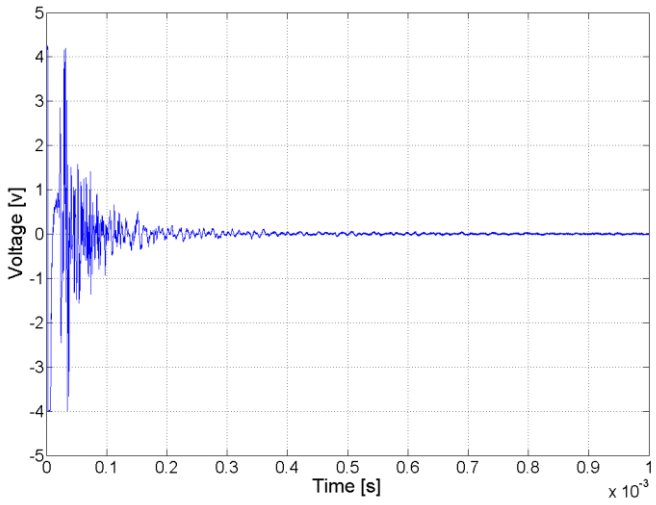

Figure 4.13: Typical diffuse ultrasound signal

The same set of equipment as in the previous experiments (a high voltage pulse generator (Panametrics 5058 PR), a pre-amplifier (DigitalWave DW2040G/A), and A four channel digital Tektronix TDS 5034 B oscilloscope) is used. All measured signals

are sampled with a sampling frequency *fs* of 50 MHz, recorded with 200000 record points, and then averaged 1000 times to obtain a signal to be processed. A viscous couplant is used to couple both of the transducers to the specimen. A time-frequency analysis is performed to calculate the measured spectral energy density $\langle E(x,t,f)\rangle$ at a 500kHz frequency *f* and at the measurement position *x*.

To recover the model parameters (P_0, D and σ) from the experimentally determined spectral energy density $\langle E(x,t,f_c)\rangle$ (calculated for a frequency band with center frequency f_c), the energy density curve is fitted to the quasi two-dimensional model in Eq. (4.4). Only data on a limited time range in which the energy density is clearly above the noise level is considered for the curve fit. The coordinates of source and receiver are (x_0, y_0) = (2.22 *m*, 0.41 *m*,) and (x, y) = (2.28 *m*, 0.41 *m*,) in the uncracked beam. In the cracked beam, the source and receiver were moved to the position around crack. The Matlab function **lsqnonlin** is used for the curve fitting. Experiments are first conducted on the uncracked concrete beam to recover the diffusivity and dissipation coefficients. A typical time-frequency analysis and curve fitting are performed on the measured ultrasonic signals to retrieve these diffusion parameters. Note that the recovered diffusion parameters at 500 kHz are 10 m^2/s and 45000 /s in this concrete beam; note that the measured dissipation is much higher than that of the concrete block samples. The reason for this is thought to be the fact that this concrete beam is 10 years old. These parameters were used in the numerical simulations to predict the peak arrival times for different crack depths. The experiments on the cracked specimens are essentially identical to those on the uncracked one, but conducted at a different location.

Transducers are placed 30 mm off on both sides of the crack. Figure 4.14 shows experimental setup with a real crack produced by loading in the concrete beam.

.

Figure 4.14: Experimental setup with a real crack in the concrete beam

Note that in all these experiments, the effective diffusivity and effective ATME are also obtained using the diffusion parameters from the uncracked beam. It should be noted that these effective diffusivity and ATME are not absolute values and cannot be a standard indicator to vertical crack depth, but these are still useful to estimate vertical crack depth experimentally. The experimental ATME will be compared with the numerical ATME obtained from FE simulations to determine vertical crack depth later. Figures 15 and 16 show effective ATME and diffusivity as a function of applied load in three different experiments. As shown in these figures, the concrete beam was loaded and unloaded three times while the ultrasonic measurements are performed during loading

stages. And in the first loading stage, interestedly, ATME and diffusivity has been changed without any significant macro cracks in the beam until load has increased up to 5000lb.It is inferred that microcracks are triggered to be opened due to this loading so that it affects both the above-mentioned the ATME and diffusivity to be changed. Also the results from two different locations are consistent; this verifies assumption such that microcracking has happened at even different locations with same loading condition. In the second and third loading stages, a macro vertical crack was observed to be opened in the surface of the beam and then developed up to more than 5 cm until 20000 lb. There is sudden jump of ATME between 7500 and 14500 in the second loading stage and between15000 and 20000 in the third loading stage. In addition to that, it is found that there exists hysteresis behavior in each loading stage, which explains that once the crack has fully opened, the crack still remains open although the load is fully released and that also demonstrates the ATME can be a good indicator to monitor crack development in the monotonic test of real concrete beam.

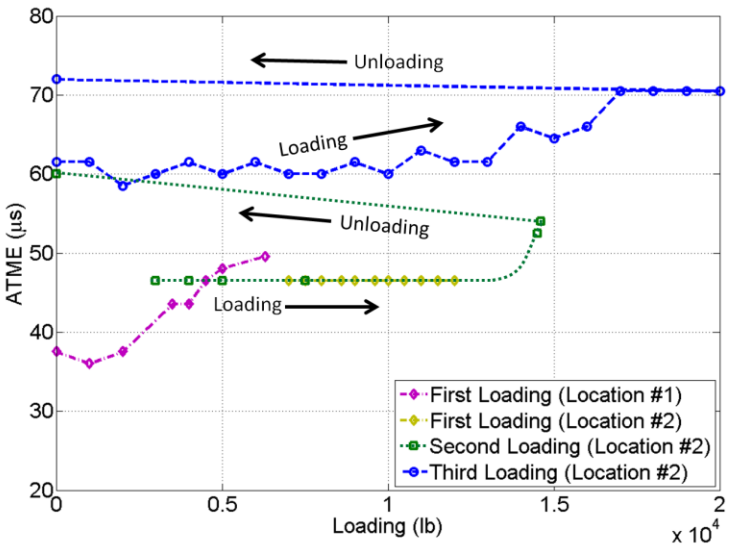

Figure 4.15: The effective ATME versus loading

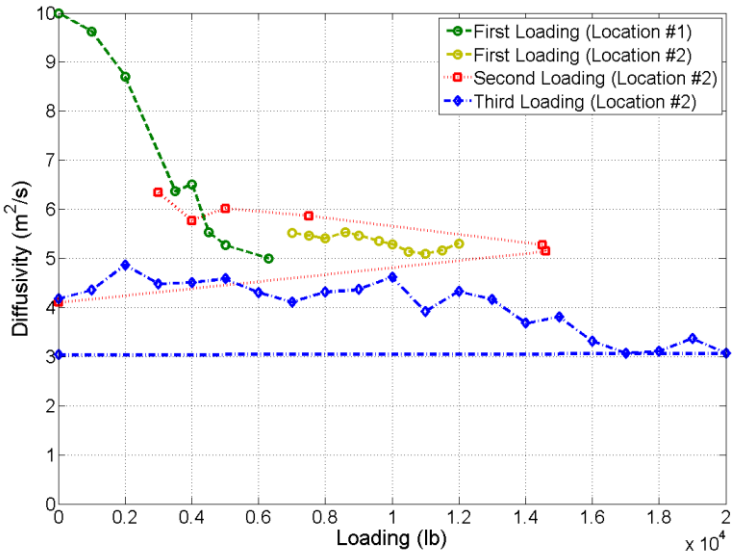

Figure 4.16: The effective diffusivity versus loading

4.6.2 **Determination of crack depth during repeated loading on concrete beam**

As mentioned in section 4.5.2, an FE simulation package, ANSYS, is used for the solution of the diffusion equation given by equation 4.4 with a forcing condition. The cross sectional details of the concrete beam specimens given in table 4.6 are used for creating a rectangular domain for this model.

The ultrasonic diffusion parameters in this research obtained from the experimental measurements on the beam using the analytical solution for a bounded two-dimensional domain given in equation 4.4 are given in table 4.7.

Parameter	Height	Width
Dimension	410mm	4500mm

Table 4.6 Dimensions of concrete beam

Parameter	Diffusivity D	Dissipation σ
Value	10 m^2/s	45000 1/s

Table 4.7 Diffusivity and dissipation parameters at 500 kHz for the simulations.

Figures 4.17 and 4.18 show a comparison of the experimentally measured diffuse energy with the numerical prediction for 2cm and 4cm crack depth with a separation distance of 60 mm, respectively. The results are scaled such that the initial rise of the experimental and numerical data matched.

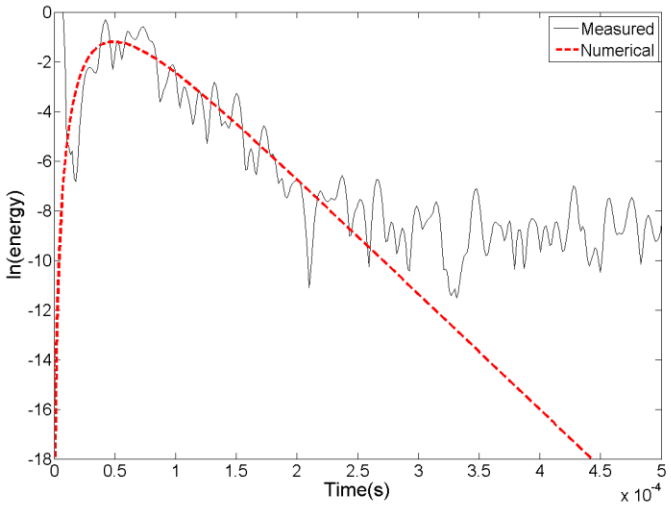

Figure 4.17 Comparison of the experimental diffuse energy curve with numerical energy curve in 2 cm cracked beam

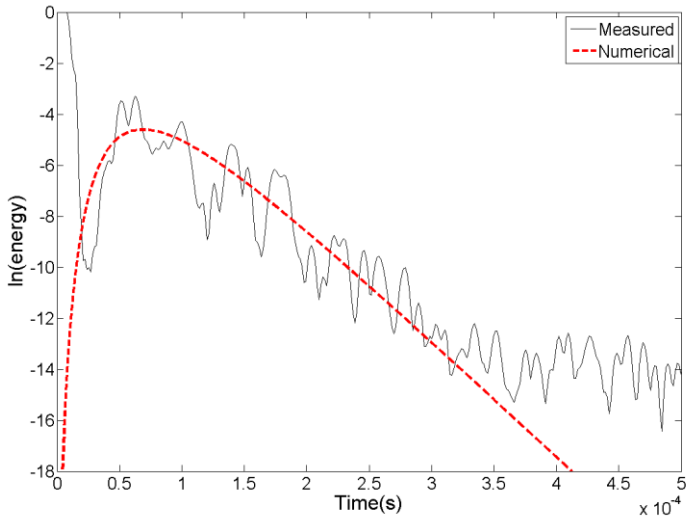

Figure 4.18 Comparison of the experimental diffuse energy curve with numerical energy curve in 4 cm cracked beam

4.6.2.1 Crack Depth Determination via Lag Time

As defined in section 4.5.2, the lag time is used here to infer the crack depth. By comparing the peak arrival time of the energy density curve across the crack with the peak arrival time of the data obtained at the uncracked region, the lag time for different crack depths are determined. Figure 4.19 shows the lag time obtained by numerical analysis for different crack depths. As compared with the experimental ATME (effective ATME), the largest surface open crack depth is inferred to be approximately 5cm.

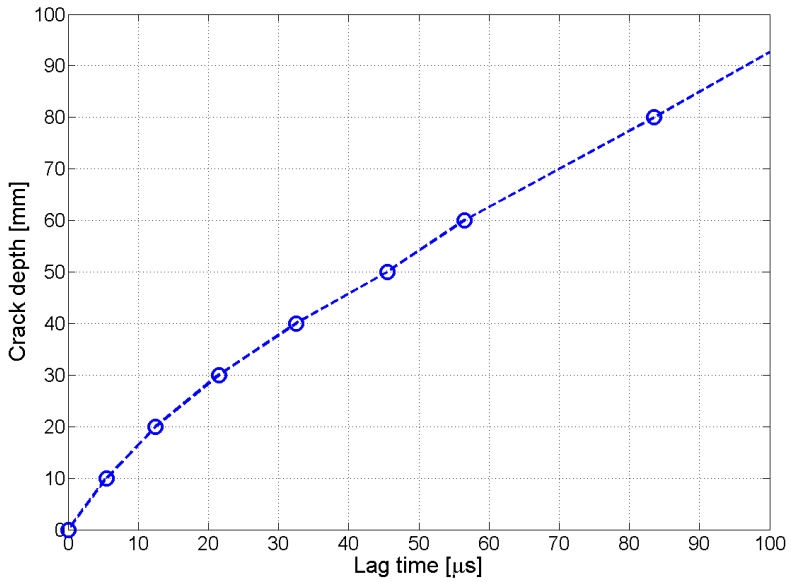

Figure 4.19 Lag time vs crack depth by numerical analysis in concrete beam

4.6.2.2 Energy velocity based crack determination via ATME

In this section, different approach is developed and utilized to estimate vertical crack depth in concrete. It is based on diffused energy velocity. According to Seher, et al. (Matthias Seher, Chi-Won In, Jin-Yeon Kim, Kimberly E. Kurtis, & Laurence J. Jacobs, 2012) (or see Appendix), diffused energy velocity depends on the frequency (i.e. the diffusion parameters) and it is reported that there is an approximately linear relationship between the minimum propagation distance and the peak energy arrival time and diffused energy velocity at 500 kHz is approximately 912.3 m/s for the diffusion parameters (diffusivity: 10 m^2/s and dissipation: 21000 /s). Thus, based on this assumption, the ATME can be calculated from this known velocity and shortest propagation path of diffuse wave for each vertical crack depth. In order to calculate the diffused energy velocity, further FE simulation has been performed for 500 kHz frequency with

diffusivity (10 m^2/s) and dissipation (45000 /s) for the vertical crack cases. Figure 4.20 clearly shows that the linear relation between the peak arrival time and minimum travel distance at 500 kHz is still hold for these vertical crack cases. In this specific case, the energy velocity (slope) is determined to be 1398.9 m/s in figure 4.20. Figure 21 shows diffuse energy velocity based curve is in good agreement with the previously defined lag time based curve.

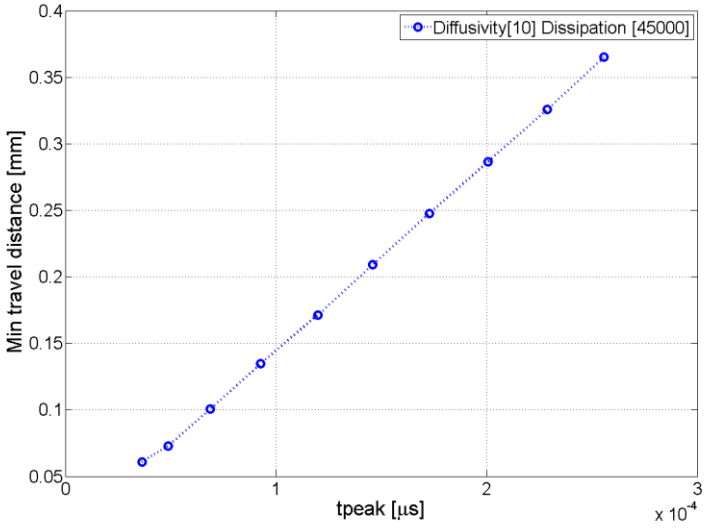

Figure 4.20: tpeak vs min travel distance at 500 kHz

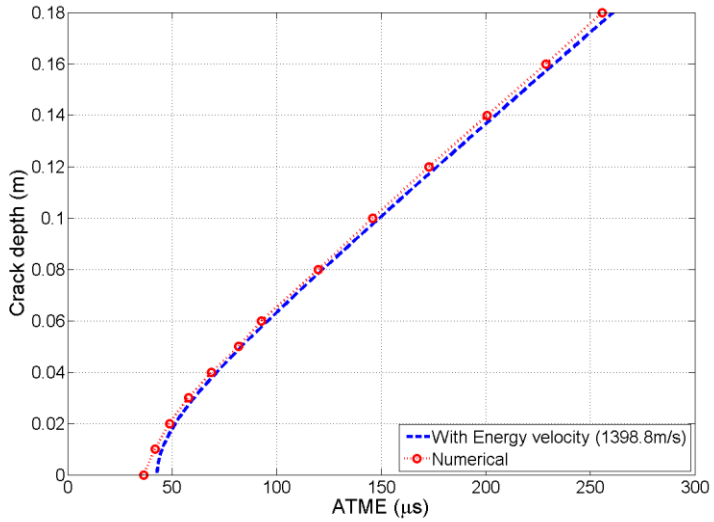

Figure 4.21: comparison of two methodologies (energy velocity based method and lag time based method)

Therefore, once the ATME is obtained from an experimental energy evolution curve, crack depth can be inferred from this energy velocity based method. Figure 4.22 shows the results of crack depth estimation from the three different experiments and figure 4.23 demonstrate the estimation of surface crack depth as a function of applied load in three different experiments. As mentioned above, the hysteresis behavior is clearly shown in this figure.

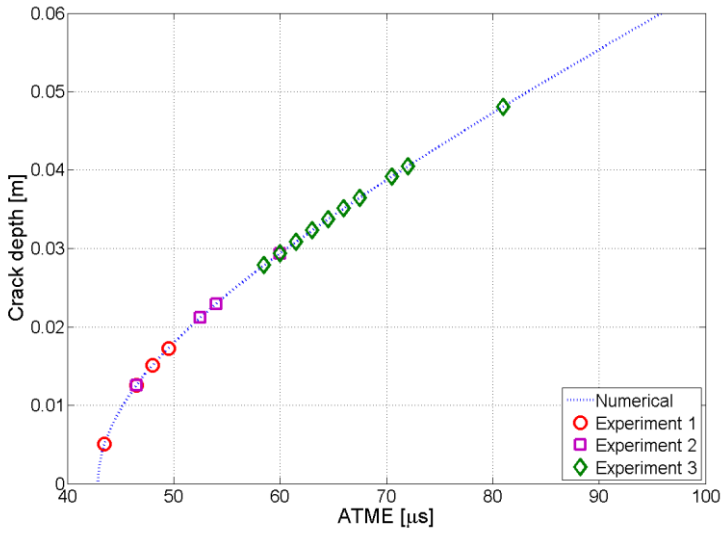

Figure 4.22: Crack depth estimation from experimentally determined ATME

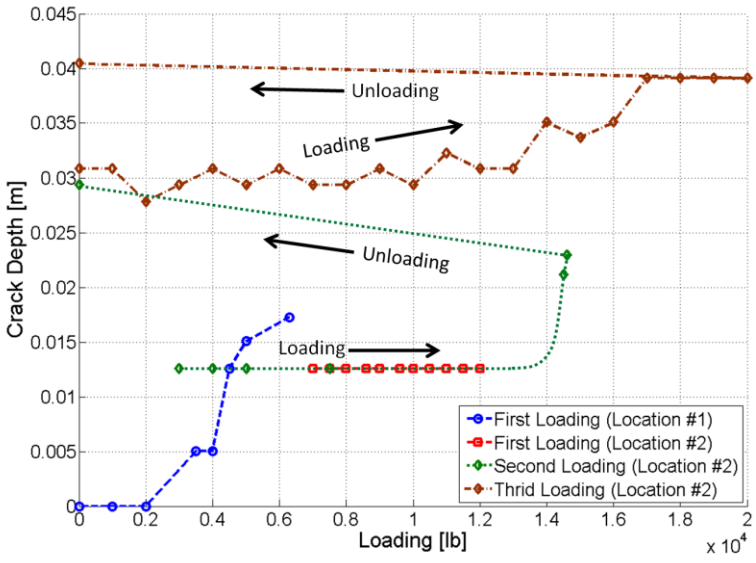

Figure 4.23: Crack depth estimation in terms of loading

4.7. Conclusions and Recommendations

This research demonstrates that the arrival time of the maximum energy (ATME) is a good indicator for the characterization of the crack depth and that open crack depth can be determined from the lag time or the ATME by the diffuse ultrasonic method in concrete samples in a reliable and reproducible way for both these idealized samples and real beam. However, in order to be more applicable to a realistic civil infrastructure, the technique requires a high signal to noise ratio to guarantee reliable curve fitting and point like receiver is necessary to avoid the phase cancellation effect.

The main steps to determine the depth of a single vertical crack in concrete are straightforward. As described previously, the diffusion parameters that are retrieved from experimental measurements in the uncracked region of the sample are used as a input parameters for the simulation. The peak energy arrival time is then determined from the numerical energy evolution curves of two different simulations, one without a crack

and the other with a crack. The lag time, defined previously as the difference between the peak arrival time in the cracked and uncracked regions, is the measure used here to infer the single vertical crack depth. The lag time is obtained by comparing the peak energy arrival time obtained above from two different simulations. Once the relation is established, the depth of the single vertical crack can be determined from the curve and the experimental lag time.

Second proposed method is based on diffused energy velocity. Once the energy velocity is known and shortest path of diffuse wave from transmitter and receiver, ATME can be obtained from this relationship numerically, then vertical crack depth can be inferred from this numerical curve with experimentally determined ATME.

In conclusion, this research provides promising results in the characterization of surface opening vertical crack depth in concrete and an understanding of the important necessary steps and the difficulties that come with the method. Thus, further research should employ the technique to characterize different crack geometries and size, and more complex configurations.

CHAPTER 5

MONITORING SELF HEALING PROCESS IN CONCRETE

This chapter demonstrates the capabilities of the diffuse ultrasonic technique to quantify the degree of self-healing of cracks in concrete. The diffuse ultrasonic parameters from a two-dimensional (2-D) diffusion model are evaluated to characterize the self-healing process and microscopic measurements of crack width over a 120 day exposure period is compared to verify the sensitivity of the technique to crack healing.

5.1. Introduction

The cracks in concrete can have a large influence on the transport and durability of structures. Cracks increase the penetrability of concrete, reduce concrete strength, decrease aesthetics of structures, and may indicate deterioration of the structure (Rodriguez, 2001).

It has been reported by many authors that under certain conditions cracks in concrete can self-heal and reduce the penetrability of chlorides into the fractured section.(Jacobsen, Marchand, & Gerard, 1998). Autogenous healing of cracked concrete can occur by: (1) the formation of calcium carbonate or calcium hydroxide (Neville, 1997), (2) sedimentation of particles (Edvardsen, 1999), and (3) continuing hydration and swelling of the cement matrix (Neville, 1997). The composition of the matrix (e.g., the amount, type, and particle size distribution of the cement and any supplementary cementitious materials (SCMs) like fly ash, slag, silica fume, or

metakaolin), then, can play an important role in the ability of a concrete to self-heal (Rodriguez, 2001; M. Sahmaran et al., 2008; Ter Heide, 2005).

Previous research by Heide (Ter Heide, 2005) and Lauer and Slate (Lauer & Slate, 1956) has shown that the following environmental conditions must be present for self-healing to occur: the presence of water; stability of the crack; and that the liquid may not lead to a leaching or dissolution reaction. With interest in extending the service life of coastal infrastructure, investigation of self-healing of precast prestressed concrete piles in the marine environment is of practical, economic relevance. The marine environment provides all of the necessary environmental conditions for self-healing to occur.

In addition, the width of the crack has been found to be a critical parameter for both the occurrence and rate of self-healing. Research has shown that cracks with an initial effective width of 50 microns can reduce to 20 microns within 24 hours, and that cracks with an initial effective width of between 50 and 100 microns reduce to an effective width of 20 microns within seven days due to self-healing (Clear, 1985). Other studies have shown that cracks with initial effective widths of 200 microns can completely seal after five to seven weeks of exposure to a moist environment (Edvardsen, 1996). In wider cracks, self-healing is less effective (Edvardsen, 1999; M. Sahmaran, 2007).

In the past decade, a number of techniques have been used to detect and possibly to quantify the extent of self-healing in concrete. In many cases, the mechanical and transport properties of the concrete have been measured with different methods including uniaxial tension testing and water permeability testing. Recently the ultrasonic phase

velocity (UPV) method has been applied to assess the healing capacity of cracked specimens (Abded-Jawad & Haddad, 1992). Jacobsen et al. (Jacobsen et al., 1995) found that the self-healing of microcracking due to freeze/thaw cycling can be monitored by UPV and that UPV parameters correlate moderately with the extent and stage of deterioration (Jacobsen et al., 1996). Sahmaran et al. (M. Sahmaran et al., 2008) have investigated the influence of fly ash on self-healing process by measuring the rate of change of UPV in concrete. Zhong and Yao (Zhong & Yao, 2008) also used the UPV method to define the ratio of damage degree to self-healing in high and normal strength concrete damaged at different ages. However, it has been found that although UPV measurements can detect the occurrence of crack healing, the method is not capable of quantitatively determining the extent of crack healing (Aldea et al., 2000).

A stress wave transmission technique (Aldea et al., 2000) has also been used to characterize the process of self-healing by quantifying the extent of healing in concrete through measured ultrasonic parameters. It has been demonstrated that the ultrasonic signal transmission measurement, when performed under laboratory conditions, can be very sensitive to the presence of cracking damage in concrete (Sellick et al., 1998). Plus, it is noted that the signal transmission measurement is more sensitive to the extent of cracking in concrete than the UPV measurement (Song et al., 1999). However, the practical application of the signal transmission measurements in concrete has not been realized because of inconsistency associated with coupling variability. In addition, this transmission measurement is unable to clearly distinguish among crack widths above 100 microns (Aldea et al., 2000).

Recently, diffuse ultrasonic techniques have demonstrated their capability to characterize microcracking and to measure the depth of large cracks in cement based materials. Deroo et al. (Deroo et al., 2010) quantified microcracking damage in concrete due to alkali silicate reaction (ASR) and thermal shock and by measuring ultrasonic diffusivity and dissipation. It has also been confirmed that diffusivity is sensitive to microcracking and microstructural behavior as also indicated in [(Becker et al., 2003; Punurai, Jarzynski, Qu, Kurtis, et al., 2007; Schurr et al., 2011). Ramamoorthy et al**.** (Ramamoorthy et al., 2004), In et al. (In et al., 2012), and Seher et al. (M. Seher et al., 2012) have numerically and experimentally shown that the diffuse ultrasonic technique can measure the depth of surface opening cracks using the arrival time of maximum energy (ATME).

5.2. Ultrasonic Measurement Procedures and Preliminary Results

5.2.1. Experimental setups and procedures

Same experimental setups and measurement procedures as described in previous chapter (Determination of crack depth in concrete) have been applied to all concrete prism specimens (5 x 5 x 18 in) to measure the material parameters (the diffusivity and dissipation) as well as the ATME. All measurements are conducted with 6cm separation distance between transducers, which is systematically centered with respect to the opening point of the crack. The transducers are placed away from the edges of the specimens to avoid edge effects. A viscous couplant is used to couple both transducers to the specimen. During the measurements, the transmitting transducer is fixed, while the receiving transducer is completely removed and reattached three different times to

generate a reliable data set and give an error analysis. All measured signals are filtered with a 4 MHz low pass filter and amplified by 40 dB with a preamplifier (the receiver part of Panametrics 5058 PR) to improve signal-to-noise ratio, and then post-amplified by 20dB with a signal conditioning amplifier (Digital Wave DW FTM 4000). The signals are sampled with a sampling frequency of 50 MHz, recorded (200000 record points), and then averaged (1000 signals) all using an oscilloscope. A schematic of the ultrasonic diffusion measurement setup is shown in figure 5.1.

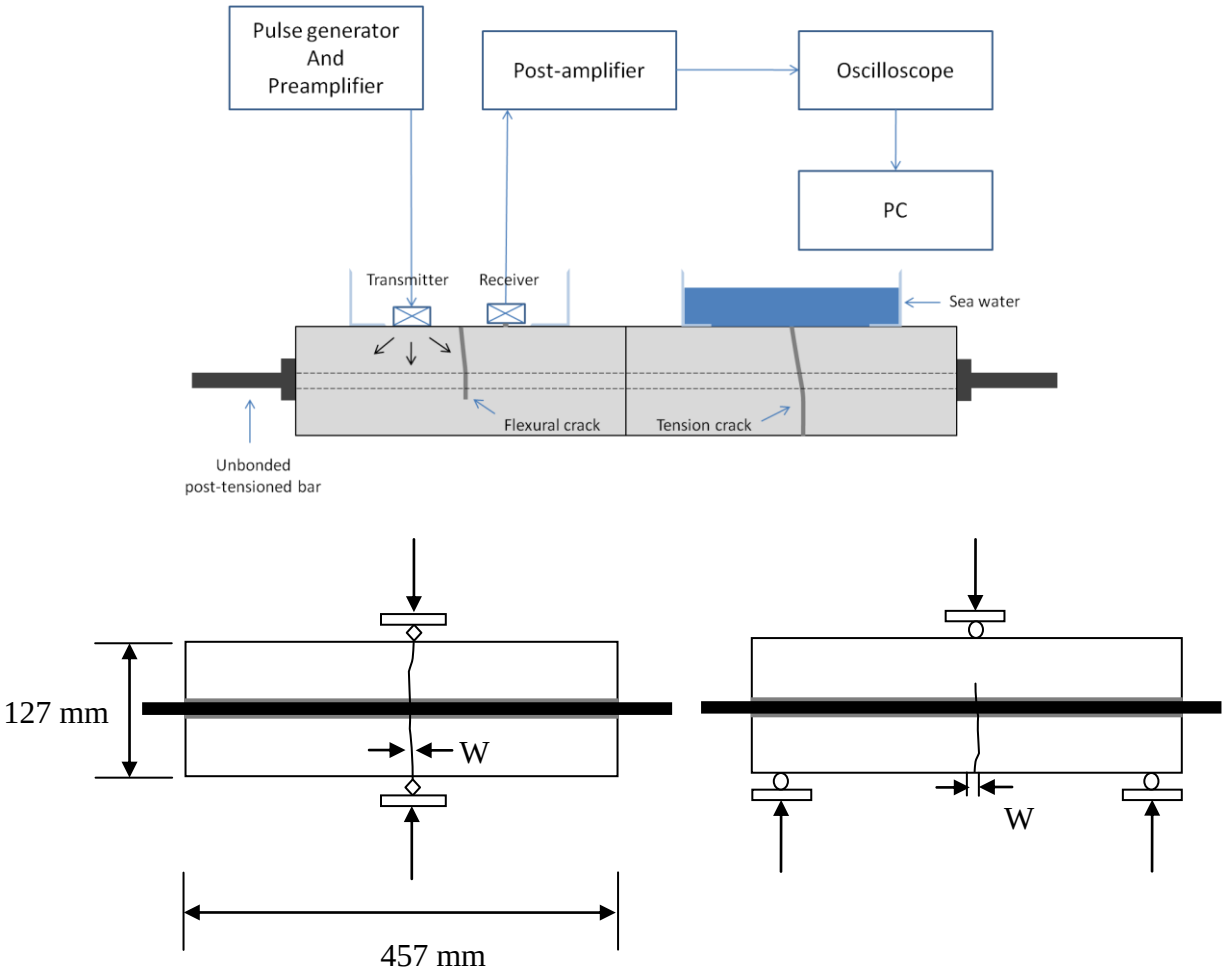

Figure 5.1: Layout of experimental setup

5.2.2 Preliminary Measurements

To obtain the initial diffuse ultrasonic parameters, experiments are conducted on the concrete specimens after cracking but before exposure to the self-healing environment. A typical measured ultrasonic signal without cracks is shown in figure 5.2. A straight forward time-frequency analysis is performed on the measured ultrasonic signals to calculate the spectral energy density $\langle E(x,t,f)\rangle$ at frequency f (and at the measurement point x). As shown in figure. 5.3, data points of the experimentally determined spectral energy density $\langle E(x,t,f_c)\rangle$ (calculated for a frequency band with the center frequency f_c,500 kHz) in a limited time range, in which the energy density is clearly above noise level, is considered for the curve fit. Figure 3 shows curve fit for the time domain signal shown in figure 5.2.

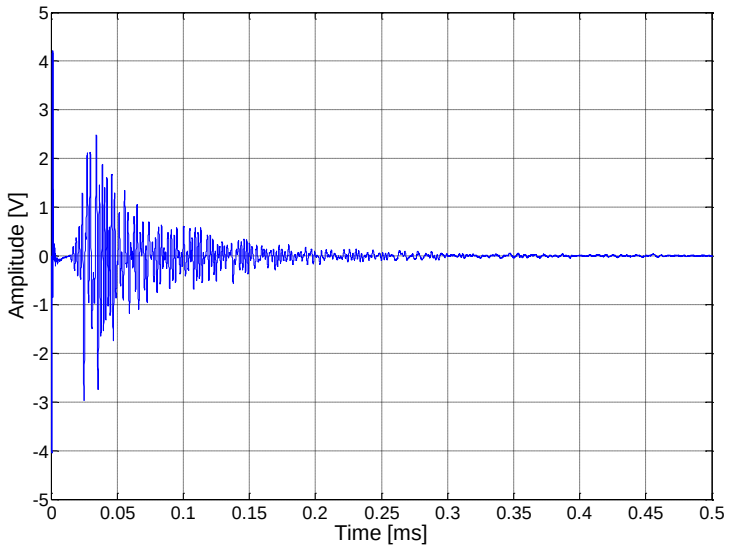

Figure 5.2: Typical diffuse ultrasound signal in uncracked control S50MK5 specimen

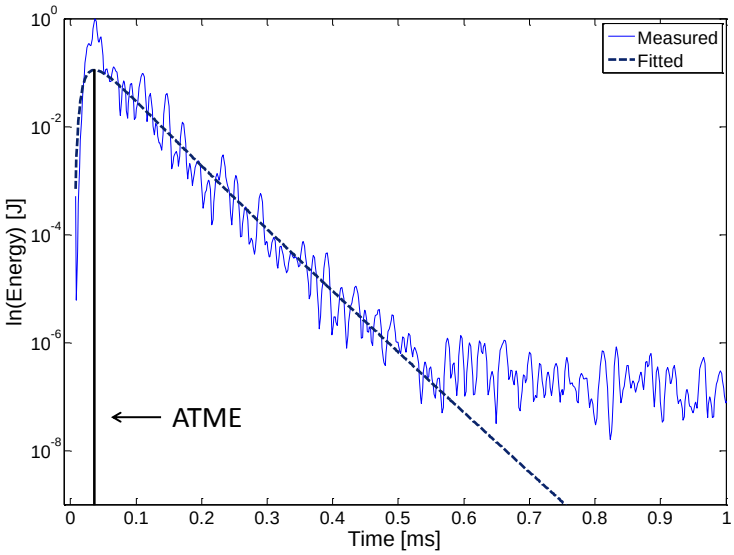

Figure 5.3: Energy density curve and curve fitting in uncracked control S50MK5 specimen

The experiment on the cracked specimens is identical to that on the uncracked control specimens. Transducers are placed consistently 30 mm off on both sides of the crack after water in the container is removed. Figure 5.4 shows the example waveform from one (T2) of the S50-MK5 specimens with a tension crack before self-healing. As expected, comparison of figures 5.2 and 5.4 clearly shows a delay of the peak arrival time, so that the crack causes the waveform to be stretched due to the more tortuous wave paths which takes the waves a longer time to reach the receiver; this effect causes the measured diffusivity, D, to be lower. The delay of the ATME, which is related to the D, is also confirmed in the comparison of figures 5.3 and 5.5. Physically, the delay in the diffuse waveform or energy is due to low transmission or absence of diffuse energy transfer across the open parts of the crack. As a result, the ATME also increase.

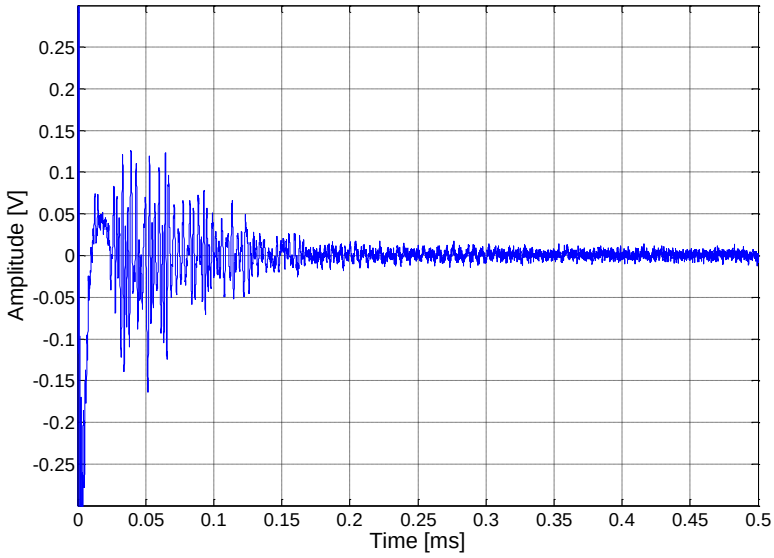

Figure 5.4: Diffuse ultrasonic wave after tension crack in S50-MK5 specimen (T2)

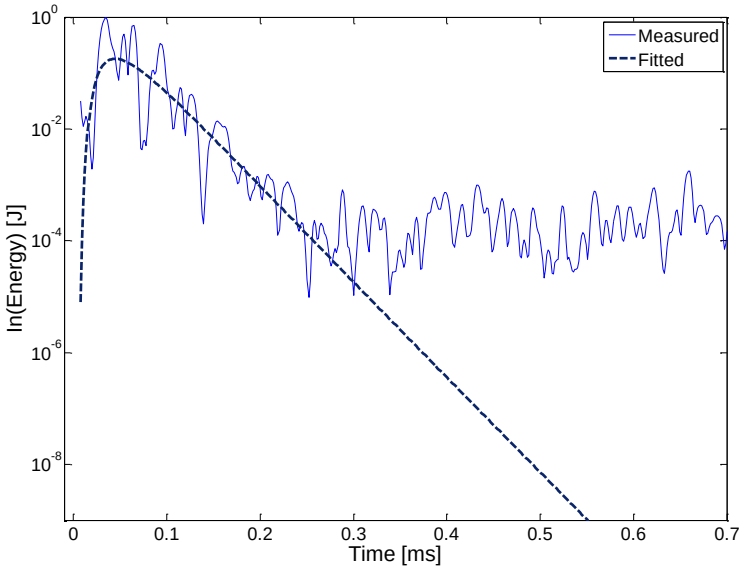

Figure 5.5: Energy density curve in tension-cracked S50MK5 specimen (T2)

5.3 Sample Preparation and crack initiation

Five mix designs are chosen for this study based upon the finding of Holland (Holland, 2012) which demonstrated that these concretes exhibit varying levels of self-healing

capability. The mix designs are a 0.30 water to cementitious materials ratio (w/cm) mix design with total cementitious material content of 950lb/cu. Yd(564kg/cu m), developed using ACI 211.4R-08 (ACI, 2008). Table 5.1 gives the cementitious material compositions of each mix design investigated; six specimens (5 x 5 x 18 in.) are cast from each mix design: two uncracked control specimens (C1, C2), two tensile crack specimens (T1, T2), and two flexure crack specimens (F1, F2). Further details on the materials, mix designs, and cracking process can be found in (Holland, 2012)

Table 5.1: Self-healing mix design binder compositions

Mix ID	Cement fraction in binder (%)	ASTM C 150 Cement Type	Slag (%)	Metakaolin (%)	Fly Ash (%)
F25	75	II	0	0	25
T3-F15	85	III	0	0	15
Type II	100	II	0	0	0
S35-MK5	60	II	35	5	0
S50-MK5	45	II	50	5	0

The specimens are moist cured and then pre-cracked to generate a through-specimen tensile crack or a flexural crack at 14 days of age. The crack orientations are designed to represent the likely cracking patterns in the field, based upon observations of cracking in piles formed due to reflective tension cracking and flexural cracking during handling. Through tensile cracks are created using knife edge bearings and flexural cracks are created using a three-point (center-point) bending configuration. After cracking, 6.2 MPa of prestressing is applied to the specimens to simulate the current level of prestressing and to control the crack widths. To initiate self-healing, specimens are then ponded with a simulated seawater solution (165g/L NaCl) for 120 days to represent conditions which may exist in the field in submerged structural elements.

5.4 Results at monitoring self healing

The average diffuse ultrasonic parameters (diffusivity, dissipation, and ATME) of each uncracked control specimens recovered using Eq. (4) for each mix design at 500 kHz are shown in table 5.2. It is noted that the average diffuse ultrasonic parameters are statistically different among mix design with significance level, 0.1. The properties of the uncracked specimens show that the values of diffusivity and dissipation depend on the porosity or density of concretes, which in turn depends upon their composition. Note that the water-to-cementitious materials ratio, aggregate contents, types are maintained all the same except for the T3-F15 specimens (Type III cement), so that differences in initial diffusivity and dissipation values can be related to the variation in the cementitious materials used in these concrete designs. For example, Type II specimens, which contain cement only, show a lower diffusivity and higher dissipation than those of mix designs containing SCMs (fly ash, metakaolin and slag). This is presumably due to the coarser and more microporous microstructure with a less pronounced aggregate/paste interfacial transition zone resulting from the use of SCMs. (Thomas, Scott, Bremner, & Bilodeau, 2008). The increase of diffusivity and the decrease of dissipation indicate that the ultrasonic energy diffuses faster (i.e. a low level of scattering events and low energy loss) due to the increased density and decreased interfacial defects.

The average diffuse ultrasonic parameters tabulated in table 5.2 are measured after exposure to the seawater ponding. As shown in table 4, the results from before ponding demonstrated that diffusivity is influenced by the saturation state of the specimens; diffusivity and dissipation showed a 31 to 49% increase and 10 to 13 % decrease in Type II, 26 to 36% increase and 29 to 38 % decrease in S50-MK5, 14 to 21% increase and 28 to27% decrease in S35-MK5, respectively. Note that average diffusion

parameters for F25 and T3-T15 are not measured before ponding. These changes can again be explained by the different microstructures, which affect the rate at which seawater can penetrate from the surfaces into the surrounding concrete(Holland, 2012). In addition, the increase in diffusivity the decrease in dissipation occur over time in all uncracked control specimens as shown in table 4 and 6. This suggests that hydration of the binder continues to occur, as are expected on specimens monitored from the beginning after only 2 weeks of age. Moreover, the long-term diffusivity values in cracked specimens are statistically equivalent to uncracked specimens. This suggests that given a sufficient period of time for small cracks (< 200 microns) to self-heal, the cracked specimens will approach the behavior of the uncracked specimens. It is very important from an experimental perspective that the recovery of the diffusivity and dissipation simply indicates that the crack has fully healed.

Table 5.2: Initial average diffuse ultrasonic parameters for each mix design

	MIX ID	F25	T3-F15	TYPE II	S35-MK5	S50-MK5
C1	ATME (μs)	-	37	35.77	36.58	36.67
	Diffusivity (m^2/s)	-	12.52	12.06	12.76	13.05
	Dissipation(1/s)	-	26573	31295	25512	24911
C2	ATME (μs)	34.1	35.5	33.18	35.96	37.38
	Diffusivity (m^2/s)	12.94	12.62	12.2	12.89	13.07
	Dissipation (1/s)	32186	29334	38291	27459	23069

5.4.1. Effect of self healing process on crack width

The crack widths were measured immediately after cracking and post-tensioning using an Elcometer 900 crack microscope with a 50x magnification and 25.4 μm tolerance rotating scale. The readings were continued weekly until the end of the 120 day ponding to measure crack closure due to swelling and continued hydration of the cement

matrix. The exposure face of flexure samples was the tension face during cracking, where the maximum crack widths would be observed. For through tensile crack samples, the exposure face was the face of the sample not subjected to the knife edge bearings. Readings were taken along the exposure face of each sample at 12.7 mm increments, for a total of 9 crack width measurements being used to calculate the mean and standard deviation.

The average crack widths measured with a crack microscope after different durations of ponding on the tension and flexure crack specimens for the five mix designs are given in table 5.3. From these data, it is clear that the cracks in all samples experience self-healing , and that this occurs after 35 to 50days of ponding, but samples from S35-MK5 or Type II demonstrate the fastest crack closing compared to others. Also, the results verify that crack healing is occurring from both faces of the crack towards the interior of the crack. This leads to a decrease in crack width over time, which may eventually bridge the crack (Qian, Schlangen, Ye, & Brreugel, 2009), and as a result, the diffusivity will be expected to increase over time. Figure 5.6 to 5.10 show a comparison of the measured crack width and diffusivity over time.

Table 5.3: Crack width measurements over time

		Exposure time (day)	0*	7	14	21	28	35	42	49	63	77	91	105	119
F25	F1	Crack width (μm)	33.34	25.4	19.05	8.47	-	4.23	-	4.23	8.47	8.47	8.47	8.47	8.47
	F2		-	-	-	-	-	-	-	-	-	-	-	-	-
	T1		120.65	59.27	33.87	25.4	-	25.4	-	21.17	21.17	21.17	21.17	16.93	16.93
	T2		116.11	29.63	25.4	33.87	-	4.23	-	8.47	8.47	8.47	8.47	8.47	8.47
T3-F15	F1	Crack width (μm)	34.93	19.05	19.05	16.93	-	15.88	-	12.7	12.7	8.47	8.47	8.47	8.47
	F2		28.58	25.4	25.4	21.17	-	12.7	-	12.7	8.47	12.7	12.7	12.7	12.7
	T1		139.7	63.5	42.33	21.17	-	29.63	-	21.17	21.17	25.4	25.4	21.17	21.17
	T2		152.4	38.1	38.1	25.4	-	8.47	-	19.05	19.05	19.05	19.05	19.05	19.05
Type	F1	Crack	80.43	31.75	50.8	59.26	55.03	42.33	-	38.1	38.1	38.1	33.86	38.1	29.63

II	F2	width (μm)	96.24	67.73	50.8	42.33	50.8	50.8	-	46.57	46.57	46.57	38.1	38.1	33.87
	T1		186.3	76.2	88.9	63.5	42.33	50.8	-	50.8	46.57	46.57	42.33	46.57	42.33
	T2		121.4	67.7	59.3	50.8	50.8	38.1	-	42.3	38.1	38.1	33.9	38.1	33.9
S35-MK5	F1	Crack width (μm)	64.91	42.33	67.73	33.87	50.8	38.1	38.1	38.1	38.1	38.1	38.1	38.1	38.1
	F2		82.55	25.4	33.87	42.33	33.87	25.4	29.72	29.63	25.4	25.4	21.17	21.17	25.4
	T1		76.2	33.87	33.87	29.63	33.87	29.63	29.72	29.63	29.63	25.4	25.4	25.4	21.17
	T2		94.54	44.45	25.4	38.1	41.28	22.23	25.4	25.4	25.4	29.63	29.63	25.4	29.63
S50-MK5	F1	Crack width (μm)	121.36	42.33	57.15	38.1	44.45	25.4	33.78	33.87	33.87	29.63	33.87	29.63	38.1
	F2		73.03	34.93	22.23	25.4	38.1	31.75	31.75	33.87	33.87	29.63	29.63	29.63	29.63
	T1		104.78	69.85	44.45	53.98	57.15	41.28	41.4	41.28	38.1	38.1	34.93	34.93	31.75
	T2		158.75	46.57	29.63	59.27	55.03	46.57	46.48	46.57	42.33	38.1	33.87	38.1	29.63

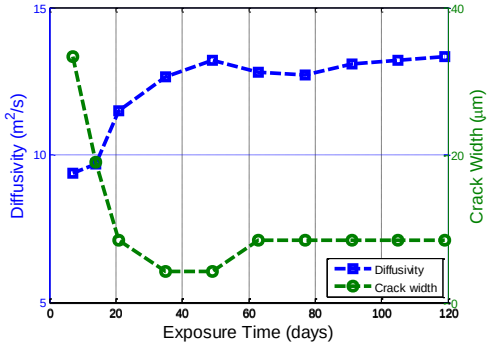

F1

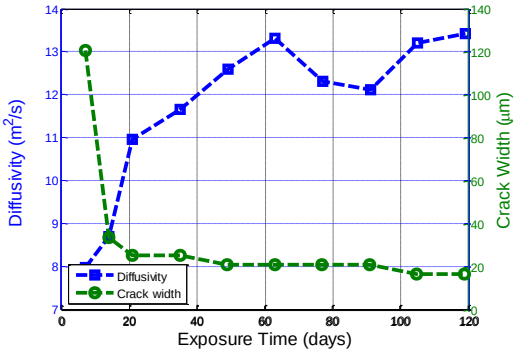

T1

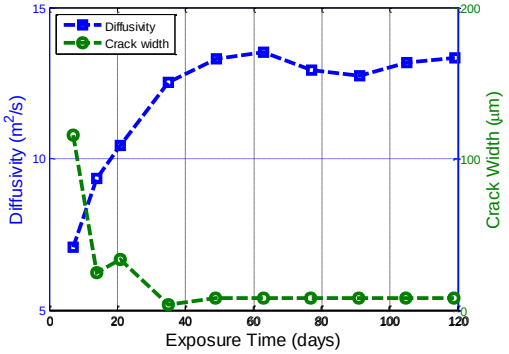

T2

Figure 5.6: Comparison of diffusivity and crack width in F25 sample

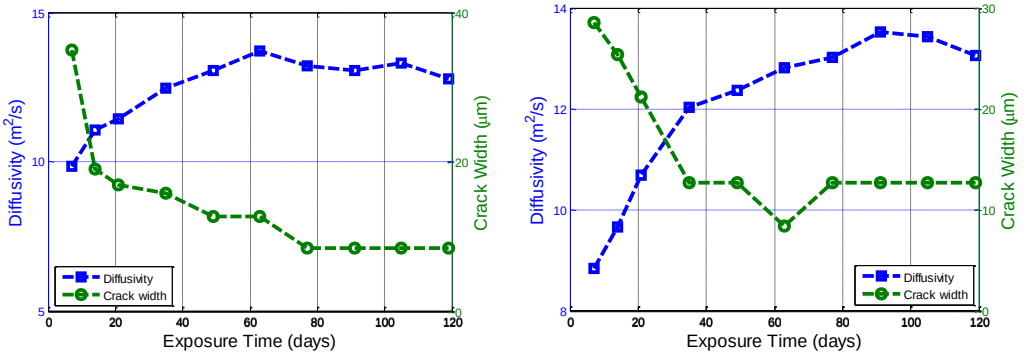

F1 F2

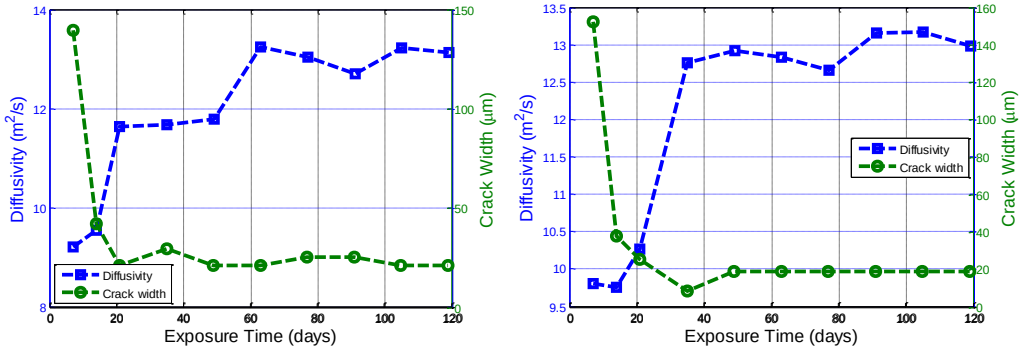

T1 T2

Figure 5.7: Comparison of diffusivity and crack width in T3-F15 sample

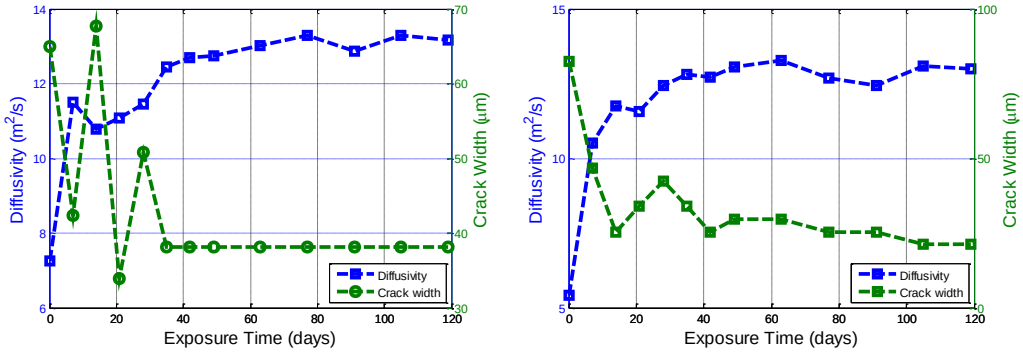

F1 F2

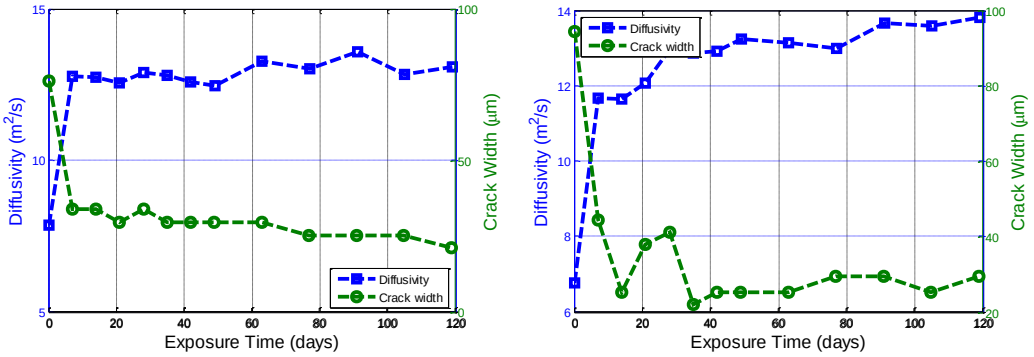

T1 T2

Figure 5.8: Comparison of diffusivity and crack width in S35-MK5 sample

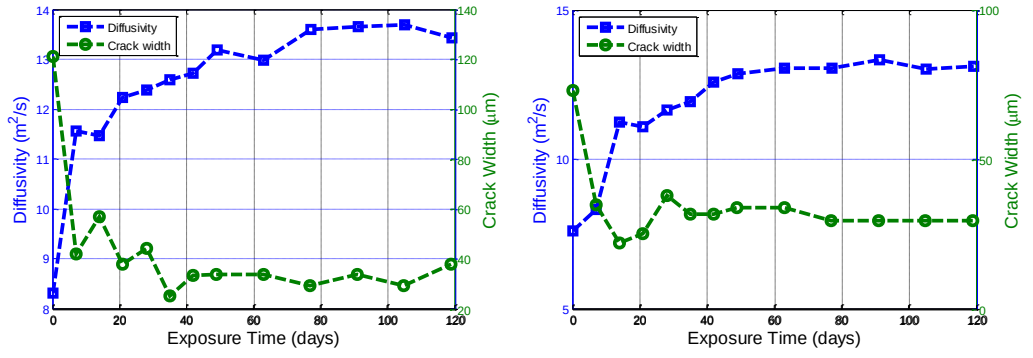

F1 F2

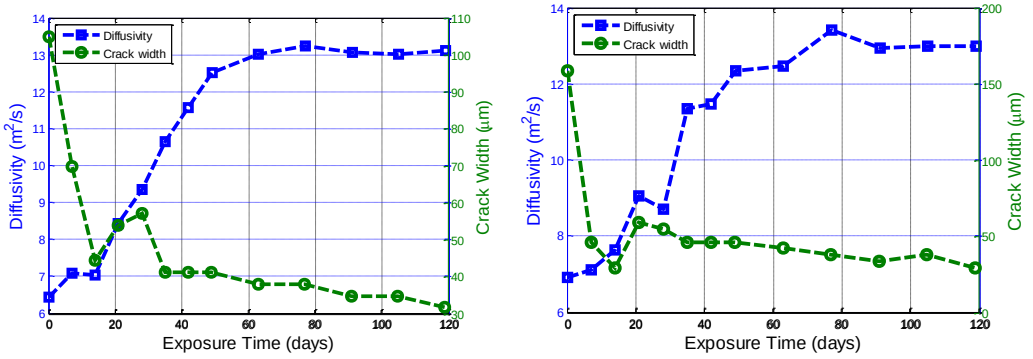

T1 T2

Figure 5.9: Comparison of diffusivity and crack width in S50-MK5 sample

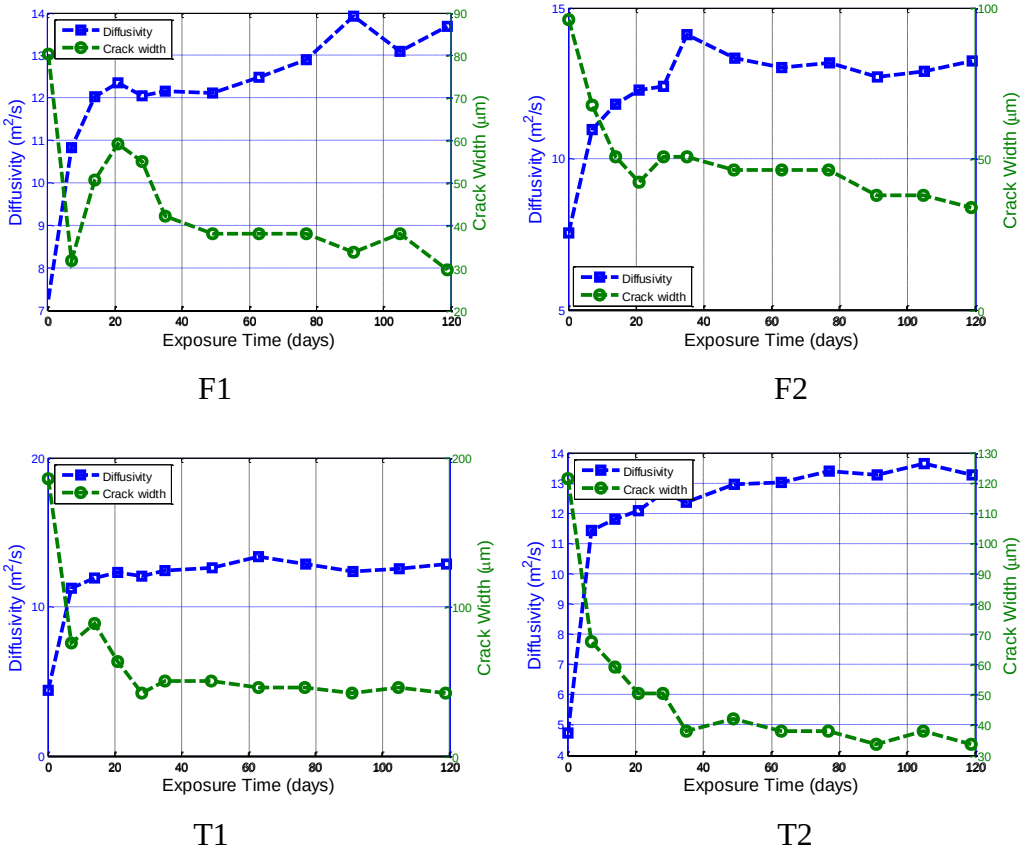

Figure 5.10: Comparison of diffusivity and crack width in Type II sample

5.4.2 Effect of self healing process on diffusion parameters

This research shows that diffusion parameters (diffusivity, dissipation, and ATME) are sensitive to microcracking and microstructural behavior and can be a good indicator for the autogeneous healing process in concrete.

5.4.2.1 The arrival time of maximum energy (ATME) and diffusivity

The results of diffusivity and the ATME with flexure and tension cracks for the five mix designs until 120th day are presented in table 5.4 and 5.5, respectively. Figures 5.11 and 5.12 show diffusivity and the ATME. The results on the tables show that each mix design had different healing capabilities. For example, S35-MK5 samples exhibits the relatively fast rate of extent of self-healing in the beginning of exposure to the healing

environment, while in contrast, S50-MK5 shows the lowest rate of extent of self-healing. The results confirm the studies of Holland (Holland, 2012), where crack width measurements was used to examine self-healing in these concretes and showed that the S35-MK5 shows the fastest self-healing process. In addition, it is observed that diffusivity of some samples after exposure to water ponding excesses averaged parameters of intact samples. Thus, It can be drawn that existing microcracks even not initiated by tension or flexure crack in such samples can be sealed with self healing process , which in terns will cause to increase diffusivity.

Ramamoorthy et al. (Ramamoorthy et al., 2004) and Quiviger et al. (Quiviger et al., 2012) have shown that the ATME is sensitive to the open crack depth in concrete. Here the ATME is also shown to be correlated with crack width, which can be interpreted in this condition to represent the extent of healing. However, it should be noted that the measured ATME values can be influenced by the fact that bridging will occur at relatively closer crack faces, and the hydration products and other precipitates could fill and bridge the portions of crack behind the crack tip, so that the diffuse ultrasonic energy can transmit through healed spots in the face of the crack (without circumnavigating around the crack tip). Therefore, the ATME is not necessarily proportional to the crack depth, and, therefore, the ATME values will strongly depend on where on the crack face self-healing occurs. This leads to fluctuations in the measured ATME values as the path of the diffuse energy varies with time, although their trends are quite similar to those of diffusivity. Also, the ATME can be influenced by small changes in the separation distance between transducers. This effect can contribute to the ATME measurement errors. These points help explain why the ATME has a larger fluctuation in results than

the diffusivity measurements. Therefore, the diffusivity appears to be a more reliable and robust indicator of the degree of self-healing, and also the diffusivity measurement does not require a very accurate separation distance between the two transducers. Additionally the diffusivity is not influenced significantly by the pathway that can be changed by the partial closure of the crack due to healing, thereby showing a more consistent result for the extent of self-healing compared to the ATME.

Table 5.4: Diffusivity measurements over time

		Exposure time (day)	0*	7	14	21	28	35	42	49	63	77	91	105	119
F25	F1	Diffusivity (m^2/s)	-	9.39	9.69	11.50	-	12.65	-	13.20	12.82	12.72	13.07	13.21	13.32
	F2		-	-	-	-	-	-	-	-	-	-	-	-	-
	T1		-	7.97	8.68	10.96	-	11.66	-	12.59	13.32	12.31	12.10	13.21	13.42
	T2		-	7.08	9.34	10.43	-	12.51	-	13.31	13.52	12.92	12.74	13.17	13.32
T3-F15	F1	Diffusivity (m^2/s)	-	9.83	11.06	11.42	-	12.45	-	13.05	13.70	13.21	13.06	13.29	12.76
	F2		-	8.84	9.66	10.68	-	12.03	-	12.36	12.80	13.02	13.52	13.42	13.06
	T1		-	9.21	9.53	11.64	-	11.67	-	11.79	13.25	13.04	12.71	13.21	13.14
	T2		-	9.81	9.75	10.26	-	12.76	-	12.92	12.83	12.66	13.16	13.17	12.98
Type II	F1	Diffusivity (m^2/s)	7.26	10.15	11.30	11.82	12.05	12.17	-	12.10	12.49	12.89	13.93	13.10	13.68
	F2		7.55	10.98	11.80	12.28	12.39	14.11	-	13.32	13.03	13.18	12.70	12.88	13.25
	T1		4.42	11.26	11.94	12.29	12.07	12.43	-	12.65	13.39	12.87	12.38	12.54	12.86
	T2		4.73	11.44	11.81	12.08	12.67	12.35	-	12.95	13.03	13.38	13.26	13.65	13.26
S35-MK5	F1	Diffusivity (m^2/s)	7.26	11.50	11.31	11.08	11.44	12.45	12.69	12.74	13.01	13.29	12.88	13.29	13.16
	F2		5.42	10.52	11.76	11.57	12.44	12.81	12.72	13.06	13.26	12.68	12.45	13.10	12.99
	T1		7.86	12.77	12.73	12.56	12.91	12.82	12.57	12.46	13.26	13.02	13.58	12.85	13.09
	T2		6.75	12.39	11.65	12.07	12.97	12.87	12.91	13.23	13.15	13.00	13.67	13.60	13.82
S50-MK5	F1	Diffusivity (m^2/s)	6.44	7.09	7.03	8.44	9.36	10.66	11.56	12.53	13.03	13.23	13.07	13.03	13.11
	F2		6.90	7.11	7.63	9.06	8.70	11.35	11.46	12.34	12.46	13.42	12.94	13.00	13.00
	T1		8.30	11.55	11.47	12.24	12.38	12.59	12.71	13.19	12.98	13.59	13.66	13.69	13.43
	T2		7.60	8.31	11.25	11.10	11.64	11.94	12.59	12.87	13.06	13.06	13.32	13.04	13.13

Table 5.5: ATME measurements over time

		Exposure time (day)	0*	7	14	21	28	35	42	49	63	77	91	105	119
F25	F1	ATME (µs)	-	33	35	35.5		31		32	34	33.75	32.5	33.5	33.5
	F2		-	-	-	-	-	-	-	-	-	-	-	-	-
	T1		-	35.25	33	31	-	30	-	28.5	31	28.5	29.5	33.5	31
	T2		-	31.5	32	30.5	-	30.5	-	30	27.5	33	32.5	32	32
T3-F15	F1	ATME (µs)	-	36.75	36	36	-	32	-	32.5	32	35	35	36	35
	F2		-	36	36	37.5	-	33	-	33	34.5	34	35.5	36	36
	T1		-	31.5	32.5	33.5	-	33.5	-	31.5	33.5	33	34	35.5	35
	T2		-	33.75	33.5	34.5	-	32	-	33	32	33.5	35.5	37	37.5
Type II	F1	ATME (µs)	47	37.5	33	32	32	33.5	-	30.5	29	31.5	28	30	33
	F2		45.5	31.5	31	31	29.5	27.5	-	34	33	32.5	33.5	31	30.5
	T1		59	31.5	31	29	29	31	-	33	34	33	32.5	29	27
	T2		56	30.5	29.5	31	33	32	-	31.5	31.5	33	32	34.5	32.5
S35-MK5	F1	ATME (µs)	47.5	35	37	36.5	36.5	33.5	34	34.5	33.5	34.5	37	35	34.5
	F2		54	36	34	36.5	33.5	33.5	32	33.75	32.5	36	35.5	34	34
	T1		46.5	31	32	30	31.5	32.5	31	32.5	32.5	35.5	36.5	33	34.5
	T2		49	30.5	32.5	31.5	32.5	31.5	30	33	32.5	32	35	32.5	32
S50-MK5	F1	ATME (µs)	51.5	44.5	48.5	43	39.5	37	34.5	35	34	34.5	37.5	34	31
	F2		47	40.5	45.5	42	42.5	35	37	36.5	37.5	37	40	34.5	33.5
	T1		43.5	34	34.5	33	34	33	30.5	31	33.5	33.5	34.5	32	31
	T2		45	38.5	34	35.5	35.5	34	34	33.5	34.5	34.5	34	33.5	36

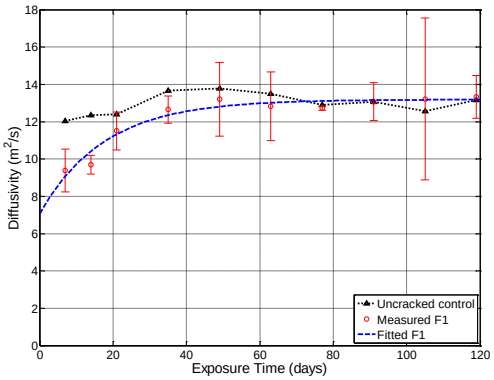

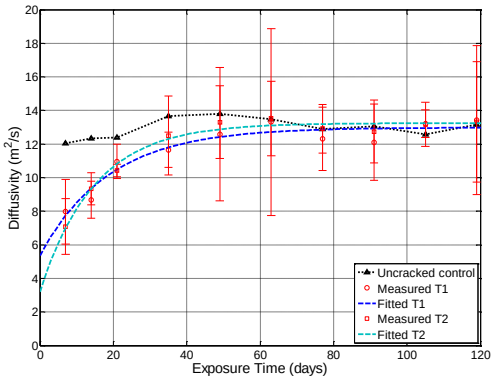

F25

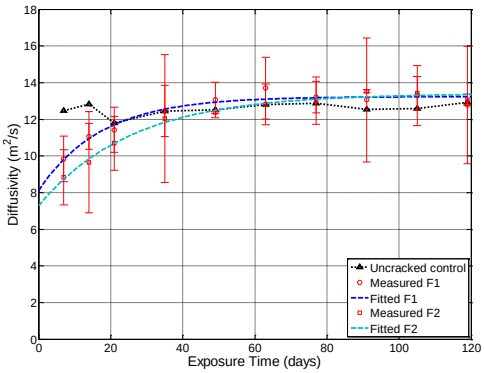

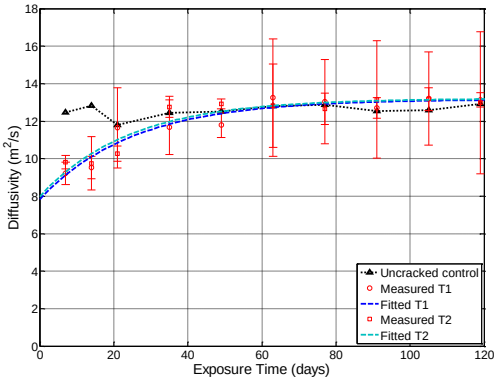

T

T3-F15

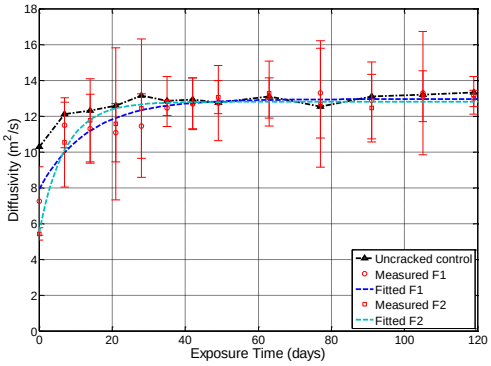

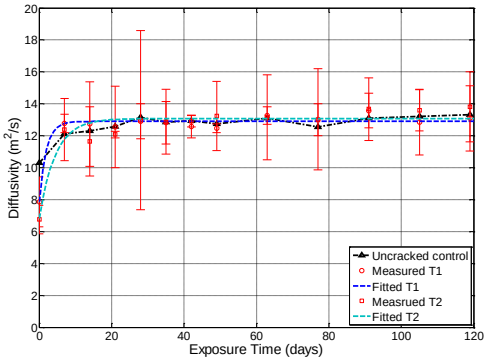

S35-MK5

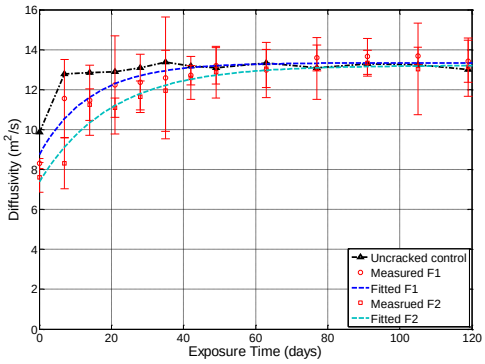

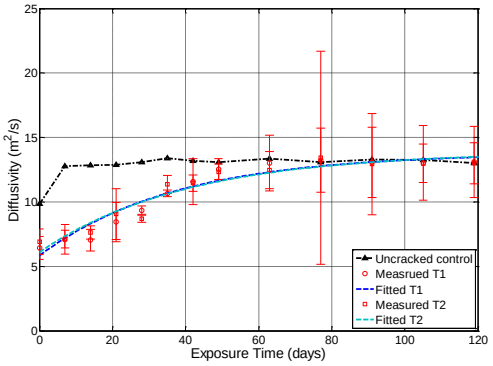

S50-MK5

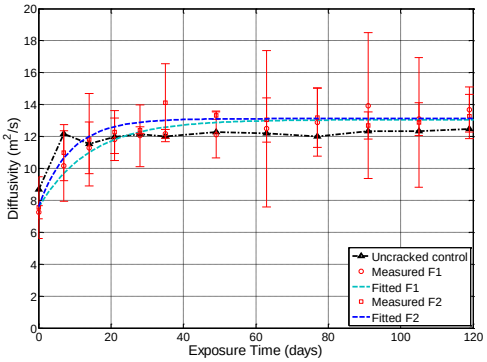

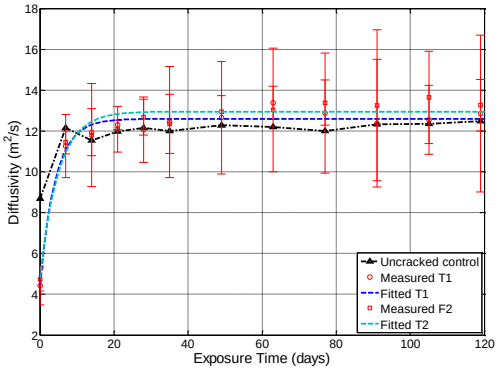

Type II

Figure 5.11: The diffusivity in each mix design (F25, T3-F15, S35-MK5, S50-MK5, Type II)

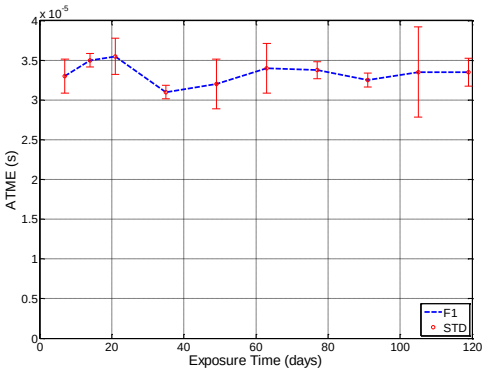

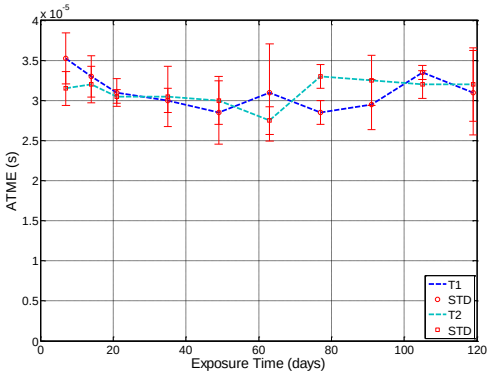

F25

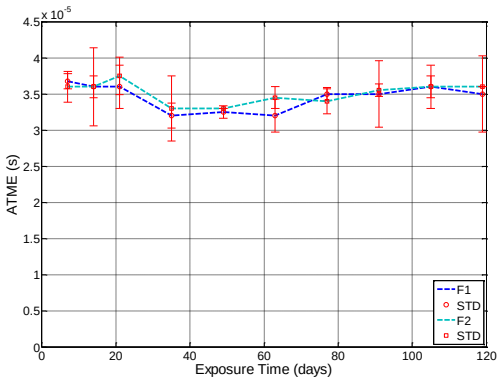

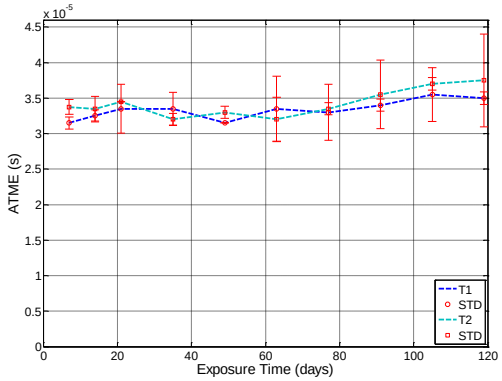

T3-F15

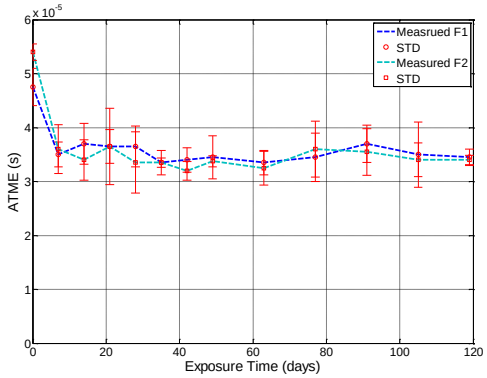

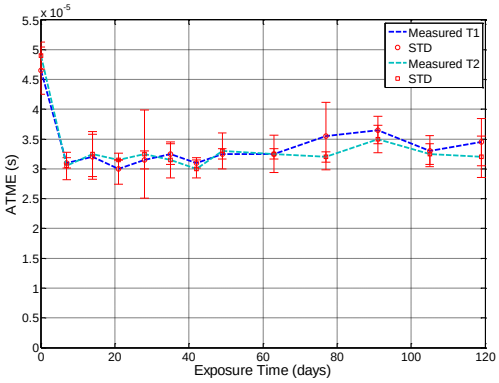

S35-MK5

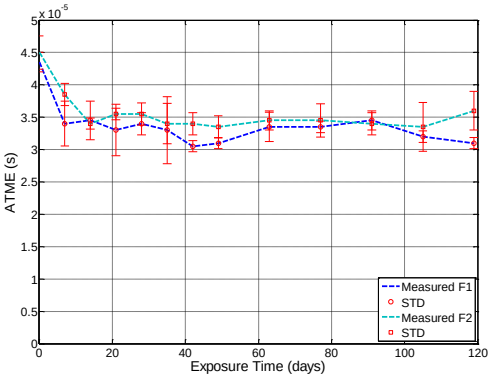

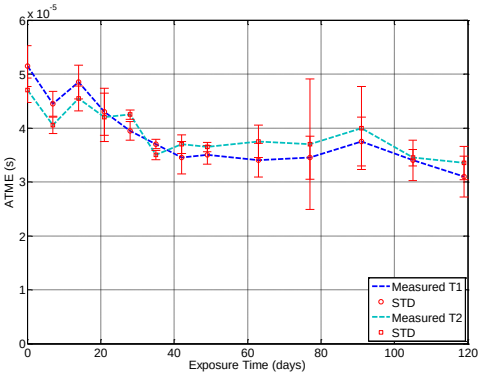

S50-MK5

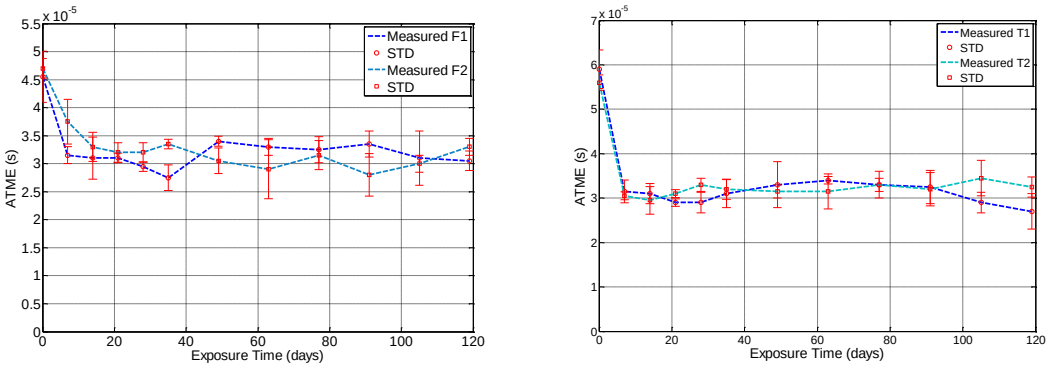

Type II

Figure 5.12: The ATME in each mix design (F25, T3-F15, S35-MK5, S50-MK5, Type II)

5.4.2.2 Dissipation

The dissipation values given in table 5.6 demonstrate that Type II samples show higher dissipation than mix designs containing supplementary cementitious materials (SCM's). This is due to a more refined, denser microstructure in mix designs containing SCM's so that the total energy of ultrasound are less absorbed in cement pastes and can be conserved in long distance. The difference of average dissipation values among five different mix designs can be explained by the fact that each cement paste has different porosities and potentially different saturation states through the depth of the sample for each mix design based upon transport properties.

Also, as shown in figure 5.13, dissipation values are retrieved for each mix design over time. It is found that as self-healing has occurred, dissipation values have shown a similar trend of decreasing, which suggests the density of material is increased and there was a low energy loss in the attenuation mechanism (dissipation is a material parameter that represents the rate of loss of energy in cement paste). Also, it should be noted that the fluctuation of diffusivity value in each samples is caused by the different state of

saturation at each measurement, which also affected by inconsistent coupling condition between transducer and specimen. In addition, decrease of dissipation happened due to water absorption would explain that there might be existed autogenous healing in preexisted microcracks and the continued hydration. More research is needed into this effect.

Table 5.6: Dissipation measurements over time

		Exposure time (day)	0*	7	14	21	28	35	42	49	63	77	91	105	119
F25	F1	Dissipation (1/s)	-	56799	46170	33344	-	40999	-	34813	32136	32268	34898	32636	29424
	F2		-	-	-	-	--	-	-	-	-	-	-	-	-
	T1		-	62582	66022	53615	-	52478	-	54251	43474	55171	51261	30453	40669
	T2		-	97773	65637	57918	-	46830	-	42029	53949	31767	36721	36232	35329
T3-F15	F1	Dissipation (1/s)	-	41843	34519	32580	-	38731	-	35653	35605	27403	30229	24904	28835
	F2		-	52176	47023	33588	-	41444	-	37952	30028	30190	24744	24448	25092
	T1		-	63997	58972	40238	-	38853	-	46294	32317	35346	30535	26347	27500
	T2		-	52351	51018	44612	-	38483	-	36452	38028	34268	27756	22434	24621
Type II	F1	Dissipation (1/s)	34805	38539	43467	41688	41804	35577	-	49190	57773	41629	49471	42836	30626
	F2		37798	51473	49518	44258	49530	47986	-	30088	33484	33978	32785	42087	40632
	T1		42419	50793	45880	51881	53771	49452	-	36741	29789	35573	38647	52339	62924
	T2		43169	53060	56661	44977	35192	38517	-	38227	40691	31112	37014	27844	33755
S35-MK5	F1	Dissipation (1/s)	35198	36142	**32232**	32819	32105	35247	32008	32763	32599	28599	24144	27502	28938
	F2		38492	40061	38178	35055	37419	32280	36476	29818	34174	28410	29870	29881	30927
	T1		32036	41649	40873	49567	37299	35333	43606	39194	32700	28589	22394	36064	29737
	T2		35990	47377	43080	42387	39045	40886	43312	34418	35723	35892	25763	31707	33471
S50-MK5	F1	Dissipation (1/s)	33845	42830	34137	34719	34988	35000	38239	30788	31169	29381	23767	30712	39922
	F2		38636	48030	35338	33453	33040	36120	30740	27114	26156	31972	20552	28998	33310
	T1		33655	40849	38377	38086	33689	36424	44635	38201	32331	30007	26945	33354	37712
	T2		37305	47272	38843	35003	32805	35716	33283	31853	28438	28145	29492	32674	25674

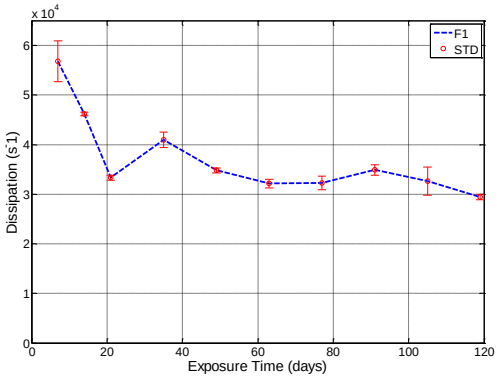

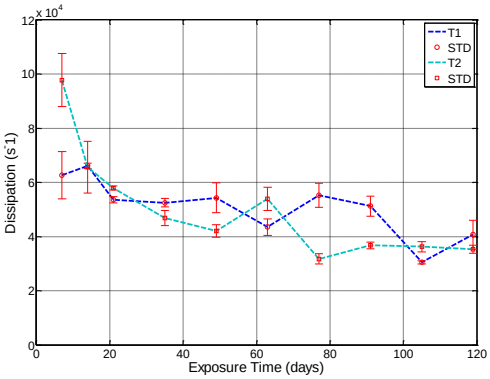

F25

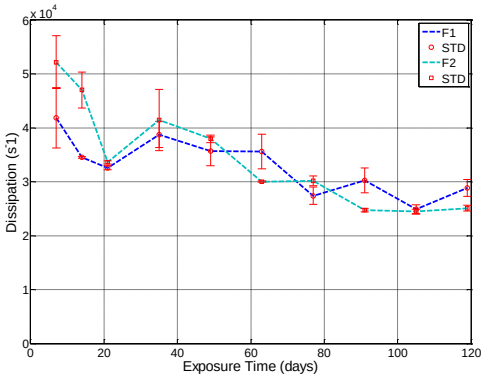

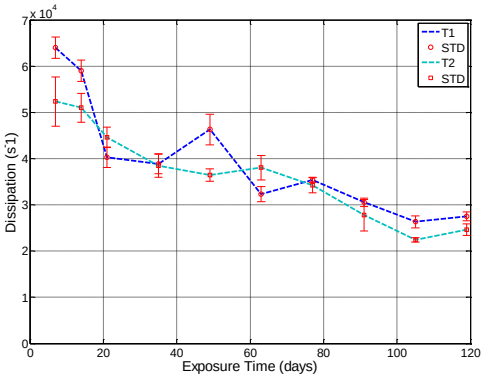

T3-F15

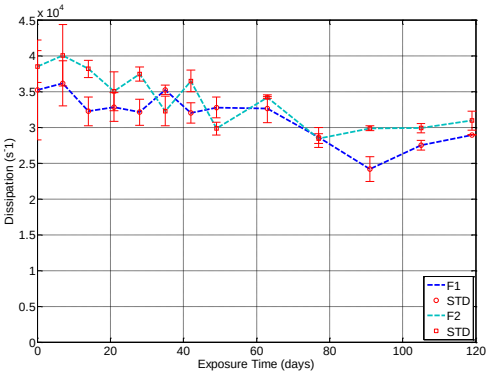

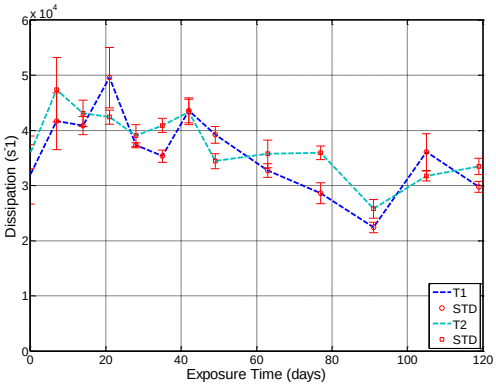

S35-MK5

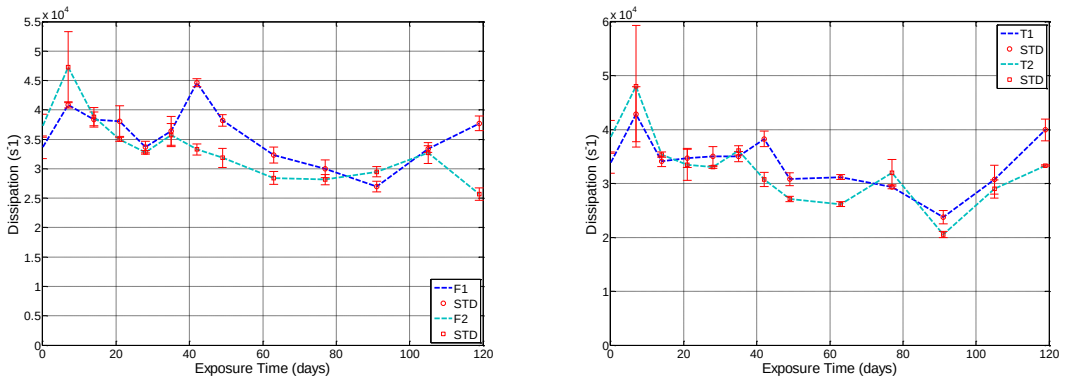

S50-MK5

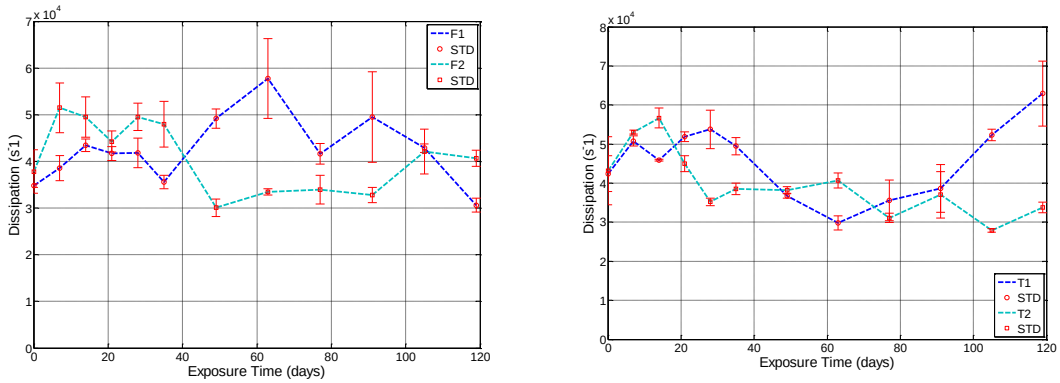

Type II

Figure 5.13: The dissipation in each mix design (F25, T3-F15, S35-MK5, S50-MK5, Type II)

5.4 Model analysis

In order to find a quantitative relationship between measured diffusivity and the amount of self-healing, this research proposes the following "exponential-recovery model,"

$$D^e = a - be^{-ct} \tag{1}$$

where D^e is the measured effective diffusivity and *a*, *b*, and *c* are fitting coefficients. Note that the coefficient *c* describes "the rate of healing" and increase in diffusivity due

to healing of the crack and, the coefficient *a* represents the asymptotic diffusivity as time approaches infinity, corresponding to the diffusivity measured in an uncracked control specimen, and *b* is related to the initial damage state in the specimen. The fitted coefficients are tabulated in table 5.7, and the curves are shown in figure 5.12. Figure 5.14 shows the coefficient *c* of each mix design for the two different crack types to compare the rate of observed self-healing in each mix design over time. These data show that the through specimen tension cracks have a larger initial damage coefficient than the flexure cracks, which indicates a wider crack and larger fractured surface. This is also consistent with the fact that specimens with a through-the-thickness tension cracks will have a higher level of damage than those with a part-through flexure crack.

Figure 5.15 shows initial damage coefficient, *b* versus rising rate coefficient, *c* for each mix design. As expected, each diffusivity curve had a different rising rate coefficient, *c* and initial damage coefficient, *b*. As was found by Holland (Holland, 2012), S35-MK5 exhibited the fastest rate and extent of self-healing, and S50-MK5 the lowest. Figure 15 suggests that the rate of self healing is related to damage degree and there appears to be a linear relationship between degree of damage and self healing until degree of damage has reached at its limit. It should be noted that one of data not shown in figure 15 is an outlier with high value of *c* coefficient in the case of the lowest damaged one (T1 sample with the lowest diffusivity value) among S35-MK5 samples. Zhong,W and Yao, W (Zhong & Yao, 2008) showed that there is relationship between degree of damage and self healing, and if the damage degree is above a certain threshold, the length of new hydration products cannot bridge the cracks, and as a result the level of self healing decreases.

Table 5.7. Fitted parameters from diffusivity curve

Mix Design	Coefficient	F1	F2	T1	T2
F25	a	13.1868	N/A	12.985	13.2463
	b	6.1229		7.6267	10.0423
	c	0.0566		0.0532	0.0676
T3-F15	a	13.2151	13.4041	13.1724	13.2127
	b	5.1239	6.1235	5.3375	5.2319
	c	0.0627	0.0387	0.0396	0.0412
TYPE II	a	13.0507	13.1178	12.5913	12.9498
	b	5.4944	5.4917	8.1505	8.1549
	c	0.0704	0.1140	0.2406	0.2014
S35-MK5	a	12.9492	12.7945	12.8967	13.0757
	b	5.0288	7.2699	5.0346	6.2554
	c	0.0746	0.1422	0.5183	0.225
S50-MK5	a	13.3417	13.2111	14.0323	13.8967
	b	4.5878	5.8289	8.3918	7.7929
	c	0.0702	0.0506	0.0254	0.0248

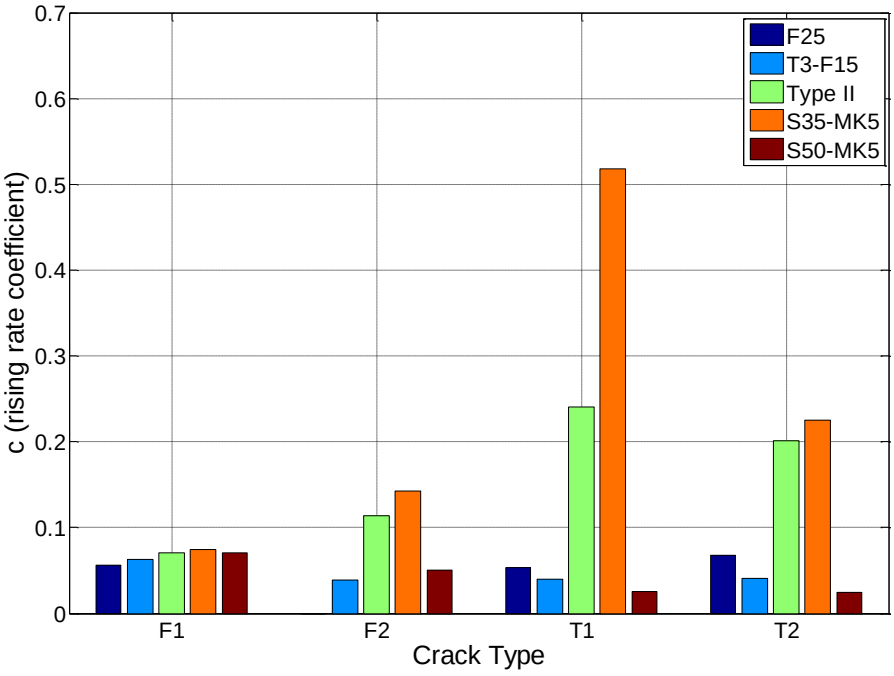

Figure 5.14 Plot for coefficient c vs. crack type in terms of mix design

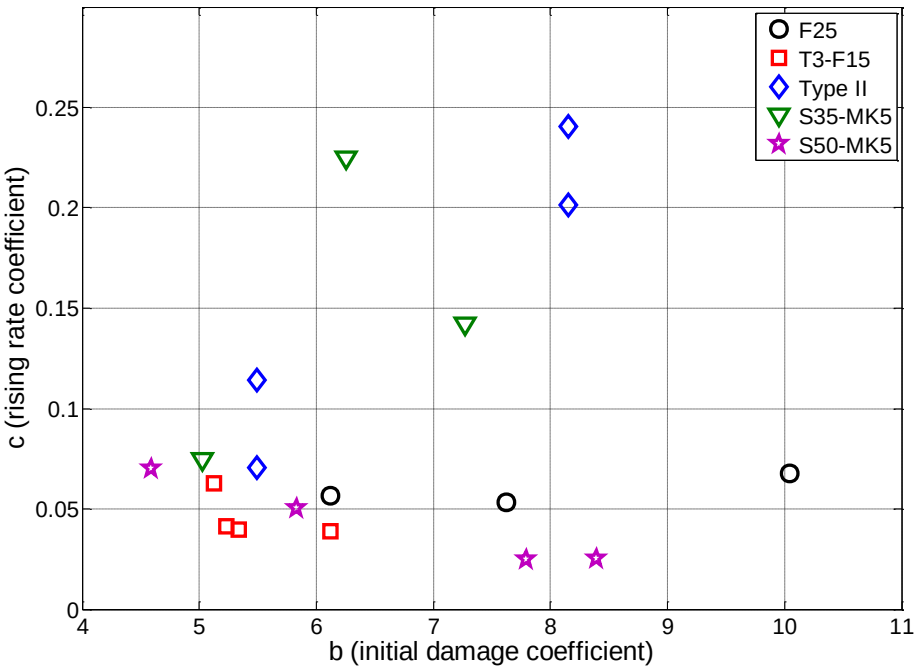

Figure 5.15. c (rising rate coefficient) vs. b (initial damage coefficient) plot

5.5 Conclusion and recommendations

The results of this investigation demonstrate that diffuse ultrasonic parameters (diffusivity and ATME) retrieved using the 2D diffusion model are sensitive to crack healing and the microstructural behavior in concrete, and thus can be an effective quantitative measure of the self-healing process over time, as well as providing the verification that self-healing has occurred. The sensitivity of the technique on crack healing is verified by comparing diffusivity with direct measurements of the crack width on the surface over a 120-day exposure period. Immediately after cracking, the ATME increases and diffusivity dramatically decreases from their initial values of the uncracked control specimens. The ATME of cracked specimens decreases significantly after exposure to the healing environment, whereas the diffusivity increases with time. Both

the ATME and diffusivity values suggest autogenous healing of the crack. In addition, Comparing among five sample types based on the proposed *exponential-recovery model,* it has been shown that S35-MK5 exhibits a relatively faster rate and extent of self-healing, and S50-MK5 shows the lowest rate and extent of self-healing. As a result, the proposed fitting parameter can be viewed as a good indicator to rate self-healing in concrete. However, it is found that the results based on the ATME show more fluctuations due to the partial crack closure (by healing that can randomly occur on the crack faces) as well as its sensitivity to the actual separation distance between the two transducers. Also, dissipation values have tended to recover its original values measured in uncracked control samples (intact samples) as self healing has occurred. This suggests that continued hydration which helps to process self-healing affects to decrease dissipation. In addition, the different dissipation values from five different mix designs suggest that different composition of cement paste have different influence on the intrinsic absorption of the materials and different microstructural behavior. This research demonstrates that diffuse ultrasound provides a viable method for monitoring self-healing of cracks in concrete and overcomes the difficulties in other ultrasonic techniques to monitor self-healing process.

6. CONCLUSION AND RECOMENDATIONS

6.1 Conclusion

This research examines the feasibility and effectiveness to characterize structural defects in heterogeneous civil materials such as asphaltic concrete and Portland cement concrete using coherent field and incoherent field analysis.

6.1.1 Segregation in asphaltic concrete

Coherent field analysis using Rayleigh surface wave has been exploited to characterize the material properties, and finally segregation in asphaltic concrete. The dispersion and attenuation characteristics of asphaltic concrete have been quantitatively measured in the frequency range from 40 to 100 kHz. Also, It is observed that the wedge to the air-coupled sensor (with a finite-size aperture) technique of Experimental setup #3 in chapter 3 appears to be the most reliable in characterizing Rayleigh waves in the present viscoelastic and heterogeneous medium. A preliminary measurement qualitatively demonstrates that the proposed measurement procedure can be used to detect segregation in asphaltic concrete specimens; Due to its different aggregate content, a segregated area will have a local attenuation coefficient either considerably higher or lower than the non- segregated area. Therefore, a judgment regarding the existence of segregation can be made by comparing the local attenuation coefficients. However, due to high viscoelasticity and high volume fraction of scatterers, which are much higher than those of cement concrete, in segregation area of asphaltic concrete, it has shown to be

difficult to achieve effectively coherent field analysis in heterogeneous civil materials, especially in asphaltic concrete.

In order to overcome the limitations found in segregation research, incoherent field analysis has been exploited to characterize defects such as surface opening cracks and monitor autogenuous crack healing in concrete structure in this research and has shown to be efficient to characterize such defects in heterogeneous civil materials.

6.1.2 Crack depth determination

The incoherent diffuse wave has been utilized in determination of surface opening crack depth. The main steps to estimate the surface opening crack depth using diffuse waves are as follows.

Lag time based technique

1) The diffusion parameters (diffusivity and dissipation) retrieved from experimental measurements in the uncracked region of the sample are used as an FE model input parameter to simulate the vertical crack configuration.

2) The peak energy arrival time is then determined from the numerical energy evolution curves of two different simulations, one without crack and the other with the crack.

3) The lag time, defined previously as the difference between the peak arrival time in the cracked and uncracked regions, is the measure used here to infer the single vertical crack depth.

4) The lag time is obtained by comparing the peak energy arrival time obtained above from two different simulations.

5) Once the relation is established, the depth of the single vertical crack can be determined from the curve.

Energy velocity based technique

1) The diffusion parameters (diffusivity and dissipation) retrieved from experimental measurements in the uncracked region of the sample are used as an FE model input parameter to calculate diffuse energy velocity at desired frequency.

2) Once the energy velocity is known and shortest path of diffuse wave from transmitter and receiver, ATME can be obtained from this relationship numerically, then vertical crack depth can be inferred from this numerical curve with experimentally determined ATME.

Also it turned out to have advantages to characterize smaller defects such as microcracks comparable to or less than size of scatterers; However, in order to be more applicable to a realistic civil infrastructure, it is recommended that the technique requires a high signal to noise ratio to guarantee reliable curve fitting and point like receiver is necessary to avoid phase cancellation. In addition, it should be noted that the maximum depth that the present diffuse ultrasonic technique can measure is limited by the fundamental physics that the technique relies on. Since the technique uses high frequency ultrasound (typically, f >300 kHz) to induce a diffuse field in the concrete structure, the attenuation caused by scattering (roughly corresponding to inverse diffusivity) and the material absorption (corresponding to the dissipation) are much higher than those in the more conventional

ultrasonic methods such as the impact-echo technique. For this reason, the propagation distance is somewhat limited and, as a result, the technique can be applied to relatively shallow cracks. The maximum measurable crack depth at, for example, 500 kHz, is about 8 inches (or 20 cm). If deeper crack needs to be measured, a lower frequency can be used; in this case, however, one should ensure that the total propagation distance is much larger than the scattering mean free path at the used frequency.

6.1.3 Self healing monitoring

This research has monitored in situ to quantify the extent of autogenuous crack healing by in a novel application of diffuse ultrasound. The diffuse ultrasonic measurements are conducted on: uncracked; tensile through-thickness cracked; and flexure partial-thickness cracked concrete specimens. Specimens made from five different mix designs are unbonded post-tensioned with a precompression force of 6.2 MPa that allows for the generation of cracks with widths less than 200 μm that should exhibit self-healing and are then exposed to a simulated marine environment.
The results of this investigation demonstrate that diffuse ultrasonic parameters (diffusivity, dissipation, and ATME) retrieved using the 2D diffusion model are sensitive to crack healing and the microstructural behavior in concrete, and thus can be an effective quantitative measure of the self-healing process over time, as well as providing verification that self-healing has occurred. The sensitivity of the technique on crack healing is verified by comparing diffusivity with direct measurements of the crack width on the surface over a 120-day exposure period. Immediately after cracking, the ATME increases and diffusivity dramatically decreases from their initial values of the uncracked

control specimens. The ATME of cracked specimens decreases significantly after exposure to the healing environment, whereas the diffusivity increases with time. Both the ATME and diffusivity values suggest autogenous healing of the crack. In addition, Comparing among five sample types based on the proposed *exponential-recovery model*, it has been shown that S35-MK5 exhibits a relatively faster rate and extent of self-healing, and S50-MK5 shows the lowest rate and extent of self-healing. As a result, the proposed fitting parameter can be viewed as a good indicator to rate self-healing in concrete. However, it is found that the results based on the ATME show more fluctuations due to the partial crack closure (by healing that can randomly occur on the crack faces) as well as its sensitivity to the actual separation distance between the two transducers. This research demonstrates that diffuse ultrasound provides a viable method for monitoring self-healing of cracks in concrete and overcomes the difficulties in other ultrasonic techniques to monitor self-healing process.

6.2 Recommendations

In conclusion, this research considers two different types of ultrasonic waves (coherent and incoherent wave) to quantitatively characterize and monitor defects in heterogeneous concrete materials and confirms that diffuse ultrasound provides a viable method for effective characterization of structural defects in heterogeneous civil materials and overcomes the difficulties in other ultrasonic techniques. However, due to the original characteristics of heterogeneous materials such as asphaltic concrete or Potland cement concrete which cause the wave to be significantly scattered and attenuated, it is recommended that for coherent wave methods, high power input is needed, especially in segregation characterization using a set of air coupled transducers, to transmit and receive the coherent wave into such materials. Also in order to use incoherent wave methods such as diffuse wave, high SNR is very important to guarantee reliable curve fitting and

point like receiver is necessary to avoid phase cancellation and detect fully diffused wave. Nevertheless, to characterize and monitor defects in these heterogeneous materials (asphaltic concrete and Portland cement concrete) has been accomplished well using either coherent or incoherent wave technique. Also, this development opens up a wide range of application in concrete for high resolution, reliable, and rapid inspection of heterogeneous materials and structures

APPENDIX A

NUMERICAL MODELING OF DIFFUSE ULTLASONIC FIELD

In this appendix, two-dimensional numerical modeling of diffuse ultrasonic field using ANSYS in concrete is demonstrated in detail and based on this numerical modeling, frequency dependency on the speed of diffuse ultrasonic energy which is used for second proposed technique in determination of crack depth is discussed.

A.1. Finite Element Modeling

A two-dimensional rectangular geometry is considered; a single crack lies in the middle of the domain and the transmitter and receiver are located symmetrically around the crack as shown in figure A.1. The height *(p)* and width *(l)* of the rectangular domain are 250 mm and 600 mm for concrete block samples and 410 mm and 4500 mm for concrete beam, respectively. At the source location, the model is excited with an impulse and then the response of the model is measured at the receiver location. The source-to-receiver distance designated by 2*d* is fixed to be 60 mm in the simulation. The experimental diffusion parameters (D = 10 m^2/s, σ = 21000/s for concrete block samples and D = 10 m^2/s, σ = 45000/s for concrete beam) are used as input parameters.

The FE model for equation 4.6 is created using the heat conduction modeling approach in ANSYS. The rectangular domain in figure A.1 is discretized using a 4-node bilinear quadrilateral element with each node having one degree of freedom (Plane55 in ANSYS). 6000 elements are used for concrete block samples and 18450 elements for concrete beam. To model the ultrasonic diffusion in terms of the heat conduction equation, the mass density and the specific heat capacity are set to be unity, and the thermal

conductivity is set to be the diffusivity *D* of the concrete sample. The impulse excitation is modeled as a heat source with a duration of 0.1 μs at the source location. The initial of the FE model are such that the initial spectral energy density in the domain B is zero and boundary conditions are that the energy flux across the boundary surface ∂B of the domain B is zero (the Neumann's boundary conditions). It is noted that each FE simulation yields only the diffuse energy density at a single frequency without dissipation. The frequency dependence of the response can be taken into account indirectly through the frequency dependent diffusion parameters. As illustrated by equation 4.5, the dissipation can be accounted for in a post-processing step.

The FE model is also validated by comparing the calculated impulse response (or the energy evolution curve) with the experimental one. For this, a specimen with a vertical crack located at the center (dash-dotted line in figure. A.1.) is used. In the FE model, the vertical crack is modeled as a thin (1 mm) rectangle with the boundary conditions of no energy flux at the crack faces. Unlike cracks in metal structures, cracks in concrete are usually open. This opening displacement of 1 mm in fact approximately matches the opening displacement of the cracks in our actual specimens. Furthermore, the mesh density near the crack and especially at the crack tip is increased to properly handle the singular behavior near the crack. Please refer to the section 4.5.1 and 4.6.2 for a comparison between the experimental and simulated impulse responses**.** It is concluded that the FE model correctly predicts features in the experimental energy evolution curves and hence can be employed to conduct further simulations with more complicated crack geometries. Please refer to (Seher, 2011) for further simulations on various crack configurations.

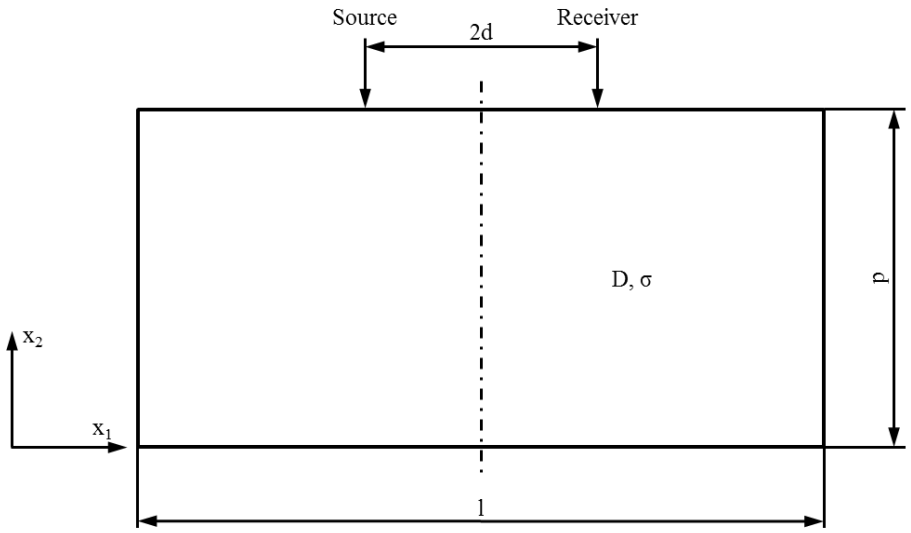

Figure A.1: Mechanical model of the experimental setup in the FE simulation

A.2 Frequency dependency on the speed of diffuse ultrasound energy

The peak energy arrival times in all simulation results for concrete block samples are plotted against the minimum propagation distance between the source and the receiver through the material and it is shown in figure A.2. The minimum propagation distance here is the shortest path between the source and the receiver under the assumption of an infinitely small crack width. It can be observed that there is an approximately linear relationship between the minimum propagation distance and the peak energy arrival time and the slope which corresponds to the speed of diffuse ultrasonic energy is 912.3 m/s. Note that this speed is about four times lower than the longitudinal wave speed in concrete. From this relationship, it can be inferred that the propagation of the diffuse ultrasonic energy follows a simple time-of-flight (TOF) principle. Note that this linear relationship and speed of diffuse ultrasonic energy holds only for one pair of diffusivity and dissipation at frequency f = 500 kHz and there is another linear relationship at another frequency. To investigate the degree of frequency dependence, further FE

simulations have been performed for two additional frequencies, 400 and 600 kHz and for the vertical and inclined crack cases. Table A.1 lists the diffusivity and dissipation values at these frequencies and at 500 kHz. Figure A.1 shows that the same linear relationship holds for other frequencies as well and the slope (diffuse energy propagation speed) is frequency-dependent. The speed of diffuse ultrasonic energy at 400 kHz is higher by about 10 % than the speed at 600 kHz as shown in table A.1. Note that the speed of diffuse ultrasonic energy is about the half the propagation speed of shear waves that are dominant in the diffuse ultrasonic field. During the simulations, it was observed that the speed is not only affected by the diffusivity but also by dissipation. Detailed reason for this behavior is subjected to further theoretical considerations.

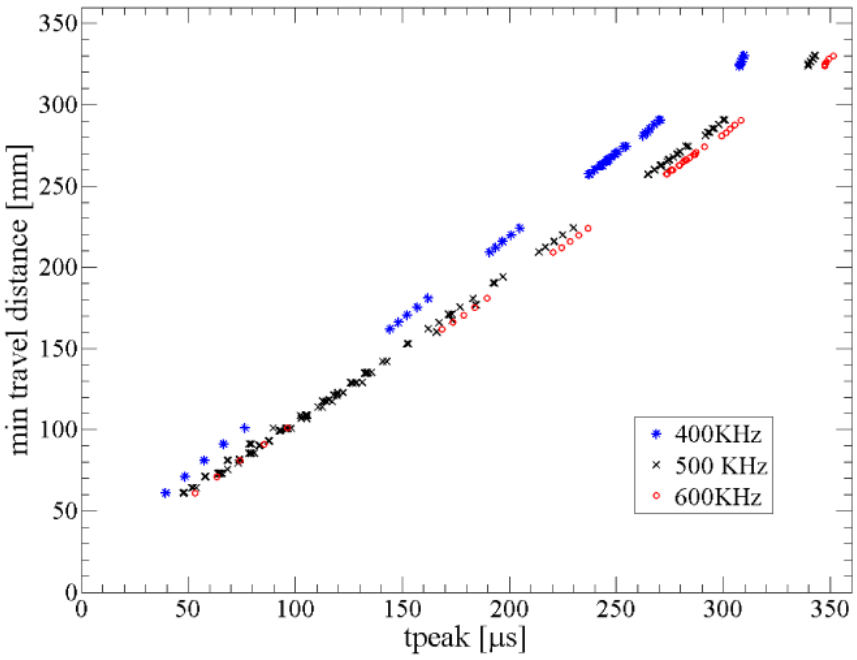

Figure A.2 : Minimum propagation distance between source and receiver through the material versus peak energy arrival time of all simulations

Table A.1: Frequency dependent diffuse ultrasonic parameters

Frequency	400 kHz	500 kHz	600 kHz
Diffusivity [$m^2\ s^{-1}$]	15	10	7
Dissipation [s^{-1}]	17000	21000	28500
Energy speed [m/s]	988.7	912.3	896.4

References

Abded-Jawad, Y., & Haddad, R. (1992). Effect of early overloading of concrete on strength at later ages. *Cement and Concrete Research, 22*(5), 927-936.

Abrams, D. (1925). Autogeneous healing of concrete *Concrete, 27*(2), 50.

ACI. (1998). Nondestructive test methods for evaluation of concrete in structures. In R. A. 228.2R-98 (Ed.). Farmington Hills, MI.

ACI. (2008). Guide for Selecting Proportions for High-Strength Concrete Using Portland Cement and Other Cementitious Materials *ACI 211.4R-08* (pp. 25): ACI Committee.

Aggelis, D. G., & Shiotania, T. (2007). Experimental study of surface wave propagation in strongly heterogeneous media. *Journal of the Acoustical Society of America, 122*(5), EL151-EL157.

Alberto Ruiz, M., & Nagy, P. B. (2002). Diffraction correction for precision surface acoustic wave velocity measurement. *Journal of the Acoustical Society of America, 112*(3), 835-842.

Aldea, C., Song, W.-J., Popovics, J. S., & Shah, S. P. (2000). Extent of healing of cracked normal strength concrete. *Journal of Materials in Civil Engineering, 12*(1), 92-96.

Ansys. (2010). *Ansys 13.0 Documentation*: ANSYS Inc.

Anugonda, P., Wiehn, J. S., & Turner, J. A. (2001). Diffusion of ultrasound in concrete. *Ultrasonics, 39*(6), 429-435.

ASCE. (2009). *ASCE Report Card for America's Infrastructure*, 2009, from www.asce.org/reportcard/index.cfm

ASTM. (2009). Standard test method for pulse velocity through concrete *C597* (pp. 4).

Bazant, Z. P., & Planas, J. (1998). *Fracture and Size Effect in Concrete and Other Quasibrittle Materials*. Boca Raton: CRC Press.

Becker, J., Jacobs, L. J., & Qu, J. (2003). Characterization of cement-based materials using diffuse ultrasound. *J Eng Mech, 129*(12), 1478–1484.

Bradfield, G., & Gatfield, E. (1964). Determining the thickness of concrete pavements by mechanical waves: directed beam method. *Concrete Research, 16*, 49.

Brendenberg, H., & Ed. (1980). *the Application of Stress-Wave Theory on Piles.* Paper presented at the International Seminar on the Application of Stress-Wave Theory on Piles, Stockholm.

Carino, N. J., Sansalone, M. J., & Hsu, N. N. (1986). A point source-point receiver, pulse-echo technique for flaw detection in concrete. *Journal of the American Concrete Institute, 83*(2), 199-208.

Carslaw, H. S., & Jaeger, J. C. (1990). *Conduction of heat in solids*. New York: Oxford.

Christensen, R. M. (1979). *Mechanics of composite materials*. New York: Wiley.

Clear, C. A. (1985). The effects of autogenous healing upon the leakage of water through cracks in concrete *Cement and Concrete Association Technical Report No. 559* (pp. 28).

Cowan, M. L., Beath, K., Page, J. H., Liu, Z. Y., & Sheng, P. (1998). Group velocity of acoustic waves in strongly scattering media: Dependence on the volume fraction of scatterers. *Physical Review E (Statistical Physics, Plasmas, Fluids, and Related Interdisciplinary Topics), 58*(5), 6626-6636.

Davis, A. G., & Hertlein, B. H. (1990, April 30-May 2). *Assessment of bridge deck repairs by a nondestructive technique.* Paper presented at the NATO Advanced Research Workshop on Bridge Evaluation, Repair, and Rehabilitation, Baltimore, MD.

Davis, A. G., & Hertlein, B. H. (1991). Developments of nondestructive small-strain methods for testing deep foundations: a review. *Transportation Research Record* (1331), 15-20.

Deroo, F., Kim, J.-Y., Qu, J., Sabra, K., & Jacobs, L. J. (2010). Detection of damage in concrete using diffuse ultrasound. *Journal of the Acoustical Society of America, 127*(6), 3315-3318.

Dunning, M. R., Karakouzian, K., & Dunning, R. L. (2007). Feasibility for the use of non-contact ultrasound for application in asphalt concrete materials. . *Journal of the Association of Asphalt Paving Technologists 76*, 851-886.

Edvardsen, C. (1996). Water permeability and autogenous healing of separation cracks in concrete. *Concrete precasting plant and tech, 62*, 77-85.

Edvardsen, C. (1999). Water permeability and autogeous healing of cracks in concrete *ACI Materials Journal, 96*(4), 448-454.

Finno, R. J., & Gassman, S. L. (1998). Impulse response evaluation of drilled shafts. *Journal of Geotechnical and Geoenvironmental Engineering, 124*(10), 965-975.

GDOT. (2011). Standard Specification : Section 828 - Hot Mix Asphaltic Concrete Mixtures, from http://www.dot.state.ga.us/doingbusiness/thesource/special_provisions/supplementals/su828.pdf

Goueygou, M., Abrakam, O., & Lataste, J.-F. (2008). A comparative study of two non-destructive testing methods to assess near-surface mechanical damage in concrete structures. *NDT&E International, 41*(6), 448-456.

Hearn, N. (1992). *Saturated permeability of concrete as influenced by cracking and self sealing.* Ph.D, University of Cambridge, London.

Hearn, N., & Morley, C. T. (1997). Self sealing property of concrete: experimental evidence *Materials and Structures/Materiaux et Constructions, 30*(201), 404-411.

Heisey, J. S., Stokoe II, K. H., & Meyer, A. H. (1982). Moduli of pavement systems from spectral analysis of surface waves. *Transportation Research Record*(852), 22-31.

Hevin, G., Abraham, O., Pedersen, H. A., & Campillo, M. (1998). Characterization of surface cracks with rayleigh waves: A numerical model. *NDT and E International, 31*(4), 289-297.

Hill, J. M., & Dewynne, J. N. (1987). *Heat conduction*: Blackwell Scientific Publications

Holland, R. B. (2012). *Durability of precast prestressed concrete piles in marine environments.* Ph.D, Georgia Institute of Technology, Atlanta.

Hornibrook, F. B. (1939). Application of sonic method to freezing and thawing studies of concrete. *ASTM Bull, 202*, 5.

Howkins, S. D. (1968). Measurement of pavement thickness by rapid and nondestructive methods (Vol. 52): NCHRP.

Huang, Y. H. (1993). *Pavement Analysis and Design* Prentice Hall.

In, C.-W., Kim , J.-Y., Jacobs, L. J., & Kurtis, K. E. (2012). *Crack depth measurement in concrete using diffuse ultrasound*. Paper presented at the QNDE.

Jacobs, L. J., & Owino, J. (2000). Effect of aggregate size on attenuation of Rayleigh surface waves in cement-based materials. *Journal of Engineering Mechanics(ASCE), 126*(11), 1124-1130.

Jacobs, L. J., & Whitcomb, R. W. (1997). Laser Generation and Detection of Ultrasound in Concrete. *Journal of Nondestructive Evaluation, 16*(2), 57-65.

Jacobsen, S., Marchand, J., & Boisvert, L. (1996). Effect of cracking and healing on chloride transport in OPC concrete. *Cement and Concrete Research, 26*(6), 869-881.

Jacobsen, S., Marchand, J., & Gerard, B. (1998). *Concrete Cracks I: Durability and Self-Healing—A Review.* Paper presented at the the 2nd International Conference on Concrete under Severe Conditions,Environment and Loading.

Jacobsen, S., Marchand, J., & Homain, H. (1995). SEM observations of the microstructure of frost deteriorated and self healed concrete. *Cement and Concrete Research, 25*(8), 1781-1790.

Jacobsen, S., & Sellevold, E. J. (1996). Self healing of high strength concrete after deterioration by freeze/thaw. *Cement and Concrete Research, 26*(1), 55-62.

Jones, R. (1948). *The Application of Ultrasonic to the Testing of Concrete, Research*. London.

Jones, R. (1962a). *Non destructive Testing of Concrete*. Londun: Cambridge University Press.

Jones, R. (1962b). Surface wave technique for measuring the elastic properties and thickness of roads: theoretical development. *British Journal of Applied Physics, 13*(1), 21-29.

Kee, S.-H., & Zhu, J. (2011). Effects of Sensor Locations on Air-Coupled Surface Wave Transmission Measurements. *IEEE Transaction on Ultrasonics, Ferroelectrics and Frequency, 58*(2), 427-436.

Kobori, O., & Udagawa, Y. (2001, JUL 29-AUG 03). *Velocity measurement on an asphalt and nondestructive detection of pipe under the asphalt.* Paper presented at the 28th Annual Conference on Quantitative Nondestructive Evaluation BOWDOIN COLL, BRUNSWICK, ME

Lauer, K., & Slate, F. O. (1956). Autogenous Healing of Cement Paste. *ACI Material Journal, 41*, 1083-1097.

Lepech, M. D., & Li, V. C. (2005). *water permeability of cracked cementitious composites.* Paper presented at the 11th International conference on Fracture, Turin, Italy.

Leslie, J. R., & Cheesman, W. J. (1949). *An ultrasonic method of studying deterioration and cracking in concrete structures.* Paper presented at the ACI Journal.

Lin, Y., & Su, W.-C. (1996). Use of stress waves for determining the depth of surface-opening cracks in concrete structures. *ACI Materials Journal, 93*(5), 494-505.

Lin, Y. C., Liou, T. H., & Tsai, W. H. (1999). Deternining crack depth and measurement errors using time-of-flight diffraction techniques. *ACI materials Journal, 96*(2), 190-195.

Liu, P.-L., Lee, K.-H., Wu, T.-T., & Kuo, M.-K. (2001). Scan of surface-opening cracks in reinforced concrete using transient elastic waves. *NDT and E International, 34*(3), 2001.

Mailer, H. (1972). Pavement thickness measurement using ultrasonic techniques. *Highway Res. Rec, 378*, 20-28.

McCann, D. M., & Forde, M. C. (2001). Review of NDT methods in the assessment of concrete and masonry structures. *NDT and E International, 34*(2), 71-84.

Mix, P. E. (2005). *Introduction to nondestructive testing: A training guide*. Hoboken, New Jersey: John Wiley & Sons.

Nazarian, S., & Stokoe II, K. H. (1986). *In situ determination of elastic moduli of pavement systems by spectral analysis of surface waves method : practical aspects*. (FHWA/TX-86/13+368-1F).

Nazarian, S., Stokoe II, K. H., & Hudson, W. R. (1983). Use of spectral analysis of surface waves method for determination of moduli and thicknesses of pavement systems. *Transportation Research Record* (930), 38-45.

Neuenschwander, J., Schmidt, T., Luthi, T., & Romer, M. (2006). Leaky Rayleigh wave investigation on mortar samples. *Ultrasonics, 45*(1-4), 50-55.

Neville, A. M. (1997). *Properties of Concrete* (4 ed ed.). New York, NY: John Wiley and Sons.

Obert, L. (1939). *Sonic method of determining the modulus of elasticity of building materials under pressure.* Paper presented at the ASTM Bull.

Olson, L., & Church, E. (1986, August). *Survey of nondestructive wave propagation testing methods for the construction industry.* Paper presented at the 37th Annual Highway Geology Symp., Helena, MT.

Olson, L. D., & Wright, C. C. (1990). *Seismic, sonic, and vibration methods for quality assurance and forensic investigation of geotechnical, pavement, and structural systems.* Paper presented at the Nondestructive Testing and Evaluation for Manufacturing and Construction, Hemisphere, Washington, D.C.

Owino, J. O., & Jacobs, L. J. (1999). Attenuation measurements in cement-based materials using laser ultrasonics. *Journal of Engineering Mechanics, 125*(6), 637-647.

Page, J. H., Schriemer, H. P., Bailey, A. E., & Weitz, D. A. (1995). Experimental test of the diffusion approximation for multiply scattered sound. *Physical Review E (Statistical Physics, Plasmas, Fluids, and Related Interdisciplinary Topics), 52*(3), 3106-3114.

Piwakowski, B., Fnine, A., Goueygou, M., & Buyle-Bodin, F. (2004). Generation of Rayleigh waves into mortar and concrete samples. *Ultrasonics, 42*(1-9), 395-402.

Popovics, J., Ryden, N., Gibson, A., Alzate, S., Al-Qadi, I. L., & Xie, W. (2008, JUL 22-27). *New developments in NDE methods for pavements.* Paper presented at the 34th Annual Review of Progress in Quantitative Nondestructive Evaluation Golden, CO

Popovics, J. S., Achenbach, J. D., & Song, W.-J. (1999). Appplicatoin of new ultrasound and sound generation methods for testing concrete structures. *Magazine of Concrete Research, 51*(1), 35-44.

Popovics, J. S., Song, W.-J., Chandehari, M., Subramaniam, K. V., & Achenbach, J. D. (2000). Application of surface wave transmission measurements for crack depth determination in concrete. *ACI Materials Journal, 97*(2), 127-135.

Popovics, J. S., Song, W.-J., Ghandehari, M., Subramaniam, K. V., Achenbach, J. D., & Shah, S. P. (2000). Application of surface wave transmission measurements for crack depth determination in concrete. *ACI Materials Journal, 97*(2), 127-135.

Popovics, S., Bilgutay, N. M., Karaoguz, M., & Akgul, T. (2000). High frequency Ultrasound Technique for Testing Concrete. *ACI Materials Journal, 97*(1), 58-65.

Posston, R., & Sansalone, M. J. (1997). Detecting cracks in beams and columns of a post-tensioned parking garage using the impact-echo method. *American Concrete Institute, 168*, 199-220.

Powers, T. C. (1938). *Measuring Young's modulus of elasticity by means of sonic vibrations.* Paper presented at the ASTM.

punurai, W., Jarzynski, J., Qu, J., Kim, J.-Y., Jacobs, L. J., & Kurtis, K. E. (2007). Characterization of multi-scale porosity in cement paste by advanced ultrasonic techniques. *Cement and Concrete Research, 37*(1), 38-46.

Punurai, W., Jarzynski, J., Qu, J., Kurtis, K. E., & Jacobs, L. J. (2006). Characterization of entrained air voids in cement paste with scattered ultrasound. *NDT and E International, 39*(6), 514-524.

Punurai, W., Jarzynski, J., Qu, J., Kurtis, K. E., & Jacobs, L. J. (2007). Characterization of dissipation losses in cement paste with diffuse ultrasound. *Mechanics Research Communications, 34*(3), 289-294.

Purnell, P., Gan, T. H., Hutchins, D. A., & Berriman, J. (2004). Noncontact ultrasonic diagnostics in concrete: A preliminary investigation. *Cement and Concrete Research, 34*(7), 1185-1188.

Qian, S. Z., J. , Schlangen, E., Ye, G., & Brreugel, K. V. (2009). Self-healing behavior of strain hardening cementitious composites incorporating local waste materials. *Cement & Concrete Composites, 31*, 613-621.

Quiviger, A., Payan, C., Chaix, J.-F., Garnier, V., & Salin, J. (2012). Effect of the presence and size of a real macro-crack on diffuse ultrasound in concrete. *NDT and E International, 45*(1), 128-132.

Ramamoorthy, S. K., Kane, Y., & Turner, J. A. (2004). Ultrasound diffusion for crack depth determination in concrete. *Journal of the Acoustical Society of America, 115*(2), 523-529.

Ramm, W., & Biscoping, M. (1998). Autogenous healing and reinforcement corrosion of water penetrated separation cracks reinforced concrete. *Nuclear Engineering and Design, 179*(2), 191-200.

Reinhardt, H., & Joos, M. (2003). Permeability and self healing of cracked concrete as function of temperature and crack width. *Cement and Concrete Research, 33*(7), 981-985.

Rodriguez, O. G. (2001). *Influence of Cracks on Chloride Ingress into Concrete.* Master's Thesis, University of Toronto.

Rogers, P. H., & Van Buren, A. L. (1974). exact expression for the Lommel diffraction correction integral. *Journal of the Acoustical Society of America, 55*(4), 724-728.

Rose, J. L. (1999). *Ultrasonic Waves in Solid Media* New York: Cambridge University Press

Ryden, N., Lowe, M. J. S., & Cawley, P. (2007, JUL 22-27). *Non-contact surface wave scanning of pavements using a rolling microphone array.* Paper presented at the

34th Annual Review of Progress in Quantitative Nondestructive Evaluation Golden, CO
Sachse, W., & pao, Y.-H. (1978). On the determination of phase and group velocities of dispersive waves in solids. *Journal of Applied Physics, 49*(8), 4320-4327.
Sahmaran, M. (2007). Effect of Flexure Induced Transverse Crack and Self-healing on Chloride Diffusivity of Reinforced Mortar. *Journal of Material Science, 42,* 9131-9136.
Sahmaran, M., Keskin, S. B., Ozerkan, G., & Yaman, I. O. (2008). Self-healing of mechanically-loaded self consolidating concretes with high volumes of fly ash. *Cement and Concrete Composites, 30*(10), 872-879.
Sansalone, M. J., & Carino, N. J. (1989). Laboratory and field study of the impact-echo method for flaw detection in concrete. *ACI, 112*, 1-20.
Sansalone, M. J., Lin, J. M., & Streett, W. B. (1997). A procedure for determining P-wave speed in concrete for use in impact-echo testing using a P-wave speed measurement technique. *ACI Materials Journal, 94*(6), 531-539.
Sansalone, M. J., Lin, J. M., & Streett, W. B. (1998). Determining the depth of surface-opening cracks using impact-generated stress waves and time-of-flight techniques. *ACI Materials Journal, 95*(2), 168-177.
Schubert, F., & Koehler, B. (2004). Numerical time-domain simulation of diffusive ultrasound in concrete. *Ultrasonics, 42*(1-9), 781-786.
Schurr, D., Kim, J.-Y., Sabra, K. G., & Jacobs, L. J. (2011). Damage detection in concrete using coda wave interferometry. *NDT & E Int 44*, 728-735.
Sebesta, S., & Scullion, T. (2003). Application of infrared imaging and ground penetrating radar to detect segregation in hot-mix asphalt overlays. *Transportation Research Record:Journal of the Transportation Research Board, 1861*, 37-43.
Seher, M. (2011). *Finite element simulation of crack depth measurements in concrete using diffuse ultrasound.* Master, Georgia Institute of Technology, Atlanta.
Seher, M., In, C.-W., Kim, J.-Y., Kurtis, K. E., & Jacobs, L. J. (2012). Numerical and Experimental Study of Crack Depth Measurement in Concrete Using Diffuse Ultrasound. *J Nondestruct Eval*.
Seher, M., In, C.-W., Kim, J.-Y., Kurtis, K. E., & Jacobs, L. J. (2012). Numerical and experimental study of crack depth measurement in concrete using diffuse ultrasound. *Journal of Nondestructive Evaluation*.
Sellick, S. F., Landis, E. N., Peterson, M. L., Shah, S. P., & Achenbach, J. D. (1998). Ultrasonic investigation of concrete with distributed damage. *ACI Materials Journal, 95*(1), 27-36.
Shashidhar, N. (1999). X-Ray Tomography of asphalt concrete. *Transportation Research Record 1681*, 186-192.
Sheng, P. (2006). *Introduction to wave scattering, localization and mesoscopic phenomena*: Springer.
Shin, S. W., Zhu, J., Min, J. Y., & Popovics, J. S. (2008). Crack depth estimation in concrete using energy transmission of surface waves. *ACI Materials Journal, 105*(5), 510-516.

Song, W.-J., Popovics, J. S., & Achenbach, J. D. (1999). *Crack depth determination in concrete slabs using wave propagation measurement.* Paper presented at the the 1999 FAA Airport Technology Transfer Conference, Atlantic City, NJ.

Song, W.-J., Popovics, J. S., Aldrin, J. C., & Shah, S. P. (2003). Measurement of surface wave transmission coefficient across surface-breaking cracks and notches in concrete. *Journal of Acoustical Society of America, 113*(2), 717-725.

Stain, R. (1982). Integrity testing. *Civil engineering London*, 53, 55, 57-59.

Stroup-Gardiner, M. (2000). Identifying segregation in hot mix asphalt pavements using rolling nuclear gage measurements and infrared imaging. *Journal of Testing and Evaluation, 28*(2), 121-130.

Stroup-Gardiner, M., & Brown, E. R. (2000). Segregation in Hot- Mix Asphalt Pavements. *Transportation Research Board, 441*, 101.

Suaris, W., & Fernando, V. (1987). Ultrasonic Pulse Attenuation as a Measure of Damage Growth during Cyclic Loading of Concrete. *ACI Materials Journal, 84*, 185-193.

Ter Heide, N. (2005). *Crack healing in hydrating concrete.* Master, Delft University, Netherlands.

Thomas, M. D. A., Scott, A., Bremner, T., & Bilodeau, A. (2008). Performance of Slag Concrete in Marine Environment. *ACI Materials Journal, 105*, 628-634.

Thomson, W. T. (1940). *Measuring changes in physical properties of concrete by the dynamic method.* Paper presented at the ASTM.

Tigdemir, M., Kalyoncuoglu, S. F., & Kalyoncuoglu, U. Y. (2001). Application of ultrasonic method in asphalt concrete testing for fatigue life estimation. *NDT and E International, 37*(8), 597-602.

Vankuten, H., & Middendorp, P. (1982). Testing of foundation piles. *Heron, 26*(4), 3-42.

Viktorov, I. A. (1967). *Rayleigh and Lamb Waves*. New York: Plenum Press

Wang, W., Jansen, D. C., Shah, S. P., & Karr, A. F. (1997). permeability study of cracked concrete. *Cement and Concrete Research, 27*(3), 381-393.

Weaver, R. L. (1982). On diffuse waves in solid media. *Journal of the Acoustical Society of America, 71*(6), 1608-1609

Weaver, R. L. (1990a). Diffusivity of ultrasound in polycrystals. *Journal of the Mechanics and Physics of Solids, 38*(1), 55-86.

Weaver, R. L. (1990b). *Ultrasonic diffuse field measurements of grain size.*, Hemispere, New York.

Weaver, R. L. (1998). Ultrasonics in an aluminum foam. *Ultrasonics, 36*(1-5), 435-442.

Yang, Y., Lepech, M. D., & Li, V. C. (2005). *Self healing of ECC under cyclic wetting and drying* Paper presented at the International workshop on durability of reinforced concrete under combined mechanical and climatic loads, Qingdao, China.

Zhang, Z. Q., Jones, I. P., Schriemer, H. P., Page, J. H., Weitz, D. A., & Sheng, P. (1999). Wave transport in random media: The ballistic to diffusive transition. *Physical Review E (Statistical Physics, Plasmas, Fluids, and Related Interdisciplinary Topics), 60*(4), 4843-4850.

Zhong, W., & Yao, W. (2008). Influence of damage degree on self-healing of concrete. *Construction and Building Materials, 22*(6), 1137-1142.

Zhu, J., & Popovics, J. S. (2005). Non-contact imaging for surface-opening cracks in concrete with air-coupled sensors. *Materials and Structures, 38*(9), 801-806

Zhu, J., & Popovics, J. S. (2007). Imaging concrete structures using air-coupled impact echo. *Journal of Engineering Mechanics (ASCE), 133*(6), 628-640.